DEVELOPMENT OF AUSTEMPERED DUCTILE IRON FOR AUTOMOBILE AND MACHINE PARTS.

BY

ADEWUYI, BENJAMIN OMOTAYO
MSc. (Metallurgical and Materials Engineering)

A THESIS IN THE DEPARTMENT OF METALLURGICAL AND MATERIALS ENGINEERING SUBMITTED TO THE POSTGRADUATE SCHOOL IN PARTIAL FULFILLMENT OF THE REQUIREMENTS FOR THE AWARD OF THE DEGREE OF DOCTOR OF PHILOSOPHY (Ph.D.), FEDERAL UNIVERSITY OF TECHNOLOGY, AKURE

NOVEMBER 2002

CERTIFICATION

We certify that Engr. B.O. Adewuyi of the Department of Metallurgical and Materials Engineering, Federal University of Technology Akure carried out this study.

Prof. A.A. Afonja
(Major Supervisor)

Prof. C.O. Adegoke
(Co-Supervisor)

REFLECTION

There is a land beyond the stars,

Glory Land, bright Glory Land,

Beyond the sunset's crimson bars,

A Land of peace without Alloy,

Of joy beyond all earthly joy,

And naught its calm can ever destroy

The city of our God is there,

Its Jasper walls with beauty fair,

Its Gates of Pearl like Silver gleam,

Its skies with fadeless sunlight beam,

And through it rolls life's crystal stream,

Glory Land Bright Glory Land.

DEDICATION

This project is specially dedicated to:

- **My Senior Partner, The Holy Spirit, Who is always by my side, to COMFORT, INSTRUCT and SHOW the way to go. Who constantly reminds me "whatever God determines in His heart, NOBODY can change."**
- **My wife, LOLA, for her understanding, prayer and encouragement, and**
- **My Children:**

(Dr.) 'Demola,

Tolu

And

Feranmi.

ACKNOWLEDGEMENT

I am very grateful to God, the Alpha and Omega who kept on assuring me that whatever He decides in His heart nobody can change and whenever He lifted up His hand to promote nobody can demote. His ordinances remain unchangeable from generations to generations. I thank Him for His redemption power and deliverance from the hand of those that are stronger than me, (Jeremiah 15:21). The Lord remains forever the source of my strength.

I thank my Major Supervisor, Professor A.A. Afonja, who made research work on the new material "Austempered Ductile Iron" so simple and interesting. His wealth of experience became a source of inspiration. Likewise my sincere appreciation goes to my Co-Supervisor, Prof. C.O. Adegoke, (Dean, SEET), who stood his ground on the side of the TRUTH despite serious opposition. I will forever be grateful to the duo.

I will also seize this opportunity to remember Late Prof. T.O. Adepoju. Even though he is no more, the legacy of hard work that he left behind still lingers on.

Prof. O.O. Onyemaobi, you are indeed a child and minister of the living God. "those who are led by the Spirit of God, are sons of God" (Romans 8:14). The Spirit of the Lord directed your footsteps to FUTA to save life and you indeed delivered me from the "snares of the fowlers". The living God will forever reward you with open heaven for obeying His voice. I would also like to express particular appreciation to Dr J.O. Borode, Dr. A Oguntuase, Prof. O.O Adewoye, Engr. J.A. Omotoyinbo, Dr. A. Odeshi, and Mr. Alo Francis as well as to other colleagues, friends and students of whose immense technical contributions and generous advice and support have culminated in the success of this work. I thank Mrs. Kate Lebile, the Departmental Secretary, Messers. Aboginije,

Alaneme, K; Afolabi A.S; Ogunniyi, O.T; Oloruntoba, Saliu, Oyetunji, A and Mrs Y.Ola-Omole. You all made my work as the Coordinator of the Department and at the same time a "postgraduate student" easy. Also I appreciate Mr. Alowolodu and Mrs. Ogundiminiyi.

The criticisms from Dr. J.A. Ajayi and Prof. A.Oni were motivating and helpful and are gratefully acknowledged. I cannot but mention the moral and spiritual support from a dear friend, Engr. Z.O. Opafunso. You have been most wonderful.

Foundry and heat-treatment facilities and technical assistance were generously made available by FUTA, OAU, Adeyera Foundries, Machine tools Oshogbo, Nigerian Foundries and Ajaokuta Steel Company.

I thank the Federal University of technology Akure, for granting me the opportunity for this research through the Staff Development Program.

Appreciation is expressed to my family, without whose patience and encouragement this work would not have been completed.

Finally, for the many contributors and others who find their essence in the pages without specific reference, I wish to express my appreciation and acknowledgement.

B.O. ADEWUYI.

November, 2002

TABLE OF CONTENTS

LIST OF TABLES

LIST OF PLATES

LIST OF SYMBOLS

SYMBOL	DEFINITION.
a_C	Critical Crack Length (mm)
α	Ferrite
γ	Austenite
d	Particle Size (μm)
ε	Strain
ζ	Fraction of Transformation (%)
K_{IC}	Critical value of Fracture Toughness
κ	Constant of Proportionality
κ_k	Kinematics Shear Yield Stress
λ	Lambda Factor
n	Strain Hardening Coefficient
p_o	Maximum Hertz Stress
ρ	Dislocation density (m^{-2})
σ_γ	Austenite Proof Stress (MPa)
σ_α	Proof Stress of Bainitic Ferrite (MPa)
σ	True (Applied) Stress (MPa)
σ_u	Ultimate Tensile Strength (MPa)
σ_y	Yield Strength (MPa)
R	Stress Range
S_C	Fatigue Limit (MPa)
S_u, S_m , S_{max}	Nominal Static Ultimate Tensile Stress, Mean Stress and Maximum Stress
T_A, t_A	Austempering Temperature and Time (^{0}C, Min)
T_γ , t_γ	Austenitising Temperature and Time (^{0}C, Min)
V_γ , $V_{\gamma r}$	Volume Fraction of Residual and Retained austenite, (%)
X_γ	Volume Fraction of Austenite (%)

ABSTRACT

An investigation has been carried out on the effect of silicon level on austempered ductile iron in order to determine the suitability of the material in the development of structural materials that can be used in the production of automobile and machine parts that undergo constant cyclic loading. This is in response to pressures on engineering and automobile industries to produce components that provide improved properties and performance, save energy cost or reductions in overall manufacturing cost and also to further increase the opportunity for wider commercial exploitation of cast irons. The study involved initial production of three ductile iron alloys containing different levels of silicon. The effect of austenitising temperature (850, 900 and 950^{0}C for 1hour) and rapid quenching and holding in a salt bath maintained at austempering temperature (280, 300 or 350^{0}C for different time intervals 15,30,60,90,or 120) on the mechanical properties were subsequently investigated. The silicon level sensitivity on the fatigue strength, impact toughness and the hardness properties of the three alloys containing increasing silicon levels (2.0%, 2.6%, 3.0%) were characterized using optical micrography and the results were used to correlate the phase relationship with the mechanical properties. Computer modeling was used to measure the volume fraction of retained austenite. The austempering applied to the ductile cast iron alloys produced different bainitic structures, as a function of heat treatment conditions that led to an attractive combination of mechanical properties. These render the low silicon, medium silicon and the high silicon austempered ductile iron useful in the production of automobile and machine parts as an economical substitute for high strength steels. While the bainitic transformation in steels

gave a mixture of ferrite and carbides, the presence of silicon in the ductile iron led to significant austenite volume fractions being retained in the microstructure. The best overall results were obtained from a high silicon alloy austenitised at 950^0C and austempered at 350^0C while optimum impact energy of 70 and 115 Joules respectively was obtained from the medium silicon alloys and high silicon alloys austenitise at 950^0C and austempered at 350^0C. Both alloys have the same optimum values for fatigue limits, 450Nmm^{-2} at these austempering conditions. The results show that alloys of different silicon levels can be used to produce machine parts by altering the austempering parameters. The model developed to predict the fatigue limit from the impact toughness value and the opening and closure of the processing window can be used to optimize production processes in foundries.

CHAPTER ONE

1.0 INTRODUCTION.

Austempered ductile iron (ADI) has been recognized as an important engineering material because of its excellent properties. Only recently, there has been an increasing demand for the introduction of austempered ductile iron (ADI) as a new engineering material because the material has a good combination of high strength, ductility, toughness, fatigue strength and wear resistance over other ductile irons, (Aranzabal et al, (1997); Prasad and Putatunda, (1990).; Shieh et al. (1995)). Several organizations worldwide are now making use of the wide range of properties offered by ADI.

Austempered Ductile Iron (ADI) is a material that is composed of bainite and austenite matrix. According to Dommaco et al, (2001), ADI matrix microstructure contains up to 35 - 40% austenite, that may transform in service by mechanical solicitations. Bainitic matrix in ductile iron can be obtained in two ways: (i) in as-cast form where bainitic transformation is achieved by judicious alloying; and (ii) by subjecting normal ductile iron castings to a specialised heat treatment known as "austempering". Austempered Ductile Iron offers to the engineer the typical benefits of conventional ductile iron in addition to enhanced mechanical properties.

Researching and developing ADI became prominent in the 1980's, although ADI has been around for some time and austempering as a treatment for alloy steels was discovered in the 1930s. Today, the research dedicated to ADI technology has made it a widely accepted engineering material with a worldwide production that is expected to exceed 10^5 tons by the new millennium, (Trudel and Gagne, (1997); Neuman (1965) Smith (2001)).

The production of bainitic matrix structures using austempering heat treatments was first demonstrated in the early stages of the commercial development of nodular graphite irons. Such treatments were shown to produce materials with desirable combinations of properties including high strength, ductility, toughness and wear resistance. Until the last decade, however, little had been done to exploit commercially the material properties that could be achieved.

Having a lower weight than steel and a higher capacity to absorb vibrations, some ADI varieties can also reach mechanical properties only comparable to high-resistance alloyed steels, (Harding, 1986). Hence, the material can provide an alternative to the use of steel in a number of demanding applications, with the added advantage of being cheaper to produce in the form of complex shapes. ADI exhibits remarkable machinability and resistance to wear in conjunction with design flexibility and low cost, (Roberts (1992), Bhadeshia (1992)).

One of the restraints in the widespread availability of ADI has been the need to subject the components to a very carefully controlled heat-treatment defined to obtain the required properties. Of particular importance is the As-Cast quality of the castings subjected to austempering as the heat-treated castings remain sensitive to casting defects. The opportunity for wide commercial exploitation of these materials has risen in response to pressures on engineering and automobile industries to produce components that provide improved properties and performance, or reductions in overall manufacturing cost.

It is known that steel component either in the casehardened or forged-condition can be heat treated and alloyed to obtain a beneficial change in the matrix structure and hence provide a range of useful properties. The beneficial use of this heat treatment had encouraged many

researchers to apply this to ductile iron so that it could become a tougher, corrosion resistant, wear resistant and stronger material, (Haseeb et al (2000), Kobayashi (1996)).

Ductile iron subjected to austempering treatment is often referred to as **"AUSTEMPERED DUCTILE IRON"** (ADI) in most international forums. The term 'Austempered Ductile Iron' therefore describes a family of materials whose properties can be varied over a wide range by the correct choice of heat treatment variables. It is now known that ADI offers an ideal combination of strength, ductility and wears resistance, with a maximum tensile strength of 1600N/mm^2 and high hardness. Materials of lower hardness having tensile strengths of 900 to 1200N/mm^2 and elongation of up to 14% can also be produced for engineering applications where considerable ductility is required, (Bahmani and Elliot(1994); Bayati and Elliot (1987)).

AUSTEMPERED DUCTILE IRON VERSUS STEEL = NO CONTEST

Whether specifying a new casting, forging or fabrication or improving an existing one, the potential benefits of Ductile Iron over steel are clear: Improved strength to weight ratio; better surface definition and finish; easier machinability and a reduced machining allowance; reduced component weight; (Ductile iron is approximately 10% lighter than steel); and reduced component cost. ADI with high strength, impact energy and wear resistance is used in gears, crankshafts, rollers and wheels, gravel crushers, mining drill heads, wear plates, cam-tracks, brake rotors, heavy machinery, diggers and agricultural machinery, and many other applications. In the abrasive wear mode, the wear rate of ADI is comparable to that of alloyed hardened AISI 4340 steel, and approximately one-half that of hardened medium-carbon AISI 1050 steel and of white and alloyed cast iron. The excellent wear resistance of ADI is attributed to the strain-affected transformation of high-carbon austenite to martensite that takes place in the surface

layer during wear tests, (Ahmadabadi et al, (1999)). Ductile iron castings have production and machining cost advantages over steel fabrications, forgings and castings within the limitations of the ductility and impact properties and have strength to weight advantages over grey iron where breakage is a problem.

Some applications of austempered ductile iron that have been successful are: Automobile crankshafts and camshafts replacing steel forging; gear rings and drive rings replacing fabrications, castings and forging; shear-pin housings and drive couplings replacing steel castings; main shafts and rotors for machinery drives; brackets replacing fabrications; thin section castings replacing fabrications for covers, delivery chute, housings and other machinery components. Gearwheels produced in ductile iron that is hardened or austempered give greater freedom of design than steel forging. Rolls for pelleting presses produced in Austempered Ductile Iron is a competitor to tool steel. Moulds for aluminium ingots cast in ductile iron have superior cooling characteristics and life than the normal grey iron moulds, Magalhaes et al, (2000). As engineering design practices become increasingly sophisticated and service conditions more demanding, the need for engineering materials and components, particularly in conditions of high dynamic loading is expected to increase.

Materials for making machine elements generally referred to as structural materials are characterized by a large diversity of shapes, dimensions, and operating conditions. These materials operate at static, cyclic and impact loads, high and low temperatures, and in contact with various aggressive media. These factors shape the requirements set forth to structural materials, which can be divided into three main groups: operating, technological and economic. Operating requirements are of prime importance. A structural material must have a high

structural strength in order to ensure the serviceability of particular machines. The structural strength is a complex of mechanical properties of a material, which can ensure reliable and long operation of the material under specified operating conditions. The required values of mechanical properties of a material for a particular element depend not only on the force factors, but also on the effects of the working media and temperature. The medium in which an element has to operate may be liquid, gaseous, ionized, irradiated, etc. and can produce an essentially and mostly negative effect on its mechanical properties and reduce the serviceability of the elements. In particular, the working medium can cause damage to the surface of the elements due to corrosion cracking, oxidation or scaling material in the surface layer resultant from saturation with unwanted elements (for instance, hydrogen which causes embrittlement in metals). To withstand the action of the working medium, a material must possess proper mechanical properties: resistance to electromechanical corrosion, heat, radiation, moisture, capability for operating in vacuum etc.

Depending on the technological processes employed, the term workability may include machinability, deformability, weldability, castability, hardenability, liability to deformation and buckling on heat treatment, etc. The workability of a material is of prime importance, since it determines the productivity of manufacture of machine elements and structures.

Traditional areas of application of ADI are the production of engine and other components which could raise fuel efficiency. According to Hemanth (2000), the major users of ductile iron components include the automobile and machine tool industry.

Compared to steel, ADI exhibits superior functional properties in terms of machinability, better resistance to contact fatigue, damping capacity and hence better noise attenuation, amenability to

heat treatment, lower density and hence better weight reduction, energy and other cost requirements from molten metal to finished product. Also ADI castings can have uniform properties even with complex shapes, a characteristic not always possible with steel forging or weldments, Hemanth. (2000); Dommarco et al, (2001); Fan et al (1993).

Developments in ADI have made it possible to replace such costly engine components as camshaft, crankshaft, connecting rods, axle shaft, steering knuckles and tractor parts of forged steel with nodular iron castings. The prospects of ADI as alternative material to the rather expensive, forged, casehardened steel in other critical components operating under severe dynamic conditions such as hypnoid ring, pinion gears, bearing and toothed gear power transmission (since it is significantly machinable for the teeth to be cut after the heat treatment, thus giving the best possible dimensional accuracy) is expected to open new vistas for cast iron production. Furthermore, major engineering components requiring complicated manufacturing from high-grade steels by, for example, forging, rolling, welding, and surface hardening, all of which may preclude the use of normal machine tools, can now be made in near-net shape casting in austempered nodular cast iron. Nevertheless, as for other engineering materials, the production parameters have a significant influence on the performance of ADI castings. Of particular importance is the as-cast quality of the castings submitted to austempering, as the heat-treated castings remain sensitive to casting defects.

Some of the restraints on the widespread availability of ADI according to Trudel and Gagne 1997; Imasogie et al, (2000), Putatunda, (2001) include:

1. When compared to grey iron the sensitivity of a DI component to its chemical composition is very high. Therefore the careful selection of the charge materials is critical.
2. Special attention must be paid to the spheroidization practices, which control the crystallization of spherullitic graphite particles. In order to obtain high-level quality DI components, the maximum possible level of these must be achieved.
3. The need to subject the components to a very carefully controlled heat treatment regime to obtain the required properties and the need to establish a process technology capable of sustaining high volume production of castings of the required integrity.
4. There has been limited metallurgical data available to explain the relationship between microstructural features of ADI and its mechanical properties.
5. There has been insignificant fatigue and impact toughness properties' data available to the design engineer for development of structural application.

Conversion-cost reduction is a common motive for switching to ductile castings. Imasogie, (1994), reported that manufacturing costs were slashed 69% in converting a two-piece fabrication of a steam turbine governor case, formally made from a steel bar stock steel tubing joined together by welding to a one piece ductile iron casting. Remarkably, the one-piece casting exceeds maximum engineering requirements. Another notable case involved a conversion from a steel forging. Primarily, as a forging, the part, a wire rope clamp for conveyor idler and support stand, cost $2.31 per unit to manufacture. But by going to a sandcast clamp of an 80-55-06 grade of ductile iron, it became possible to save part cost by 91%. Also, the castings had more than adequate strength and toughness while eliminating machining because functional surfaces had

sufficient accuracy in the as-cast condition. Another special case involves the use of the 65-45-12 grade of ductile iron casting lined with Teflon. The complex plug valve, which controls the flow of extremely corrosive liquids in chemical processing plants, was formerly made of a variety of exotic materials, including type 316 stainless steel, Monel alloy, Castelloy B, titanium, and tantalum. In some specific cases, unit cost ran as high as $229, the item is now down to $79 with cast recesser and machined grooves in the body and plug locking the Teflon in place preventing it from collapsing even in a high vacuum or during thermal cycling. In addition to cost, other considerations such as mechanical properties, corrosion resistance, welding and thermal (spalling) qualities, recommend ductile irons over and above all other materials. Specifically, the oil manifold for earth-moving equipment is presently made of ductile iron because the application called for a combination of high strength and good ductility, (Dommarco et al, (2001)). Ductile iron piston for diesel locomotive engines is stronger and has more wear resistance than previously used types. Reduction in weight (by 50%) also means less stress on other parts, such as bearings. Ductile iron has the potential to replace costlier materials in many significant engineering applications. The requirements concerning safety and reliability are always on the increase and therefore resistance to fatigue and impact toughness is ever more crucial. In view of the paucity of data on the fatigue and impact toughness of ADI, the present research is intended to fill the void.

The method of obtaining ADI with excellent properties depends on the effective control of metallurgical and process variables. Hence in considering the technological implication of this investigation, special emphasis is placed on the production process of the ductile iron and the test

parameters. Results obtained are expected to indicate whether these irons have improved properties such as would recommend them for applications pertinent to those earlier mentioned.

The project is approached in the following ways:

1. Production of Ductile Iron samples with varying levels of silicon. Yan (1995) reported that during austempering, silicon restrains formation of carbide and makes carbon atoms saturate in retained austenite when bainitic ferrite grows, so that the stability of supercooled austenite is improved. In a certain range, the volume fraction of retained austenite increases with the content of silicon. Silicon is one of the elements contracting the austenite zone of phase diagram. It reduces the transformation rate of austenitising. Furthermore, silicon shifts the eutectoid point in phase diagram to lower carbon content and decreases the carbon solubility in austenite matrix. However with excessive silicon content, the carbon content in austenite may be cut down and the retained austenite reduced. An increase in the amount of silicon in cast iron reduces the amount of pearlite but increases that of ferrite. In iron with a very high silicon content, the matrix becomes completely ferritic (silico - ferritic). Due to its large affinity for oxygen, silicon easily forms protective oxide films (SiO_2) on the surface of castings and also increases its heat resistance, (up to 5 -6%).

Silicon has a key role to play in the development of microstructure of austempered irons. Hence the sensitivity of silicon level to the fatigue strength and impact energy of austempered ductile iron will be considered, so also is the interdependence of austenitising temperature and silicon content.

2. Developing and investigating an ADI with different silicon content with the aim of improving the fatigue strength through the effect of isothermal transformation. According to Putatunda and Sing, (1995), the yield strength of ADI depends on the finess of ferrite and austenite, and the fracture toughness of ADI depend on austenitic carbon content. Hence by combining the effect of silicon with austempering holding time and temperature, it is envisaged that there is the possibility of obtaining an ADI with high fatigue strength and impact toughness. During the austempering process, ferrite forms out of austenite by nucleation and growth process, Bahmani and Elliot, (1994). When ferrite forms out of austenite, carbon is rejected from ferrite and diffuses into the surrounding austenite. Since nucleation depends on the supercooling, very fine ferrite and austenite will be produced when supercooling is high, i.e. when ADI is quenched to a lower austempering temperature from the austenitizing temperature. It is expected that silicon will affect the diffusion of carbon at a faster rate. This is expected to produce a material with improved fatigue and impact toughness. The austempering time is selected to ensure that the formation of bainitic ferrite adequately enriches the residual austenite with carbon, allowing much of it to be retained to room temperature.

It is expected that the research findings will be useful to the foundry industry in the following ways:

(a) As a tool for the optimisation of the production process.

(b)To attain the desired mechanical properties in crankshafts and gears through selection of a specific alloy composition and heat treatment parameters.

(c) As a guideline for the production of ADI alloys which can be a substitute for existing steel alloys used in automobile and machine parts

The primary objective of this research is to develop ductile cast iron alloys suitable for the production of automobile and machine parts.

Specific objectives of the research are to:

a) Investigate the effect of silicon on the microstructure of austempered ductile iron.

b) Evaluate the effect of austenitising temperature, austempering temperature and time and silicon level on the impact and fatigue strength of austempered ductile iron.

c) Use computer models for the prediction of the amount of the retained austenite and the prediction of the fatigue limit from impact strength data in ADI as a function of austempering variables.

d) Investigate the relationship between microstructure features and impact and fatigue strength of ADI

e) Establish an optimum set of compositional and heat treatment variables for the production of ADI of high impact and fatigue strength, suitable for the manufacture of automotive and other machine components.

The great interest in using ADI in many applications requires a more comprehensive database on the fatigue and other mechanical properties of ADIs. The published data regarding the effect of silicon level and austempering temperature on ADI fatigue properties are still limited, thus providing a need for further experimental work. The present study is intended to increase the database and understanding of ADI's impact toughness and fatigue properties. The aim is to characterise the effects of silicon level and austempering temperature and time on the impact toughness and fatigue properties of ADI by systematic experimental studies on specimens.

CHAPTER TWO

2.0 LITERATURE REVIEW

2.1 AUSTEMPERED DUCTILE CAST IRON.

The history of Austempered Ductile Iron (ADI) has been influenced by a number of technical developments that have resulted in new business opportunities for the foundry industry. Austempered Ductile Iron has earned what could be termed a unique position among engineering materials. No other ferrous material can match its combination of castability and mechanical properties.

The presence of graphite contributes directly to lubrication of rubbing surfaces and provides reservoirs to accommodate and hold lubricants. This means good resistance to mechanical wear. Graphite also contributes to machinability because it acts as a lubricant during cutting. In their studies, Magalhaes et al, (2000), carried out experimental observations of contact fatigue crack mechanisms for austempered ductile iron discs. They concluded that superficial graphite nodules that lie just beneath the surface and covered by very thin layer of material do not have negative effect on the fatigue fissures but the graphite enrichment of the lubricant resulting from the voiding of these nodules is noticeable. Like grey iron, ADI has inherent corrosion resistance, Hemanth, (2000). The material can be referred to as being versatile because it can be tailored to fit an unusually broad diversity of needs. It has for instance been chosen over and above cast steel, steel forging, steel fabrications including weldments, in parts ranging from a fraction of kilograms (e.g. pump cylinder), to mill rolls.

In Austempered Ductile Iron, the free graphite is in the form of discreet nodules or spheroids. The matrix may be ferritic, pearlitic or a mixture of the two. The discrete form of the graphite nodules in comparison to the planes of weakness of the graphite flakes in grey iron means that the properties of ductile iron are determined more by the matrix of the material than the form of the graphite. Thus ADI has higher strengths, greater elongation and better resistance to impact than grey iron.

In the as cast condition a range of properties from high ductility to comparatively high strengths can be produced by control of the chemical composition and production process. This range of properties may be extended by alloy adjustment and subsequent heat treatment including surface hardening and through hardening by quenching and tempering. Whilst the production of ductile iron is more involving than grey iron, it is still possible to produce complex shapes which are more easily machined than steel. The wide range of properties means that the various grades of ductile iron could be used in a variety of applications.

ADI is a prominent cast ferrous alloy, where conversion of carbon to graphite of spheroidal shape with a matrix of pearlite imparts enhanced ductility, that is capacity for plastic deformation prior to fracture. Such improved ductility therefore opens the possibility of forging parts made of ADI. In this way energy consumption can be reduced by finish forging of readily castable rough shape in certain parts. The other route to obtain high strength and ductility in Austempered Ductile Iron is by means of austempering heat treatment. Studies conducted by Prasad (1988) of the Indian Institute of Technology concerning the upset forging behaviour of ADI clarify conditions under which it can be hot forged. Hence utilizing cast billets of ductile iron, as stock for forging is less attractive than austempering.

Two types of Ductile cast Irons are recommended for ADI production: the ferritic grade and the pearlitic grade. These two grades differ mainly by their chemical composition, Tables 1 - 4.

2.2 CASTINGS TECHNOLOGY AND CONTROL FOR ADI PRODUCTION

The casting technology to produce nearnet shape components of consistent dimensions is well established, and several alternatives are available. These include die-casting, the use of semi-permanent moulds, investment casting and certain sand casting processes in which moulds of high rigidity and excellent definition are produced. In the latter context, the use of zircon as opposed to silica sands can offer considerable advantages, the higher initial cost of the zircon sand being offset by its reclamation and re-use in a closed-loop system. Such systems have been operated with considerable success in foundries for at least twenty years, to produce components of very consistent dimensions. (Briggs, (1986). Krauze et al (1988), Neuman, (1965)).

To prevent the contamination of the castings by certain alloying elements found in steel and to maintain a high level of consistency of the microstructure, the charge materials must be carefully selected, (Imasogie (1994)). Briggs (1986) confirmed that non-metallic inclusions adversely affect the serviceability, machinability and appearance of Fe-castings. These inclusions come from slag and dross generated during the melting, alloying and pouring of cast iron. Frequently, they enter the mold cavity through the gating system. Indeed, the primary method used to prevent inclusions in the casting is a carefully designed gating system, often with elaborate slag traps. Recently, ceramic filters have been developed that are applied to the gating system to remove slag and dross from the molten Fe and so reduce the opportunity for non-metallic inclusions to find their way into the casting.

Table 1. Grades of Ductile Iron.

Grade	Tensile strength (min), MPa	0.2% Proof stress (min), MPa	% Elongation	Matrix
350 / 22	350	220	22	Ferritic
420 / 12	420	270	12	Mainly feritic
500 / 7	500	320	7	TemperedFerrite and pearlite
800 /2	800	480	2	Martensite

Table 2. Typical Mechanical Properties and Applications of Ductile Iron

Alloy Type	Chemical Composition, %	Condition	Microstructure	Typical Application
Ferritic	3.5 C –2.2 Si	Annealed	Ferritic	Pressure casting such as valve and pump bodies
Martensitic	3.5 C –2.2 Si	Quenched and Tempered	Martensitic	Pinions, gears, rollers and slides.
Pearlitic	3.5 C –2.2 Si	As – Cast	Ferritic - Pearlitic.	Crankshaft, gears, rollers.

Table 3. ASTM Standard 897M-90 for ADI grades

Grade	Tensile Strength MPa	Yield Strength MPa	% Elongation	Impact energy Joules.	Typical Hardness BHN
125/80/10	850	50	10	100	269 to 321
150/100/7	1050	700	7	80	302 to 363
178/125/4	1200	850	4	60	341to 444
200/155/1	1400	1100	1	32	388 to 477
230/185/-	1600	1300	N/A	N/A	444 to 555

Table 4. Range of Chemical Composition for DI castings

Element	Ferritic grade %	Pearlitic grade %	Function	Remark
C	3.0 to 4.0	3.0 to 4.0	Constituent of the spheroids	
Si	1.08 to 3.0	1.8 to 2.75	Graphitizer, ferritiser	Excess causes graphite location
Mg	0.03 to 0.06	0.03 to 0.08	Spheroidiser	Control as cast pearlite
Ce	0.03 max	0.03 max	Promotes formation of spheroids in combination with Mg	Excess promotes
S	0.015 max	0.015 max	Combines with Mn	Sulphur removal is essential
Mn	0.2max	0.7 max	Pearlite former	Excess promotes carbides
P	0.035 max	0.05 max	Embrittles structure	Pearlite stabilier
Cr	0.04 max	0.1 max	Very potent carbide former	Retards annealing
Cu	0.03 max	To specification.	Strength, hardness	Potent pearlite stabiliser

Such castings reduce casting defects and facilitate gating system simplification. In commercial practice the softer grades of ductile iron are made of a composition that is low in pearlite-stabilizing elements such as manganese to minimize the combined carbon content. The slow cooling of thick metal sections can influence the casting properties in three ways: (a) cause graphite floatation in high carbon iron (this can be avoided by maintaning a lower total carbon content). (b) Form a large cell and increase segregation (increase segregation at cell boundaries reduces the strength and ductility). (c) Formation of ferrite with a relatively low hardness and strength. The mechanisms of formation of graphite in pure Fe-C alloys investigated by Krauze et al (1988) established that the form of graphite is determined by the stability of the liquid phase. As a means of controlling the nature of the liquid phase, such factors as refining of the melt, the rate of its cooling, superheating, inoculation, and control of chemical composition (separately or

combined) affect the forming of graphite through their action on the stability of the melt. These findings are of great importance for the production of high strength spheroidal graphite cast iron, making it possible to select inoculant and methods of inoculation on a sound basis. The nature of their effect on the stability of the liquid phase must be taken into account.

2.3 PROCESS TECHNOLOGY FOR INTRODUCING SPHERODISING AGENTS.

One of the greatest practical difficulties in the production of ductile iron is getting the required amount of nodulizer into the melt with the necessary degree of consistency and assurance, combined with freedom from risk of danger. The practical difficulties are quite enormous due to the speed of reaction and the accompanying violence. Magnesium, for example, boils at about 1120^0C and when plunged into the molten cast iron at 1400^0C, Mg metal melts and vapourises instantaneously, escaping with violence and carrying with it some of the cast iron. Successful Magnesium treatment requires an emulsion of magnesium vapour and liquid cast iron. To obtain an intimate emulsion, liberation of the Mg should occur over a period of time and at many places in the molten iron. For this reasons the most popular methods of producing ductile iron rely on some form of carrier or indirect method of introducing the nodulizer. To improve the dissolution behaviour of nodulizing mixtures and consequently, the structure homogeneity of the castings, several methods had been adopted.

1. Spherodising treatment inside the mold is one of the recent achievements in the production of S.G. iron castings. It offers several economical and technological advantages that recommend its application, particularly in the mass-production of S.G. iron castings. Shaker and Salamoni, (1988), in their contribution in this area attempted to add sawdust to the mixture. Their result

clearly shows that an addition of approximately 5% of sawdust to a nodulising mixture of granular Mg and FeSi 75 in the compressed form at 7N/cm^2 improves both nodularising characteristics and homogeneity of the casting structure.

2. Treatment of cast iron melts with magnesium wire and inoculating wire for mass production of cast iron parts with spherical graphite was attempted by Best, (1989).

3. Various ladle processes had been adopted for mixture additions: The pouring over system is the oldest technique. The treatment alloy is lower in density hence it tends to float on the surface of the bath. The sandwich system is used, the basic idea being to trap the alloy in a bottom chamber of the ladle and hold it down whilst the molten metal is poured into the ladle in such a manner as to disturb the sandwich as little as possible. This ensures that the magnesium alloy has to travel up through the liquid iron bath - treating it as it goes. The trigger process is a variant of the sandwish process and the aim is to inhibit the magnesium reaction in such a manner that it can be controlled or initiated by external factors until it is desired that the reaction should begin. The cover is usually calcium carbide, sand or cast iron borings. This achieves delayed treatment and delayed nucleation, both desirable features. The tundish ladle process incorporates a pneumatically operated lid on a tundish (or a pouring basin) with a carefully controlled orifice so that the time to fill the ladle with base iron is equal to the reaction time of iron with the nodulizing treatment. The plunging technique is believed to give particularly clean iron by virtue of the purging action of the ascending magnesium vapour bubbles which collect impurities and lift them to the surface of the ladle. Other techniques include the holding process; the T-Neck process; the Flortet process and the In-Mold process.

Since Magnesium metal boils at about 1120^{0}C, it requires a pressure of about 10-12 atmospheres in order to offset this effect at normal cast iron treatment temperatures (1450-1500^{0}C). In view of this, various types of processes had been developed which are based on pressure treatment using either metallic magnesium or high magnesium content alloy. Such a vessel includes the invertible pressure vessel and the Fischel vessel.

The efficiency of Mg recovery depends on a number of factors, such as temperature, ladle size, method of use, sulphur content of the iron and residual magnesium required.

A range of magnesium -ferrosilicon is available containing from 3 to about 15% Mg with approximately by 45% Si. Other materials include a magnesium-impregnated coke (Mag-Coke) or compaction formed from granular mixtures of iron and magnesium. This latter material avoids the progressive pick-up of silicon from magnesium ferrosilicon and which eventually leads to the accumulation of large amounts of unusable back-scraps; Ni-Mg alloy with 5 -15% Mg); All these materials can however be used in any of the alloying systems.

Solidification of ductile iron was examined in detail by Dumpy and Pellini, 1968. They found that a large number of small graphite nodules were formed at the beginning of the eutectic arrest. Graphite nodule counts showed their numbers to be fixed at the start of eutectic freezing. The principal factor is the structural role played by spheroidizing elements when incorporated in a graphite lattice and its effects on the growth.

2.4 DEVELOPMENT OF AUSTEMPERED NODULAR CAST IRON

Austempering as a treatment for alloy steels was discovered in the 1930s. The main advantages are that although the structure formed (bainite - acicular ferrite with carbide nodules) is not as

hard as martensite which forms during a conventional quenching process, the structure is much tougher and because the cooling is interrupted, there is less distortion, Ahmadabadi et al, (1999). The morphology of bainite and techniques for producing bainitic ductile irons, structure property relations etc., have also been studied during recent years, Harding, (1986), Bahmani and Elliot, (1994). Dai et al, (2000), James and Thomson (1999) developed a model that indicates the volume changes during eutectic solidification of ductile iron. Their investigation reveals that chills are essential during solidification to eliminate shrinkage defects and to make the castings sound. In his work on the effect of Cu, Mo and Si on the content of retained austenite of austempered ductile iron, Yan (1995), observed that high silicon content suppresses the precipitation of the carbide phase associated with the normal bainitic transformation in steels and a lamellar structure of acicular ferrite and high carbon austenite is formed. Also, Bhadeshia, (1992) confirmed that the austenite is progressively enriched by the carbon rejected from the growing bainitic ferrite units. With unalloyed irons, very rapid quenching from the austenitising temperature - even of small section thichnesses - is necessary to avoid the precipitation of ferrite or pearlite. By incorporating alloying elements that lengthen the ferrite and pearlite transformation times, slower cooling rates, such as can be obtained by salt quenching or forced air cooling, can be used. The most effective alloying addition is molybdenum. The material retains the nodular graphite distribution of ductile iron, but the matrix is acicular ferrite in a high carbon austenite. The advantageous mechanical properties combined with the ability to cast parts means that these irons are replacing plain and low alloy steels for many components, UTS values of 800 to 950 MPa with elongation of 8 - 10% are readily obtained, Angus, (1976), 'Marks', (1996).

It has been proposed by Krauze et al, (1988) that the growth of spheroids in Mg treated iron occurs because of diffusion of carbon atoms through the austenite shell. However, some authors suggested that the graphite grows whilst essentially in contact with the liquid. This argument is based on the premise that the growth of phase in an isothermal melt is determined by the mechanism that leads to a maximum freezing velocity of that phase or of the eutectic grain and reference has been made to results obtained, which showed that the diffusion transport of carbon in the liquid phase was almost 20 times more rapid than in the austenite phase. Various theories have been advanced to explain the reason why graphite grows as a spheroid, these being; (i) graphite growth in the spheroidal form because of the protection offered by the austenite shell; (ii) spheroidal growth formation under cooling of the melt due to Mg treatment promoting spheroidal growth, Imasogie, (1994).

2.5. AUSTEMPERING PARAMETERS

2.5.1 Metal Composition.

A requirement for the production of austempered ductile irons having optimum combinations of properties is that pearlite formation should be avoided during quenching.

The primary aim of alloying elements in ADI is to provide sufficient hardenability to the matrix. The role of copper, manganese, molybdenum, nickel and cobalt had been identified.

Experimental work, Dorazil, 1982 on cylindrical test bars shows that, with unalloyed irons, the maximum diameter that could be transformed without pearlite formation can be increased from 15mm at a temperature of 450^{0}C to 30mm at a temperature of 250^{0}C. As the bar diameters were increased beyond these values, pearlite formed at the centres of sections as small colonies

associated with graphite nodules, and fully pearlitic matrices were obtained in 30mm diameter bars austempered at 250°C.

In studying the effect of pearlite formation on mechanical properties of austempered ductile iron, Bahmani and Elliot (1994) observed that the presence of pearlite will generally be detrimental to the mechanical properties, although its effect has not yet been fully quantified. When a high enough quenching rate cannot be achieved to prevent pearlite formation in heavier sections sizes, alloying additions must be made to the iron to delay the start and finish of the decomposition of austenite to pearlite and bainite. An addition of 0.3% molybdenum approximately doubles the bar diameter, which can be satisfactorily austempered. The maximum section size can be further increased by larger molybdenum additions although, when such additions exceed approximately 0,5%, significant segregation occurs at the cell boundaries and results in stable carbide formation which has an embrittling effect, Elliot (1997), Tiziani et al, (1988), Juneja (1989), Imasogie, (1994), Trudel and Gagne,(1997).

-Carbon

Ductile irons produced commercially usually have carbon contents, which fall into a relatively narrow range around 3.6%. A systematic investigation at BCIRA has shown that increasing the carbon content from 3 to 4% resulted in a progressive reduction in the tensile strength and proof-stress values after any given austempering treatment, whereas elongation at failure and hardness were attributed to the increase in graphite volume fraction and consequent reduction in the load-bearing cross-section as the carbon content increased.

-Manganese

Manganese has been identified to have two-fold effects: in small section castings. It has been shown to favour the formation of eutectic carbides whose presence require either a longer austenitizing time or an annealing of the casting prior to austempering, Gagne, (1984). In castings solidifying at an intermediate or slow rate, manganese segregates at cell boundaries, causing the precipitates of intercellular complex Fe-Mn carbides. These manganese-stabilized carbides usually remain as a highly brittle phase in the structure after the austempering treatment. The effects of manganese content on the tensile properties of irons austempered for 1 hour in the range 300 to 400°C have also been established, Gagne, (1984); Harding, (1986). It was found that with manganese contents of about 0.9%, tensile and 0.2% proof strengths fell progressively at all austempering temperatures, and ductility was always within the range of 1-3% elongation, even after austempering at higher temperatures. It is therefore suggested that the manganese content in ADI castings should not exceed 0.3%. Beyond this limit, the as-cast quality of the material as well as the kinetics of the solid state reactions occurring during austempering will be affected.

Segregation of manganese at cell boundaries alsc results in a heterogeneous hardenability of the matrix by increasing the stability of the intercellular austenite. These segregated regions may either transform to martensite after cooling from the austempering temperature, or remain as large unreacted austenite areas. The effect of manganese content on the quantity of such intercellular phases in the austempered component and on the austempering time needed to avoid martensite formation had been evaluated, Gagne (1987); Faucher (1987). These intercellular phases severely affect the mechanical properties of ADI castings especially the fracture

toughness. With the heavy segregation which can occur in irons of high manganese content, the intercellular austenite is stable over the normal range of austempering temperatures and will have an M_s temperature of around 150°C. On air-cooling after the isothermal heat treatment, therefore, much of the intercellular retained austenite transformed to martensite.

-Molybdenum

Molybdenum has been discovered as the most potent hardenability agent in ADI. Like manganese, it also segregates at cell-boundaries during solidification to form carbides, Gagne and Fallo, (1986), Elliot, (1996), Tiziani, et al (1988). The Mo-rich carbides serve as nucleation sites as well as propagation paths for cracks. ADI casting containing 3.6%C, 2.5%Si, 1%Cu, 0.2%Mn and 0.25%Mo was observed to have ruptured after only a 2% tensile elongation. The use of molybdenum should be limited to the minimum concentration needed to obtain the required hardenability for a given section size. For practical purpose, molybdenum should be used in combination with nickel and/or copper and its combination should not, in any situation exceed 0.02%. Tensile strength, hardness, and elongation fell progressively as the molybdenum content was increased, and these effects were particularly marked at molybdenum contents above 0.2%. This reduction is due to the segregation of molybdenum during solidification, resulting in the formation of martensite in the segregation regions. In this latter respect, molybdenum acts in a similar manner to manganese. The influence of molybdenum on austempering behaviour of ductile iron was extensively studied by Yazdani and Elliot, (1999). Austempering kinetic measurements and mechanical property measurements of a ductile iron of composition Fe-3.56C-2.77Si-0.25Mn-0.45Mo-0.43Cu-0.04Mg (wt-%) after austenitising at 870°C and

austempering at 400, 375, 320, and 285° C show that increasing the Mo content of the iron with the aim of increasing the hardenability, does not delay the austempering reaction significantly and the processing window is open for all temperatures studied. The mechanical properties determined for austempering temperatures of 400 and 375°C show that the higher ductility grades of the austempered ductile iron standards can be satisfied as predicted by open processing windows. The ductility of the 0.45% Mo austempered iron is reduced compared with that measured in 0.13% Mo and 0.25% Mo iron austempered under the same conditions. This is attributed to an increased amount and continuity of intercellular carbide as the Mo content increases. It is most likely that increasing molybdenum additions, owing to the segregation effects noted above will also reduce these properties, but this is still to be confirmed.

-Copper

There is no evidence to suggest that copper affects the amount of retained austenite in isothermally heat-treated ductile irons. It has been suggested that copper additions suppress the formation of carbides in lower bainite and this would account for the enhanced ductility of copper-containing irons austempered at temperatures of 350°C and below, Elliot, (1996). A study was made to determine the influence of intercellular segregation during tempering on the microstructure of austempered ductile iron in unalloyed and alloyed ductile iron. It was postulated that the acquisition of a first stage matrix exclusively composed of ferrite and carbon enriched (or stabilized) ausferrite needs a rigorous control of the following heat treatment parameters: austenitization temperature and holding time, amounts of alloying elements and thickness of the piece (cell size). The most significant influence of the intercellular segregation is

the formation of a heterogeneous upper bainite composed of ferrite and enriched ausferrite with martensite and retained austenite located in the solidification cell boundaries.

-Copper and nickel

Santos et al (1991) demonstrated that Copper addition alone does not provide sufficient hardenability to successfully austemper a casting of 2.5cm diameter, although this could be achieved by combining nickel and copper. As little as 1.5 % Ni in combination with 0.75% Cu were sufficient for the austempering of 2.5cm diameter castings. Tiziani et al (1985), suggested that increasing the nickel and or copper contents improves the hardenability but not sufficiently to avoid pearlite formation at the center of castings. Boutorabi, (1998), investigated the mechanical properties and microstructure of Cu and Ni alloyed ductile iron and stated that the tensile strength and elongation are significantly affected by austempering temperature and time, whilst the change in hardness appeared to be more dependent on the structure produced by austempering temperature. The mechanism of bainitic reaction of austempered ductile iron, including nucleation and growth of ferrite, and decomposition of retained austenite are similar to those found in austempered ductile-Si cast irons. The addition of small quantities of Mn and/or Mo is necessary to fully austemper such castings.

Combined effect of Cu and Mn on the properties and fracture characteristics of ADI (containing 3.8C, 2.7 to 0.55 Mn, 0.8Cu, 0.0065 to 0.052P, 0.07Mg) was studied by Juneja et al. The studies revealed that a high volume fraction of austenite with increased tensile strength (1150MPa) can be obtained by decreasing the austenitizing temperature from 900° to 850°C and austempering from 400°C to 300°C. However, a low ductility of 3 - 4% elongation remained unaffected by the heat treatment conditions. A material of such composition would however contain about 15%

pearlite at the center of a 5.1cm diameter austempered casting but can be fully pearlite at 0.5cm under the surface of 7.6cm diameter casting. Increasing the nickel and/or copper contents improves the hardenability but not sufficiently to avoid pearlite formation at the center of 5.1cm diameter castings. The addition of small quantities of Mn and / or Mo is necessary to fully austemper such castings. According to Viau et al (1987), Major advantages of using nickel and copper in order to minimize the concentrations of Mn and / or Mo are:

1. To avoid the segregation of the latter elements to the cell boundaries; and
2. To shorten the time required completing the austempering reaction.

2.5.2. Austenitizing Temperature and Time.

The austenitization of Ductile Iron castings of suitable chemical composition is the first step of the ADI treatment. The austenitizing temperature controls the carbon content of the austenite, which in turn affects the structure and properties of the austempered castings. Viau et al (1987) has shown that austenitizing at 900°C delays the first stage of the austempering reaction and may result in the formation of martensite if the austempering time is too short. However, austenitizing at higher temperature favours the redistribution of segregated elements and the decomposition of intercellular carbides when present.

The austenitizing time should be the minimum required ensuring that the casting has been completely transformed to carbon-saturated austenite. One hour is usually appropriate at 900°C for a 2.5cm diameter casting. Nevertheless, at lower temperatures, up to 3h are recommended to ensure the reduction of the microsegregation of alloying elements. As for steels, the austenitizing time and temperature have to be adjusted as a function of the section size.

2.5.3. **Austempering Temperature and Time.**

Austempering provides ductile irons with a wide range of mechanical properties. Austempering is an isothermal heat treatment process consisting of austenitising components at approximately 900^0C, followed by rapid quenching from this high temperature into hot oil or molten salt baths or fluidized beds. Austempering of components is carried out at a lower temperature (250 to 450^0C) and held at this temperature for a specified period of time after which the components are cooled. During the holding period, austenite transforms isothermally to bainite. For most treatments the transformation is incomplete, so that varying proportions of martensite and retained austenite are also present after cooling to ambient temperature. The hardenability of the ductile iron casting to be austempered and the severity of the cooling from the austenitizing to the austempering temperatures must be sufficient with regard to the casting section size to avoid the formation of pearlite. The structure and properties of the casting will be determined by austempering at a given temperature for an optimized time. Over the austempering temperature range, (between 250^0 – 450^0C) transformation starts by the nucleation of bainitic ferrite at interphase and grain boundaries. A high austempering temperature produces a strong casting with excellent ductility and dynamic properties while a low one results in a part with a very high strength and wears resistance. The effects of the austempering temperature are related to microstructural changes. A high austempering temperature (360^0C) results in a coarse microstructure with a fairly large amount of austenite. Reducing the austempering temperature to 310^0C favours the formation of a finer microstructure with smaller isolated austenite islets. A lower austempering temperature therefore results in a large undercooling of the austenite and a

slow diffusion rate of carbon. The nucleation of ferrite plates rather than their growth is favoured resulting in a finer structure, (Rao and Putatunda, (1997)).

Once the austempering temperature has been selected to obtain the desired properties, treatment time has to be optimized. Martensite forms in the austempering structure after short austempering times because of either the higher hardnenability of Mn-segregated areas and / or because of the lower carbon content of some austenite regions. The austempering has to be sufficiently long to eliminate the untransformed austenite and consequently the martensite that might form. Although a long austempering time ensures the avoidance of martensite due to the presence of manganese, large unreacted austenite areas may remain and embrittle the castings. An extreme austempering time would cause the decomposition of the stabilized austenite to ferrite and carbides, making the structure brittle. Tiziani et al (1988) confirmed the effect of different content of Nickel, copper and molybdenum on the austemperability, which is typically a bainitic microstructure even in larger sections

2.6 STAGE I AND STAGE II BAINITIC TRANSFORMATION

The kinetics and mechanism of the transformation of austenite to bainite have not been widely studied for austempered ductile irons but, nevertheless, a quantitative understanding has been achieved. Over the austempering temperatures range (250 to 450^{0}C) transformation starts by the nucleation of bainitic ferrite at interface and grain boundaries. The bainitic transformation is an incomplete reaction in which the volume fraction of ferrite and the final carbon content of the remaining austenite depend both on the composition and the treatment conditions, Bhadeshia, (1992). When the Bainitic formation ceases, the austenite can have a carbon content high enough

to be stable on quenching to room temperature. Aranzabal et al, (1997) reported that this structure is not stable, mainly at high temperatures, and on increasing the treatment time, when the austenite can decompose to ferrite and complex carbides. This constitutes the stage II of the transformation. For short treatment times, the volume of bainite being formed is small and as a consequence, the austenite is relatively unstable and transforms at least partially to martensite on quenching. This is the so-called Stage I of the transformation.

Changing the treatment conditions results in different distribution of bainitic ferrite and austenite. High temperatures lead to the formation of relatively low bainite volume fractions and, consequently, large pools of austenite are present in the microstructure. At low temperatures, when the diffusion of the carbon from the bainitic units is difficult and the driving force for the transformation is higher, a finer microstructure is formed with a higher volume fraction of bainitic ferrite. According to Janowak (1983), and Trudel (1997), the austempering heat treatment consists of complete austenitizing of the castings and quenching to the austempering temperature and holding for a given time at the austempering temperature followed by cooling to a room temperature. This temperature is lower than the pearlitic transformation temperature but higher than that for martensite transformation. As a result of high concentration of carbon and silicon in DI, the solid-state transformation of the austenite during austempering differs from those observed in steels, Janowak (1983).

Figure 1. Presents schematically the structural changes occurring during austempering. Individual plates of ferrite, separated from each other by layers of carbon saturated austenite, nucleate at austenite grain boundaries and grow. As the reaction proceeds, the carbon diffusion ahead of the ferritic plates becomes more difficult and the growth of the plate ceases, resulting in

a duplex ferritic-austenitic matrix, called ausferrite. The high carbon content of DI favours the formation of such a structure by slowing down the growth of the ferrite plates and stabilizing the austenite. Because ausferrite is metastable at low temperature, it will eventually transform to ferrite and very fine globular cementite. This transformation is however delayed by the high silicon content of the alloy, which retards carbide formation. Therefore, the austempering reaction can be considered as a two-stage solid state transformation of austenite,

i) $\gamma = \alpha + \gamma_{HC}$

ii) $\gamma_{HC} = \alpha + Fe_3C$

where γ is the primary austenite and γ_{HC}, the carbon enriched austenite,

(N.B. an ausferrite structure is a ferrite plate in carbon enriched austenite, Janowak, 1983).

At isothermal temperatures below about 330^0C, growth rates of the ferritic needles are high and as the rate of carbon diffusion is relatively low, this results in high carbon contents in the bainitic ferrite, which can initially, have a distorted tetragonal crystal structure. At an early stage of the austempering treatment, this carbon is rejected from the ferrite and precipitates as ε-carbide ($Fe_{2.4}C$) in the ferrite needles, and this is often referred to as 'bainitic carbide'. As little carbon is rejected from the bainitic ferrite into the residual austenite, transformation can proceed continuously so that, after austempering treatments of 0.5 to 3 hours, only small quantities of retained austenite are present after cooling to ambient temperature. This structure is referred to as 'lower bainite'. Figure 2(a). At higher treatment temperatures (above about 330^0C) a different transformation mechanism operates, resulting in the formation of upper bainite, Figure 2(b). Carbon diffusion is more rapid so most of the carbon is able to diffuse out of the growing bainitic ferrite plates, enriching the residual austenite, particularly between the growing ferrite plates. If

the austempering process is halted at an early stage, the martensite start (M_s) temperature will still be above ambient temperature and the residual austenite will transform at least partially to martensite during cooling. As the isothermal treatment is prolonged, the carbon content of the residual austenite will increase and eventually reaches a level (approximately 1.5 to 1.7%C) where the bainitic transformation is inhibited. Furthermore, the high carbon content depresses the M_s temperature, resulting in austenite being retained after cooling to ambient temperature. This retained austenite can be stable down to at least -120^0C. According to Wen and Lei, (1999), the corresponding temperature (^{0}C) of the beginning of martensite transformation M_s can be estimated using the following equation:

$$M_s = 400 - 200(C_\gamma). \quad \ldots\ldots\ldots(3); \quad \text{where } C_\gamma = \text{carbon content of the residual austenite.}$$

In studying the mechanical properties of a low alloyed austempered ductile iron in upper ausferrite region, Wen and Lei observed that the structure of upper bainite in ductile irons after austempering treatments of 0.5 to 3 hours consists of relatively coarse ferrite and retained austenite; this latter phase can account for up to 40% of the matrix structure. The presence of large quantities of retained austenite is believed to be responsible for the high levels of ductility and toughness obtainable in upper-bainitic ductile irons.

When the transformation time is prolonged beyond about 4 hours, iron carbide (Fe_3C) is precipitated from the residual austenite. As the austenite carbon content is thus lowered, further transformation to bainitic ferrite occurs. The final microstructure after cooling to room temperature will be ferrite plates, carbide and small amounts of retained austenite. Such prolonged transformation time can lead to embrittlement, but it is not clear whether this is due to the presence of carbides between the ferrite plates or to the low level of retained austenite.

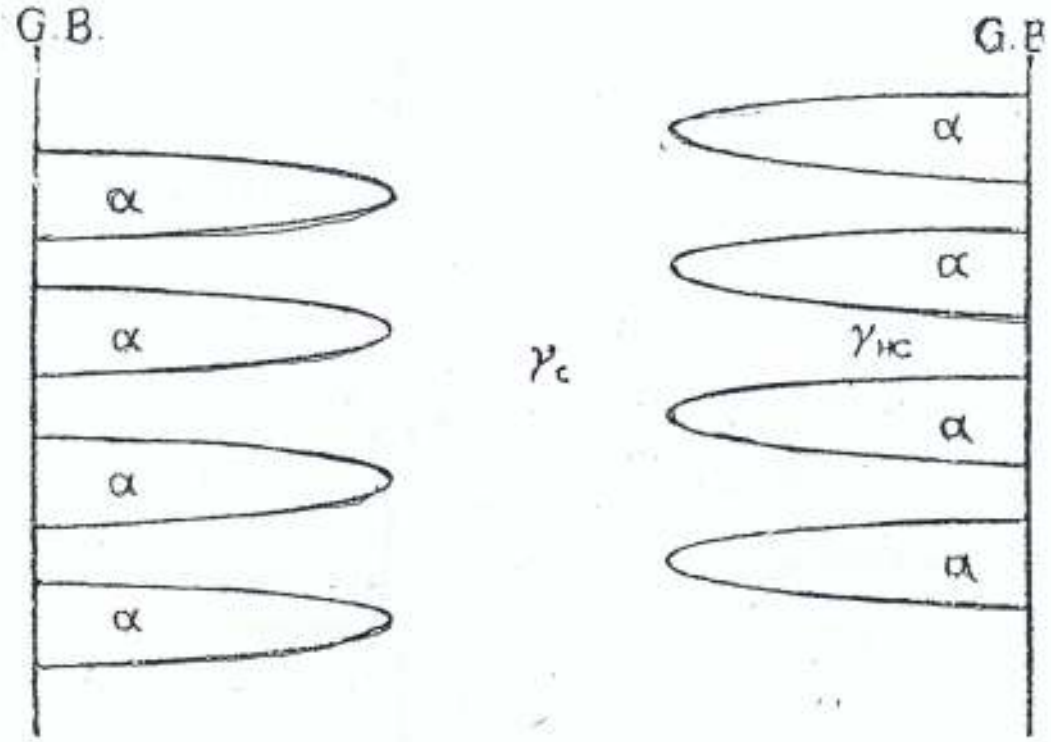

Figure 1. Schematic illustration of the solid state transformation of austenite during austempering. Plates of ferrite are separated from each other by layers of carbon saturated austenite.

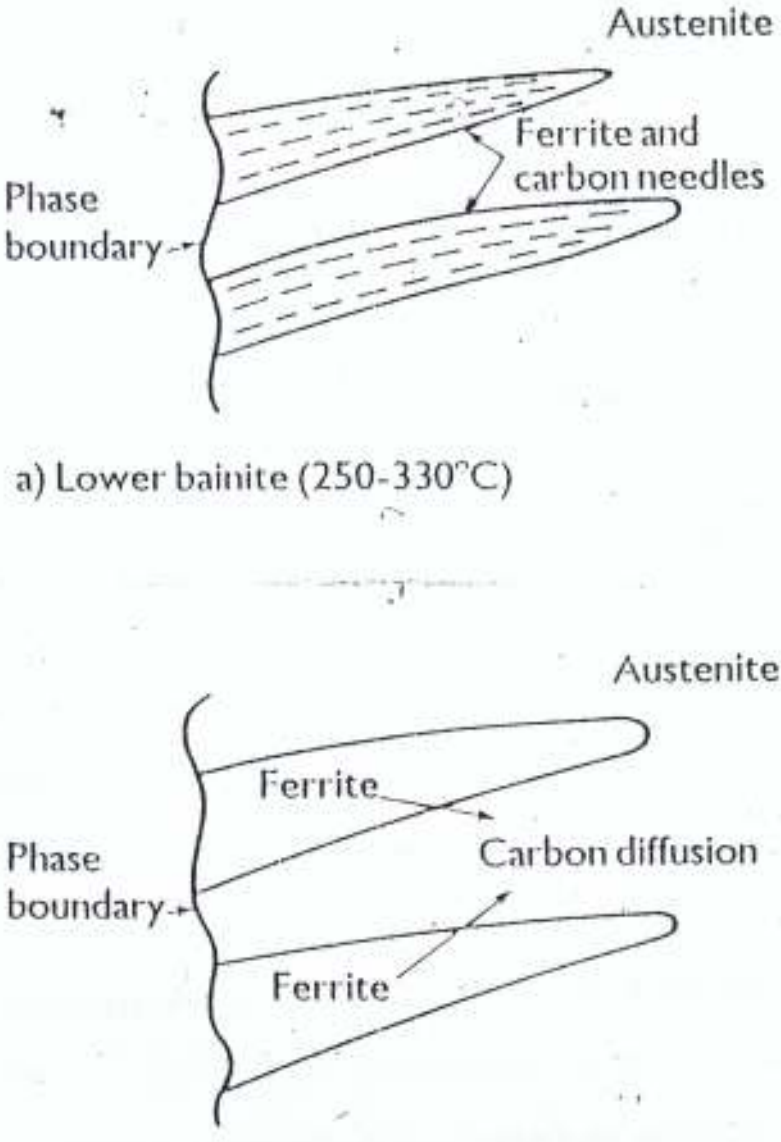

Figure 2. Mechanism of formation of lower and upper bainite.

The effects of isothermal holding time on the proportions of retained austenite after treatments at various temperatures was already studied by Dorazil, (1976). Also the influence of temperature and time of austempering on a nodular cast iron austenitised for 30 min at 900^0C was investigated by Aranzabal et al, (1994).

It has been previously reported, Aranzabal et al, (1997), that the plastic stability of retained austenite is determined by the surrounding copditions and the size of retained austenite rather than by the stability of the retained austenite itself. The evolution of the bainite formation during austempering treatment may be represented by the scheme in Figure 3. Bainite forms around the graphite nodules. If the transformation is interrupted in the early stages, the remaining austenite transforms to martensite on cooling, but if the treatment time is long enough, the bainite transformation affected regions (ferrite + austenite films between subunits + small Austenite regions between sheaves) can be represented by spheres centered at nodules. At low temperatures, the volume fraction of bainitic ferrite is high and the spheres impinge each other. In this case, an addition to the austenite films between ferrite subunits, only relatively small austenite pools between bainite sheaves can be found.

At high temperatures, the austenite morphology changes. The volume fraction of ferritic bainite is lower and the bainite reaction is interrupted, leaving large unaffected austenite regions, Aranzabal et al, 1997.

The bainitic transformation is an incomplete reaction in which the volume fraction of ferrite and the final carbon content of the remaining austenite depend both on the composition and the treatment conditions, Bhadeshia, (1992). When the bainitic formation ceases, the austenite can have a carbon content high enough to be stable on quenching to room temperature. However this

structure, as reported by Aranzabal, et al (1997), is not stable, mainly at high temperatures, or on increasing the treatment time, when the austenite can decompose to ferrite and complex carbides. This constitutes the stage II of the transformation. For short treatment times, the volume fraction of bainitic ferrite being formed is small and as a consequence, the austenite is relatively unstable and transforms, at least partially to martensite on quenching. This is the so-called stage I of the transformation.

Changing the treatment conditions results in different distributions of bainitic ferrite and austenite. High temperatures lead to the formation of relatively low bainitic volume fractions and in consequence, large pools of austenite are present in the microstructure. At low temperatures, when diffusion of the carbon from the bainitic units is difficult and the driving force for the transformation is higher, a finer microstructure is formed with a higher volume fraction of bainitic ferrite.

2.7. FACTORS AFFECTING FATIGUE STRENGTH AND ADI COMMERCIAL EXPLOITATION

The opportunity for wide commercial exploitation of ADI materials has arisen in response to pressures on engineering and automobile industries to produce components that provide improved properties and performance, or reductions in overall manufacturing costs. It is important that a much wider range of mechanical properties is determined and in particular there is an acute need for high-quality fatigue and fracture - toughness data. As an example, gear design uses bending and contact fatigue strength criteria. Many components in service are subjected to high frequency cyclic or fluctuating stresses. When this happens, the components fail in a brittle fashion at stresses which are very much less than the maximum strength of the

material under static loading conditions. Fatigue damage increases with applied load cycles in a cumulative manner, which may lead to fracture. Cumulative fatigue damage analysis plays a key role in life prediction of components and structures subjected to field load histories. To avoid sudden failure in operation, it is essential to consider the crack resistance of a material. The processes of gradual accumulation of defects in a material under the action of cyclic loads, resulting in changes of the properties of the material, nucleation and propagation of cracks, and final failure is called fatigue. In other words, failure of metals under alternating stress and the ability to resist these processes is referred to as fatigue strength or endurance. According to Gur and Hren, (1974), factors affecting fatigue strength include the surface conditions, range of stress, complex stresses (in ductile materials the significant stress is determined by the combination of all the principal stresses that act on the specimen), section size and temperature frequency. Figure 4 illustrates types of stresses that can cause breakage or spalling. Since fatigue failures originate at the surface of metallic specimens, strengthening the surface generally improves the fatigue life. Most fatigue failures in actual engineering structures are the result of macroscopic stress raisers, which were unintentionally incorporated in the object that failed.

2.8 INFLUENCE OF AUSTEMPERING PARAMETERS ON THE MECHANICAL PROPERTIES.

2.8.1 Tensile Properties Of The Duplex (Ferrite + Austenite) Microstructures.

Aranzabal et al (1997) presented work concerned mainly with a more detailed study of the tensile properties of the duplex ($\alpha + \gamma$) microstructures with a special emphasis on the transformation-induced plasticity (TRIP) effects. It was observed that short treatment times

produce the partial formation of bainite, and high volume fractions of martensite are found for all the temperatures. They observed that intermediate treatment times lead to the microstructures of a duplex ferrite / austenite structure, and also that the differences in austenite distribution and stability are dependent on austempering temperatures. High-temperature treatment leads to the decomposition of austenite into ferrite and carbides. The decomposition sequence was also reported to occur in more than one step. The homogenous precipitation of quasi-coherent epsilon carbides in austenite for relatively short times (120 minutes, 410^{0}C) seems to be the precursor for the formation of complex carbides that leads to the overall decomposition of the austenite.

Results by Aranzabal et al (1997) in studying the influence of heat treatment parameters on the mechanical properties show that the proof stress and the UTS increase with decreasing transformation temperature for austempered ductile iron and in general for bainitic steels. Strength in steels depends on grain size. However in ADI, austenitise under the same conditions, the initial austenite grain size remains constant. Schryvers et al (as reported by Aranzabal) observed that structural refinement is believed to be the main factor controlling the strength and from microstructure observations it was apparent that there is an important structural refinement of bainitic structure. As the treatment temperature decreases from 370^{0}C or 410^{0}C to 300^{0}C, the lathe size is reduced from 0.3 to 0.1μm, respectively. However the carbon content of both the austenite and the ferrite and the austenite volume fraction play important role on strength. The carbon content contributes to the solid solution strengthening and the austenite distribution, and stability can affect the strength in different ways. Also Kobayashi and Yamada (1996), studied the effect of holding time in the (α+γ) temperature range on toughness of specialty austempered

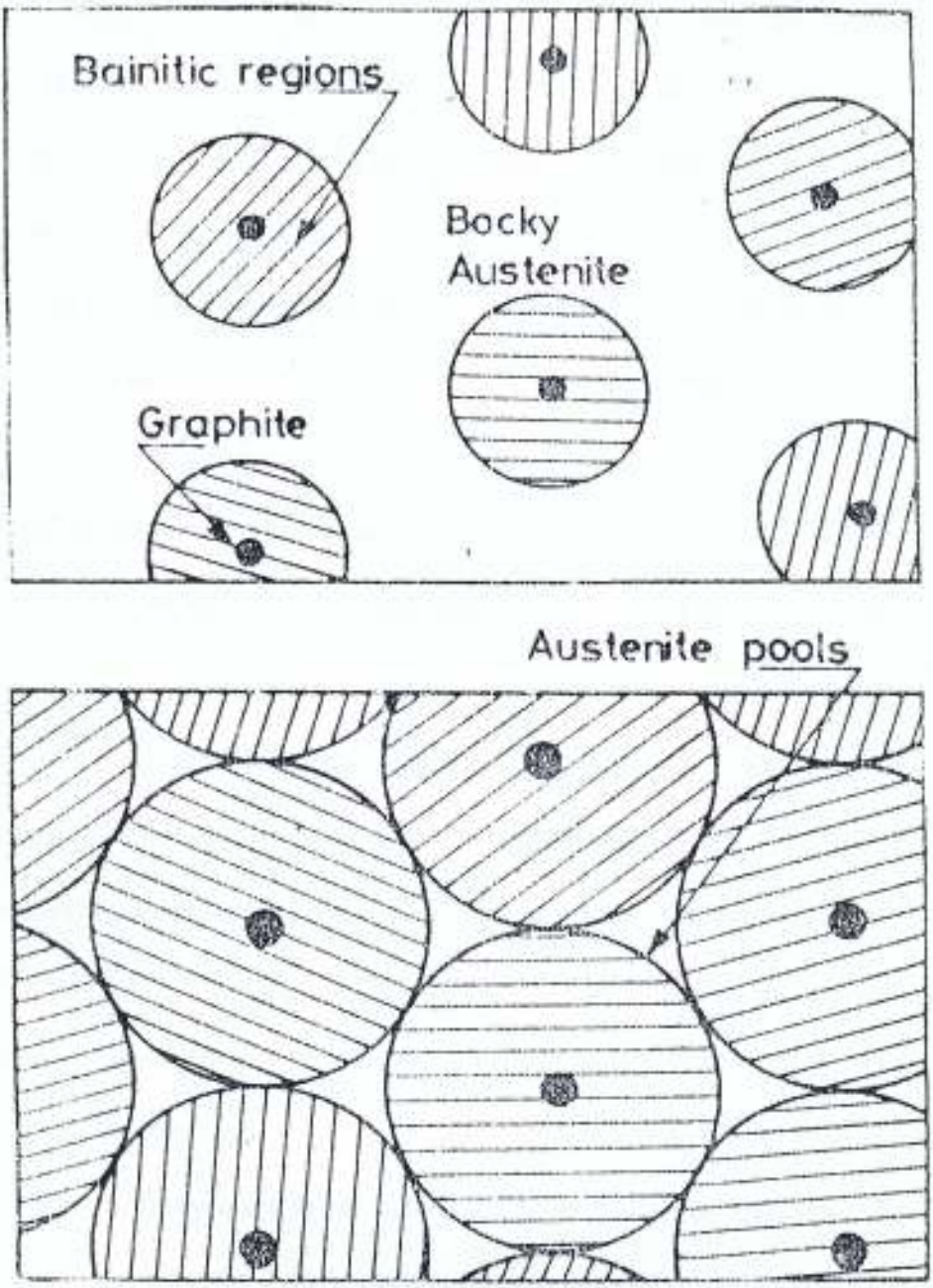

Figure 3. Scheme representing, in a simplified form, the evolution of the bainite formation, mainly nucleated around the graphite nodules. The hatched region around graphite nodules corresponds to the bainitic structure formed by ferritic bainite, austenite films between sub units and small austenite pools between sheaves oriented in different directions.

ductile iron. They concluded that the increase in toughness with the holding time was caused mainly by the increase in ductility due to the decomposition of carbide. In their work on comparative study of fracture toughness of austempered ductile irons with upper and lower ausferrite microstructures, Putatunda and Rao (1998) confirmed that the acicular ferritic structure resulting from the low austempering temperature leads to higher strength. For all heat treatment conditions, tensile toughness was estimated using the relationship:

$$\text{Tensile toughness} = (\sigma_y + \sigma_u)\varepsilon_f/2 \quad \ldots\ldots\ldots(4)$$

where σ_y and σ_u are the yield strength and ultimate tensile strength respectively, while ε_f is the fracture strain. The strain-hardening coefficient was estimated using the Hollomon relationship

$$\sigma = k\varepsilon^{n'} \quad \ldots\ldots\ldots\ldots(5)$$

where σ is the true stress, ε is the strain, n is the strain hardening coefficient and k is the constant of proportionality. Higher austenite content and higher carbon content of the retained austenite at the higher austempering temperature result in higher strain hardening capability.

Rao, (1995), studied the influence of heat treatment parameters on the microstructure and tensile behaviour of an austempered ductile iron containing 1.4 wt% Ni and 0.6 wt% Mo. It was discovered that there was an extensive carbide precipitation at higher austempering temperatures leading to loss of strength (at lower austenitising temperatures and time), as well as ductility. The formation of martensite during austempering reduced the mechanical properties of ADI but these properties could be increased by a tempering treatment at 200^0C after cooling to obtain more ductility and toughness as compared with that undergoing single heat treatment.

Putatunda et al, (1999), examined the influence of austenitising temperature on the resultant microstructure and mechanical properties of an unalloyed and low manganese ADI and with an

as cast (solidified) ferritic structure and also the influence of austenitizing temperature on the fracture toughness. Compact and round cylindrical tensile specimens were prepared from a nodular cast iron without any alloying elements (e.g. nickel, molybdenum or copper) and with very low manganese content and with an as cast (solidified) ferritic structure austenitized at several temperatures ranging from 871^{0}C to 982^{0}C and then austempered at a constant austempering temperature of 302^{0}C for a fixed time period of 2 hours. Both volume fractions of austenite and its carbon content increased with austenitizing temperature.

2.8.2. The Role of Austenite in Promoting Ductility

The role of austenite in promoting ductility in an austempered ductile iron was investigated by Bayati and Elliot, (1997), after single and stepped austempering treatments following austenitizing at 920^{0}C. The kinetics and tensile data were analysed to show how the thermal and mechanical stability of the austenite phase varies with austempering treatment. Both the thermal and mechanical instability of the austenite phase limit the activity achieved in single austempering treatments at 375 and 400^{0}C to such an extent that the impact energy fails to satisfy the ASTM standard. Stepped austempering treatment improves both the thermal and mechanical stability of the austenite phase and increases the impact energy to such an extent that the ASTM standard is satisfied over a wide range of austempering conditions. A well-defined relationship is shown to exist between impact energy and the austenite carbon content for different austempering treatments after austenitizing at 920^{0}C.

2.8.3. Austempered Ductile Iron and Automotive Technology

The use of Austempered Ductile Iron (ADI) in machine parts for the automotive industry is becoming increasingly important. The advantages of using these alloys are clear:

a) Near form cast products, with the attending reduction in machining costs.

b) 10% lower density than forged steels with comparable strengths.

c) Lower prices, etc.

Most of the production is used satisfactorily in elements subjected to dynamic and cyclic loads, fatigue and also rolling contact fatigue.

Automobiles are subjected to a full range of loads including shear and bending (due to the vehicle mass and loads being distributed), torsion (caused by irregular road, putting a wheel on a curb), lateral loading (caused by cornering), and fore and aft loading (caused by acceleration and deceleration). In practice these occur in combination together with dynamic / transient effects. Typically an automobile structure will be designed so that under the worst envisaged dynamic load condition there will still be a factor of safety based on the yield strength of 1.5, (Happian - Smith, 2001). This is usually adequate for guarding against fatigue failure, but fatigue calculations are still used where stress concentration effects are likely to be significant. In practice, vehicle design is normally governed by stiffness requirements rather than maximum permitted stress levels.

2.8.4 Cast Iron for Crankshafts.

Crankshafts suffer cyclic loading so the fatigue endurance strength of the material is critical to their performance. For cast irons, a key factor determining the fatigue performance is the

distribution of the graphite in the structure. In grey or flake irons, the graphite is distributed as long thin flakes, many of which are exposed on machine surfaces, thus providing in-built surface defects from which fatigue cracks can grow. Hence the fatigue endurance strength of such irons is quite low, (Smith, (2001).

Fatigue testing of ferrous materials indicates a stress level below, which no failure occurs, however many the load cycles applied. This is called the fatigue endurance strength or endurance limit. Normally the number of cycles to reach this limit is between 10^6 and 10^7 and if a test piece lasts this long it is assumed that it will last indefinitely. However some failures of cast iron have occurred after more than 10^7 load cycles. Consequently, fatigue testing carried out by BCIRA is done on the basis of 2×10^7 cycles, (Smith, (2001).

The ratio of fatigue endurance strength / UTS for cast iron in reversed bending is between 0.33 and 0.47, (Smith, (2001). Alloying additions and heat treatment, which raise the UTS, will normally not improve this ratio but fillet rolling / surface rolling improves the fatigue performance.

For many applications nodular irons are superior to other types of iron and can be processed to have mechanical properties similar to those of low and medium carbon steels (UTS: 370 - 800 MPa; 0.2% proof stress: 230-460 MPa, (Smith, 2001). This has resulted in considerable increase in the production and use of nodular irons for items such as crank-shafts for car engines where reasonable strength combined with the capability for economically large production is somewhat more important than obtaining the maximum possible strength.

The mechanical properties of grey cast iron depend on the properties of the metallic matrix and more substantially, on the concentration, shape and size of graphite inclusions.

Elliot, (1997), Waaders et al, (1998), and Guo et al, (1998) confirmed that the mechanical properties of austempered ductile iron are related to three microstructural variables: the bainite morphology, the proportion of retained austenite and the formation of martensite. The strength, hardness and wear resistance of cast irons increase with increasing concentration of pearlite in the matrix, which in its structure is similar to steels, Owhadi et al, (1998). The decisive effect of graphite is due to the fact that graphite lamellae, whose strength is very low, transverse the metallic matrix and act as notches or cracks. In tension (which is the most rigorous kind of stressing), fractured nuclei form easily at the ends of graphite lamellae. For that reason, grey cast iron works poorly in tension and has low values of strength and ductility. The relative elongation in tension does not exceed 0.5% irrespective of structure of matrix. The rupture strength of grey cast irons is lower when graphite inclusions are larger and have more elongated shape. On the contrary, finer and less concentrated graphite inclusions produce a less adverse effect. Spheroidal graphite is a less severe stress concentrator than lamellar graphite and therefore does not worsen so substantially the mechanical properties of the metallic matrix.

2.8.5. High Strength Cast Irons

Cast irons with spheroidal graphite possess a high strength and a certain degree of ductility. High strength cast irons are graded according to their ultimate strength and relative elongation. High strength cast irons have found wide use in parts of machinery and agricultural machines crankshafts, gears, etc. It has been demonstrated that spheroidal high strength cast iron can be used successfully and with economic benefit as a substitute for steel (forged or cast) in some kinds of machine parts. The lack of documentation available and the difficult operating

conditions which gears usually undergo have not encouraged the spread of their production in ductile iron.

Trippodo et al (1988) worked on the evaluation of mechanical behaviour of austempered nodular iron for possible use in gears. They suggested the possibility of replacing gears in nitriding steels with austempered ductile iron (ADI), since both exhibit equal fatigue strength and ADI exhibits better toughness. Also, Juneja et al. (1989) has reported the combined effect of copper and manganese on the properties and fracture characteristics of austempered ductile iron. By decreasing the temperature of austenitizing from 900 to 850^{0}C, a high volume fraction of austenite with increased tensile strength (1150 Mpa) was obtained. However, a low ductility of 3-4% elongation remained unaffected by the heat-treatment conditions.

Prasad (1988), compared the mechanical properties of hot forged SG iron requirement for the production of austempered ductile irons having optimum combinations of properties, and concluded that pearlite formation should be avoided during quenching. Experimental work on cylindrical test bars with unalloyed irons, showed that the maximum diameter that transformed without pearlite formation increased from 15mm at a temperature of 450^{0}C to 30mm at a temperature of 250^{0}C. This is due to a higher quenching rate at a lower temperature. As the bar diameters were increased beyond these values, pearlite initially formed at the center of sections as small colonies associated with graphite nodules, and fully pearlitic matrices were obtained in 30mm diameter bars austempered at 250^{0}C. The presence of pearlite will generally be detrimental to the mechanical properties, although its effect has not yet been fully quantified. When a high enough quenching rate cannot be achieved to prevent pearlite formation in heavier section sizes, alloying additions must be made to the iron to delay the start and finish of the

decomposition of austenite to pearlite and bainite. Molybdenum, nickel and copper increase the section size, which can be austempered without the formation of pearlite. An addition of 0.3% molybdenum approximately doubles the bar diameter, which can be satisfactorily austempered. The maximun section sizes can be further increased by larger molybdenum additions although, when such additions exceed approximately 0,5%, significant segregation occurs at the cell boundaries and results in stable carbide formation, which has an embrittling effect.

2.8.6. Austempered Ductile Iron and Wear Resistance Properties

A detailed review of wear resistance properties carried out by Lerner and Kingsbury, (1998) was undertaken to examine the potential application of ADI for wear parts, as an alternative to steels, alloyed cast irons and white cast irons, bronzes, and other competitive materials. Two modes of wear were studied: adhesive (frictional) dry sliding and abrasive wears. In the rotating dry sliding tests, wear behaviour of the base material (a stationary block) was considered in relationship to counter surface (steel shaft) wear. In this wear mode, the wear rate of the material was only one fifth that of pearlitic ductile iron grade 100-70-03; the wear rates of aluminium bronze and lead-tin bronze, respectively, were 3.7 and 3.3 times greater than that of ADI. Only the quenched DI with a fully martensitic matrix slightly outperformed ADI. No significant difference was observed in the wear of steel shafts running against ADI and quenched DI. The excellent wear performance of ADI and its counter surface, combined with their relatively low friction coefficient, indicate potential for dry sliding wear applications.

Previous research on the characterization of the mechanical properties of ADI over a range (220 - 360^{0}C) of austempering temperatures, Dommarco et al 2001, have shown that wear resistance increases for material treated at lower austempering temperatures. Other mechanical properties evaluated (UTS, elongation, hardness and toughness) and wear change with the austempering time according to the degree of transformation. This makes it beneficial to carry out a specific analysis for each application in order to find out the optimum combination of properties for the intended use. Field tests on soil plowing tools by Capurro et al, 1996, revealed that the wear resistance of ADI increased as austempering temperature decreased, although it never exceed the wear performance of hard faced steel tools. However, ADI was clearly superior in rocky conditions where failure by fracture often occurred. Recent field-tests by Farina et al, 1998, illustrated that ADI was superior to steel when used for chisel tips. Seetharamu et al, 1993, reported that the abrasive wear resistance (ASTM G65-91) and hardness of permanent molded ADI castings can be increased by raising the austenite level through a reduction in silicon content. Also an optimum hardness / microstructural condition that provides the highest wear resistance can be achieved at intermediate austempering temperatures.

Studies have been conducted previously, with a single pass grooving pendulum, to evaluate the potential use of ductile iron in earth moving equipment parts, Velez and Tschiptschin, 1995. The results show that at constant austempering temperature, the wear resistance increased for the austempering time, which produced the highest austenite content. For different austempering temperatures wear resistance increased with hardness, while austenite levels decreased. It was also reported, (Zhou et al, 1993; Haseeb et al, 2000), that the wear behavior of ADI is closely related to the retained austenite content, which behaved differently under different wear

conditions. In analyzing factors affecting ductile-brittleness transition of ferrite in spheroidal graphite cast iron, Vavatuk (1988) studied the influence of graphite nodule number on the fracture behaviour by means of Charpy V-notch impact tests and scanning electron microscopy. Specimens either in annealed or in quenched and tempered conditions were tested at temperature from 25 to -196^{0}C. Annealed Fe with higher nodule count presented low Charpy value at room temperature and lower transition temperature.

The wear behaviour of 1.5Mn ADI studied by Owhadi et al, (1998), revealed that impact resistance is affected adversely by untransformed austenite volume but this parameter improves the wear resistance of high Mn ADI.

2.9 LOW CYCLE FATIGUE OF ADI

As the application of ADI as engineering components involve using castings of various geometry and section sizes subjected to long-term mechanical variable loads, it is important to understand the fatigue behaviour of ADI in different section sizes. As reported in literature, mechanical properties of ductile iron usually deteriorate as the cast section size increases. Similar tendency was also observed in ADIs. Such degradation of mechanical properties in heavy section castings was mostly attributed to the increasing effects of nodule morphology, segregation of alloy elements, and other casting defects associated with the last to freeze volumes, Lin and Fu, (1997). The microstructural characteristics of ADIs with different austempering treatment and their effect on mechanical properties have been the topics of many previous studies, yet research of their effect on fatigue properties is not quite much. Lin and Fu (1997) reported that the influence of ausferritic structure on High Cycle Fatigue (HCF) and Low Cycle Fatigue behaviour

of ADI were different. ADI with larger volume fraction of retained austenite showed better HCF resistance but poorer LCF performance. This was related to the stability of retained austenite and the associated fatigue loading modes during fatigue test. In this regard, it might not be appropriate to use the HCF strength data of ADI as reference to select proper austempering conditions for ADI components subjected to strain-control loading. Therefore, in other to better predict the fatigue life of ADI components in service, a more complete data on the fatigue properties of ADI is required.

Many service fatigue failures of castings originate at a geometric stress concentration that is part of the casting design. The local high stress area is undergoing strain-controlled deformation. Therefore, strain-control approach of LCF in the finite life range has been usually applied to evaluate stress concentration effect on the fatigue behavior of structures, Bannatine et al, (1990).

The effect of Si, Al and Bi on the microstructure and mechanical properties of as-welded and austempered ductile iron weld metals was studied with SEM, TEM, X-ray diffraction, image analysing system tensile and other test methods, Sun et al, (1996). Results show that increasing weld with Si, Al and Bi content favours improving the chilling tendency of as-welded ductile iron weld and mechanical properties of austempered ductile iron weld. On this basis the optimal chemical composition of weld is determined.

2.10. INFLUENCE OF FOUNDRY DEFECTS ON CRACK FORMATION.

The position of major wears in iron castings can also be attributed to concentration of matrix defects. Typical foundry defects are usually found inside the contour cracks of spall locations. The presence of foundry defects (practically inevitable) may be of extreme importance regarding

surface failure. Affected sports near the surface are preferential crack-initiation sites, Figure 7. Magalhaes et al (2000) while studying the influence of graphite nodules on crack propagation observed that most nodules are totally spherical, but some elongated forms could also be found. Although graphite nodules tend to act as crack-arrest systems when cracks are relatively small, many situations could be found where:

. cracks propagate without deviation having nodules very near the surface;

. cracks can pass through nodules as if they are not there;

. cracks arrive to a nodule and then multiply, originating several microcracks that propagate in different directions;

. cracks enter nodules in a direction and exit in a different direction;

.secondary small cracks tend to be attracted to graphite nodules and many times stop their propagation when they get there.

Magalhaes et al, (2000), concluded that the presence of graphite nodules under the surface of ductile cast irons may be the cause for the growth of typical fatigue cracks, resulting in characteristic surface damage. Nodules acts as local stress raisers and are preferentially sports for crack initiation when operating conditions are severe enough. This is assumed to be the commonest contact long-term failure. According to Magalhaea et al (2000), conditions for crack propagation modes depend, among other things on factors such as graphite nodule size, matrix constitution, contact pressure, sliding rate, surface roughness, and of course the depth at which nodules are. Depending mainly on the depth at which nodules lay under the surface and on local stress field condition, at least two other different forms of crack evolution can be found. Figure 4 schematizes both situations.

A. Nodules close to the surface:

The thin layer above a nodule is broken.

Edges are broken and graphite expelled.

Permanent wear smoothes hole edges. Empty cavities are a less significant fatigue crack source.

B. Nodules at some critical depth (≈10 to 50 um):

Cracks grow between a nodule and the surface.

A cover particle is detached and radial cracks start to grow from the graphite nodule cavity.

Cracks propagate towards the surface (left) or along the Hertzian stressed sub-surface (right) mainly due to the strong edge effect.

Figure 4. Typical evolutions of cracks around graphite nodules near the surface of an ADI.

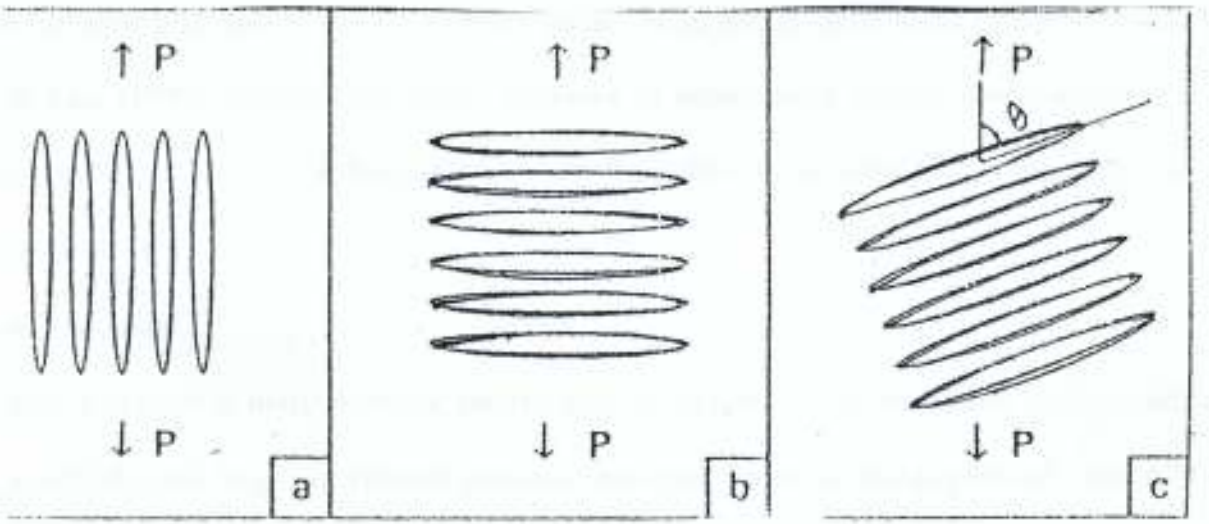

Figure 5. Schematic simplified diagram showing the possible orientation relationships between bainitic ferrite laths and the applied load direction.

2.11. FRACTURE TOUGHNESS OF AUSTEMPERED DUCTILE IRON

The influence of casting size and graphite nodule refinement on fracture toughness of austempered ductile iron was investigated by Lee et al, (1998). They observed that casting size affects the solidification cooling rate and microstructure of casting materials. Graphite nodules existing in the structure of ductile iron are inherent and inert second phase that cannot be modified in subsequent heat treatment processing. The matrix and the fineness of the second phase undoubtedly have some impact on the fracture toughness of the as-cast material, as does the subsequent heat treatment, as it alters the microstructure. This research applied austempering heat treatment to ductile iron of different section sizes and graphite nodule fineness. Putatunda and Rao, (1998) estimated the defect tolerance of austempered ductile iron materials. For an infinite plate containing a sharp crack of length 2a, the critical value of fracture toughness K_{IC} was given as:

$$K_{IC} = \sigma Y(\pi a_C)^{1/2} \qquad \text{.....(6)}$$

where Y is equal to unity. Nominal applied stress σ depends on the appropriate design code, a_C is the critical crack length at different austempering times. From the design point of view, ADI can easily be used for structural applications.

The properties of Austempered ductile iron as a gear material was extensively studied by Trippodo et al, (1988) and Magalhaes and Seabra, 1998). There is now the possibility of replacing gears in nitriding steels with austempered ductile iron (ADI), thanks to both the equal fatigue strength and the better toughness shown by the cast iron.

It has been reported that the yield strength depends on the finess of the ferrite blades, Putatunda and Rao, (1998) showed that the yield strength of ADI could be expressed as

$$\sigma_y = \sigma_o + Ad^{1/2} + BX_\gamma \quad \text{.....(7)}$$

where d is the ferrite particles size, X_γ is the volume fraction of austenite and σ_o, A, and B are constants.

2.12. INFLUENCE OF AUSTENITE AND BAINITIC FERRITE ON MECHANICAL PROPERTIES.

Aranzabal et al, 1997 carried out a study to estimate the influence of austenite and bainitic ferrite on the mechanical properties of ADI. They calculated the proof stress of bainitic ferrite through a relationship that takes into account different components:

$$\sigma_{\alpha\,0.2\%}(\text{Mpa}) = \sigma_o + 1722\,(\%C)^{1/2} + 115\,d^{-1} + 7.34 \times 10^{-1}\rho \quad \text{.....(8)}$$

The first term represents the intrinsic contribution of the pure iron in a fully annealed condition. The second term takes into account the strengthening due to the carbon dissolved in interstitial solution, %C, which is assumed to be 0.03% in bainitic ferrite. The contribution of these two terms can be calculated taking account of the material composition. The third term corresponds to the lath size effect and d is the width expressed in μm ($d_{300\,C} = 0.1\mu m$ and $d_{370\,C} = d_{410\,C} = 0.3\mu m$).

The effect of the dislocation density, ρ, generated by the transformation is expressed as

$$\log(\rho) = 9.2840 + 6880.73/T - 1780360/T^2 \quad \text{.....(9)}$$

where T is the transformation temperature in Kelvin and ρ is in m^{-2} (T varies from 570 to 920K.

Aranzabal et al further reported that the austenite proof stress can be calculated in the same way by using the relationship proposed by Pickering that includes the effect of carbon, of substitutional solutes, as well as the grain size contributions:

$$\sigma_{\gamma 0.2\%}(\text{Mpa}) = 15.4[4.4 + 23(C) + 1.3(Si) + 0.9(Mo) + 0.46D^{1/2}], \quad \text{.....(10)}$$

where C is the austenite carbon content in solution, in weight percent, and D is the austenite grain size. The silicon contribution predicted by this equation is close to 50Mpa. The original austenite grain size is estimated to be close to 30μm, this gives a contribution of about 40Mpa to the proof stress.

2.13. DEFORMATION PROCESS AND FAILURE MODES OF ADI COMPONENTS

The deformation process under uniform strain of steel having a mixed structure is generally considered to happen in three stages:

a) The preferential deformation of the ductile phase (austenite);

b) The development of a geometrical dislocation array at the interface between the two phases; and

c) The associated deformation of the two phases.

If the (c) stage were assumed to control the entire deformation process, the strength would follow the law of mixtures. The law of mixtures assumes that the proof stress should vary as a function of the austenite volume fraction, f_γ as

$$\sigma_{0.2\%} = f_{\gamma\,0.2\%} + (1-f_\gamma)\sigma_{\alpha\,0.2\%} \qquad \text{.....(11)}$$

The modified law of mixtures with an exponent 1/3 affects the volume of the softer phase, which has been applied to ferrite plus pearlite:

$$\sigma_{0.2\%} = f_\gamma^{1/3}\,\sigma_{\gamma\,0.2\%} + (1-f_\gamma^{1/3})\sigma_{\alpha\,0.2\%} \qquad \text{.....(12)}$$

It is clear that the austenite controls the proof stress in those cases where this phase is distributed in the microstructure in a continuous blocky way in addition to inter lath films. When the ductile iron is austempered at a temperature in the range of the lower bainite, the structure is more finely distributed and the proof stress appears not to be controlled only by the austenite.

According to Fan and Smallman (1994), the matrix of ADI is a rather complex mixture of bainite ferrite and austenite. Austenite is the basic phase, and on austempering, the austenite transforms into bainitic ferrite and associated high carbon stabilized austenite.

Several bainitic ferrite laths of platelets may have the same orientation, forming a cluster of bainitic ferrite laths or platelets. Commercial ADI is polycrystalline and consists of aggregates of such clusters. Each of them has a particular orientation. If an external load is applied the orientation relationship between the bainitic ferrite laths and the applied load direction can be classified into three types:

1. The longitudinal direction of a cluster of bainitic ferrite laths is parallel to the loading direction, Figure 5(a).
2. The longitudinal direction of a cluster of bainitic ferrite laths is normal to the loading direction, Figure 5(b)
3. The longitudinal direction of a cluster of bainitic ferrite laths makes an angle θ with P, Fig5c.

Most clusters of bainitic ferrite laths belong to the category of Fig. 5c but with different angles.

Fan and Smallman, (1967) further observed that precipitated carbides in the matrix of ADI influence the fracture characteristics of ADI. In order to analyse the situation we can assume that there are two clusters of bainitic ferrite laths between two graphite nodules, one nearly parallel to the applied load direction, the other nearly perpendicular to the applied load direction. The effects of carbides on the crack propagation path and the fracture mode of ADI can be classified into three models, (Figure 6). Model 1 - without carbide in matrix; Model 2 - with carbide in bainitic ferrite laths or platelets; Model 3 - also with carbides at the austenite / ferrite interfaces.

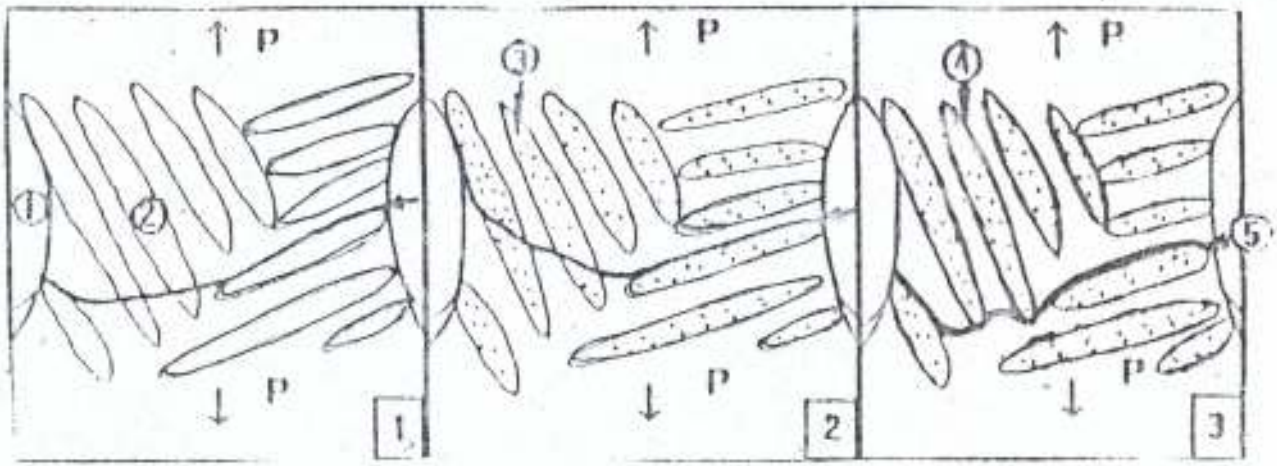

Figure 6. Models of crack propagation

1. Microvoids at graphite matrix interfaces
2. Bainite ferrite laths
3. Carbides in bainitic / ferrite laths
4. Carbides at austenite / ferrite interfaces
5. Possible crack paths.

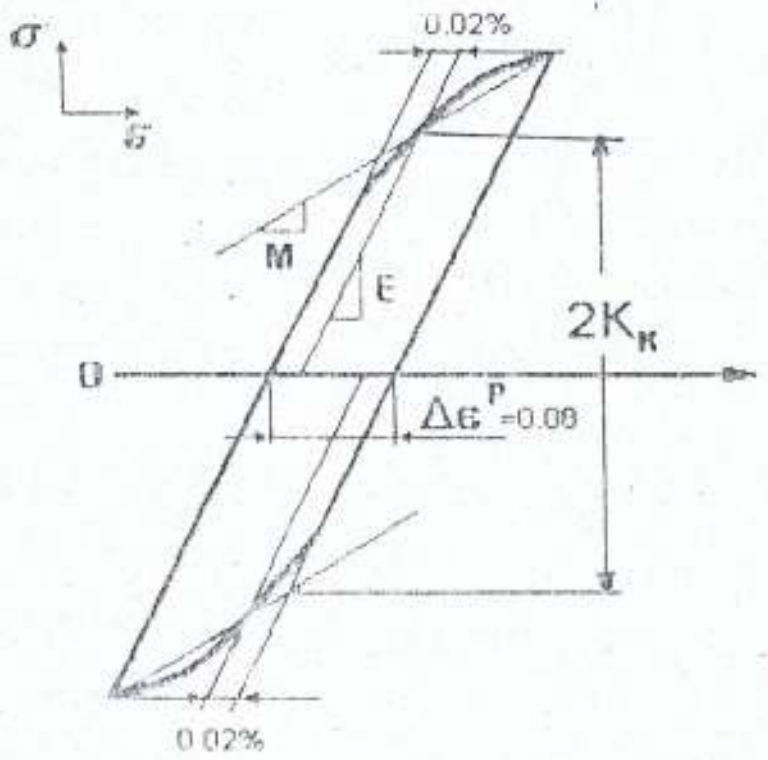

Figure 7. Schematic representation of ADI behaviour under cyclic tension-compression fatigue test. The values of the kinematics yield strength, k_k, the elastic modulus, E, and the plastic modulus, M, are indicated on the hysteresis loop.

3.0 THEORETICAL BACKGROUND AND MODEL DEVELOPMENT

3.1. Failure Mode Predictions

The design of components subjected to variable loads requires reference values that are currently scarce or unavailable. With the advent of modern steel manufacturing technologies, i.e. cleaner materials, subsurface nucleated failures initiated at metallic and non-metallic inclusions have diminished. Modern power trains require higher transmitted specific power, which stresses material to its endurance limit. According to Dommarco et al, (2001), these severe mechanical solicitation lead to metallic contact (micro-asperities and debris interactions), and have shifted the failure mode from a subsurface to a surface - dominated one, The failure mode can be predicted using the value of the specific film thickness Lambda factor (λ). This parameter is the ratio between h_o, the minimum oil film thickness and $(\sigma_1 + \sigma_2)^{1/2}$, the compound roughness of the machining surface. For $\lambda > 2$, the oil film is thick enough to completely separate the contacting surfaces and the failure mode will be the subsurface type; For $\lambda < 2$, the failure mode will be surface controlled. Dommarco et al (1998) studied the rolling contact fatigue resistance of ADI. They considered the elastic kinematics plastic response under tension = compression cyclic loading and also conducted tests at loads above the shakedown limit i.e. $p_o/k_k = 4$, where p_o is the maximum Hertz stress and k_k the kinematics shear yield Stress. The kinematics shear yield strength for the ADI was obtained from the hysteresis loop measured during cyclic tension-compression loading tests, represented schematically in Figure 7. They suggested that the fatigue

life in components subjected to rolling contact loading is composed of two distinct stages, i.e. nucleation and propagation.

3.2. Model Development for Fatigue Limit Prediction

It has been suggested that the fatigue limits of several ductile irons including ADI depended mainly on the graphite nodule size. An empirical equation between fatigue limit and graphite nodule size was then introduced for ADI, (Tanaka et al, 1995 as reported by Lin and Wei, 1997). Similar concept is applied to the current study to generate the relationship between fatigue limit and nodule size for ADI's

According to Tanaka et al, given an austempering treatment, the fatigue limit decreased linearly with an increase in mean nodule diameter on logarithmic scales. The correlation coefficients of the fitting curves are $r^2 = 0.91$ and 0.84 for austempering temperatures of 350 and 300^{0}C respectively. Therefore given a mean nodule diameter, the fatigue limit of ADI austempered at 350^{0}C is distinctly greater than that austempered at 300^{0}C. The degree of sensitivity of ADI fatigue limit to the nodule size is different as the austempering temperature changes. In order to find a universal equation for predicting fatigue limits of ADIs obtained from different austempering treatments, other factors needed to be considered. Tanaka et al (1995) suggested using Vickers hardness value of the matrix to relate to ADI fatigue limit. However as mentioned by other authors, fatigue limit was not dependent on either tensile strength or hardness for any given graphite nodule morphology.

Therefore it is considered to be more appropriate to use impact toughness value instead of hardness to correlate with ADI fatigue limit. Therefore the impact toughness value is proposed in

the present study to combine with the mean nodule diameter to correlate with the fatigue limits of ADIs tested. This can be expressed as follows:

$S_e = k * I^n * d^m$, ...(13), (Tanaka et al (1995)).

where S_e is the fatigue limit (Nmm^{-2}), I is the impact toughness (J), and d is the mean nodule diameter, (μm). The results of fatigue limit predictions are presented in Table 10 and Figure 39.

3.3. Empirical Formulae Embodying Experimental Fatigue Test

The most satisfactory empirical formular embodying experimental fatigue test data is due to Gerber and may be written as,

$$S_{max} = R/2 + \sqrt{(Su - nRSu)} \quad \text{.....(14)}$$

Where S_{max} is the maximum stress during each cycle at the fatigue limit, R is the stress range, S_u is the nominal static ultimate tensile stress and n is a material constant.

Goodman suggested a simple straight-line law relating stress range and mean stress:

$$R = \frac{S}{n}(1 - \frac{Sm}{Su}), \quad \text{.....(15)}$$

where S_m is the mean stress.

The S_m , the mean stress and S_v , the variable stress are defined as follows:

$S_m = ½ (S_{max} + S_{min})$; and

$S_v = ½ (S_{max} - S_{min}) = R/2$. .....(16)

The most commonly used empirical fatigue failure equations defining the relationship between the mean and variable stresses are written as:

1. Gerber parabolic equation:

$$\frac{S_r}{S_e} = \left(\frac{S_m}{S_u}\right)^2 = 1 \quad \text{.....(17)}$$

2. Modified Goodman equation:

$$\frac{Sr}{Se} + \frac{Sm}{Su} = 1 \quad \text{.....(18)}$$

3. Soderberg Relationship:

$$\frac{Sr}{Se} + (\frac{Sm}{Syp}) = 1 \quad \text{.....(19)} \ ,$$

where S_e is the fatigue strength for complete strength reversal; S_{yp} is the static yield stress.

3.4. Effect Of Austenitising Temperature in Modifying Fe-C Phase.

When ductile iron is heated to the austenitising temperature, it enters the austenite plus graphite regions of the Fe-C phase diagram Figures 8, 9 and 10. Figure 10 is used to determine the maximum carbon content that dissolves in the austenite at the solution treatment temperature. Austenitizing temperature is an important heat treatment parameter as it determines the matrix carbon content that dissolves in the austenite and has a significant influence on the kinetics of the first stage transformation reaction. It can be seen from the free energy diagram (Figure 9) that there is a corresponding increase in the driving force for the transformation of austenite to the metastable product ferrite plus carbon enriched austenite, (Grech and Young, 1984). The resulting higher driving force (b-b>a-a) increases the number of ferrite nuclei. The activity gradient driving the carbon in the austenite, in advance of the growing ferrite plates is also increased, thereby increasing the diffusion rate of carbon. Thus the transformation to ausferrite

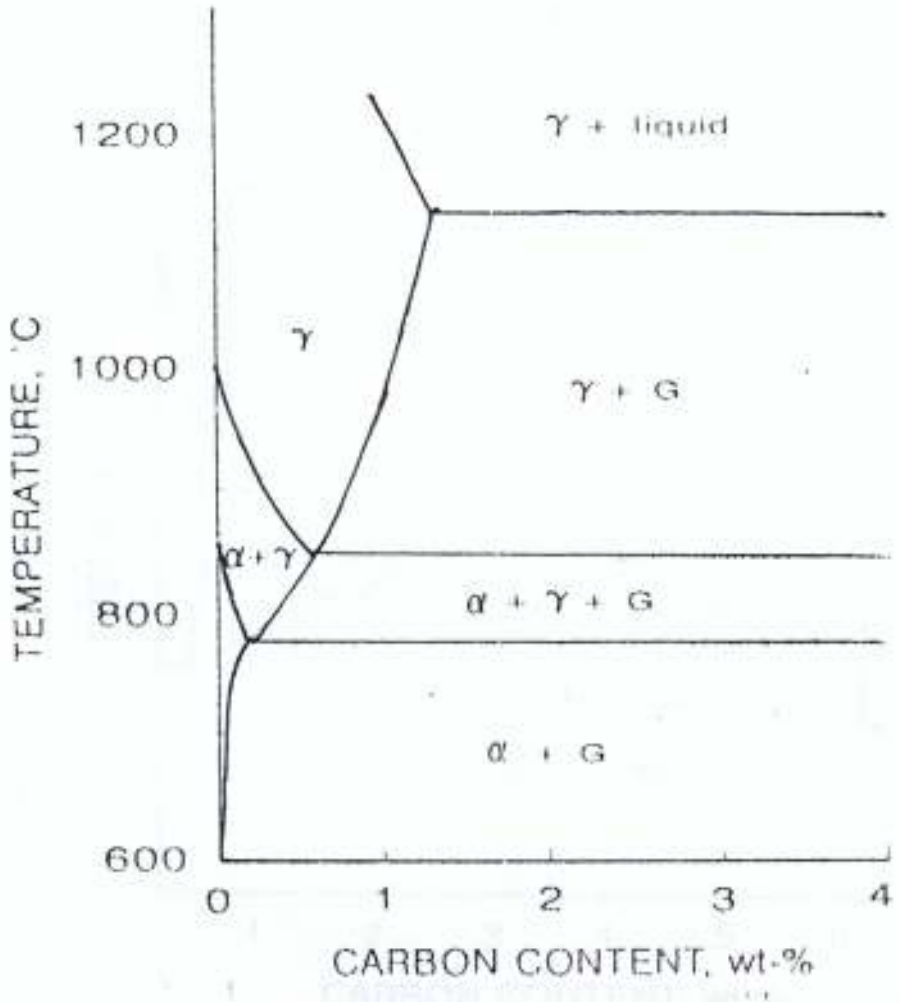

Figure 8. Schematic Fe-C-Si phase diagram and free energy curves for ferrite, α, austenite γ, and cementite Fe_3C phases

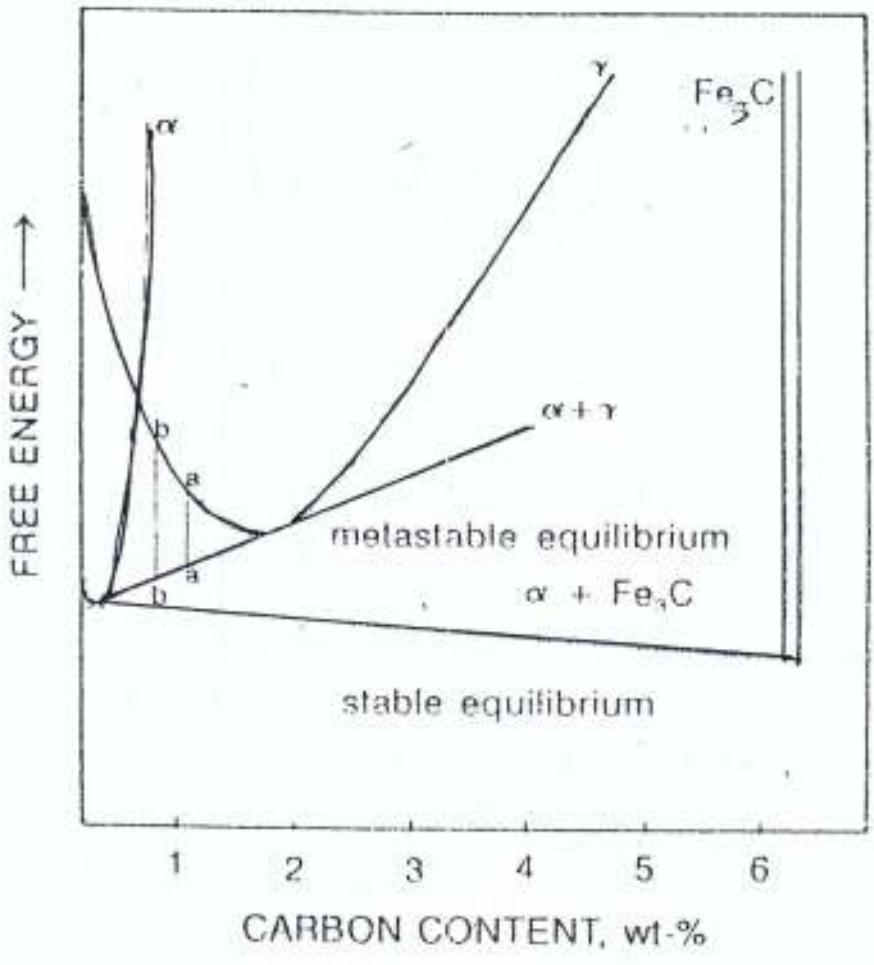

Figure 9. Schematic free energy diagram for λ (austenite), α (ferrite), and Fe_3C (cementite).

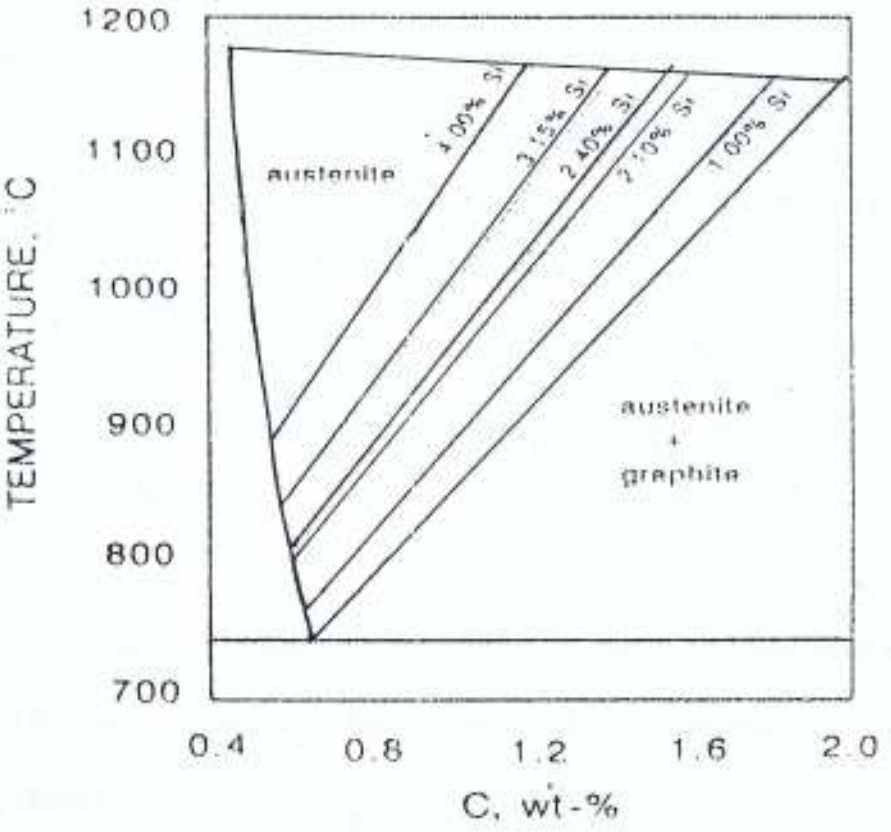

Figure 10. Modified Fe – C phase diagram

occurs more rapidly due to a combination of better ferrite nucleation and growth. This leads to a reduction in austempering time needed to attain optimum properties and more uniform microstructure which in turn has a positive influence on the mechanical properties. Austenitising temperature is an important factor in austempering. Austenitising within the range of 900 to 950^{0}C enables finer bainite morphology to be obtained and also prevents the retention of prior austenite due to carbon segregation at cell boundaries. A network of retained prior austenite is undesirable because it can transform to martensite under strain. The presence of this strain-induced martensite will lead to a loss of toughness and reduction in fatigue strength. Gundlach and Janowack reported that, in order to obtain good ductility, the austempering temperature must be such that an optimum amount of retained austenite is formed, say about 40%. As the austenitising temperature is raised, this will necessitate a reduction in austempering temperature. The present work studies the influence of austenitising temperature on the fatigue and impact toughness of austempered ductile irons.

3.5. Relationship Between Austenitising Temperature, Silicon Level And Austenite Carbon

3.5.1 Estimate Of Austenite Carbon in Equilibrium with the Graphite.

The following equation

$$Co = T\gamma - \frac{0.17Si}{420} - 0.95 \quad \text{.....(20)}$$

where Tγ is in ^{0}C and Si in wt %

provides an estimate of austenite carbon in equilibrium with the graphite, which decreases with decreasing Tγ and increasing silicon content.

3.5.2 Carbon Equivalent

The carbon equivalent for the various cast alloys were calculated using the following equation:

$$C.E. = \%C + \%Si / 3. \quad \ldots\ldots\ldots\ldots\ldots\ldots (21)$$

3.6. Defining the Processing Window for Austempering Conditions

Austempering basically consists of austenitising the ductile iron, quenching to the austempering temperature, holding for a controlled time and then cooling to room temperature. The austempering process is conventionally defined in two stages, figure 11. In the first stage, the initial austenite decomposes into ferrite and high carbon or transformed austenite. Ferrite is a stable phase but carbon enriched austenite is a metastable phase. When this transformation is completed, the ausferrite exists metastably for only a certain time. It thus becomes difficult, if not impossible, to define an ideal austempering time for the whole of the cast iron component. The processing window of ADI is derived from microstructural features, mechanical properties or predicted by measuring the volume fraction of retained austenite. The optimum mechanical properties can be achieved when setting the holding time of austempering within the range of the processing window. The processing window can be calculated from the graphs of various tests with austempering time. This calculation can be achieved by drawing a line parallel to the time axis on the above relationship at a level of about 90% of the maximum. The line intercepts the curve at each side of the maximum at times t_x and t_y. The time t_2 corresponds to an austempered microstructure that contains insufficient carbide for it to be detrimental to the desired mechanical properties and the closure of processing window can be calculated from the equation:

$$Ln\ t_2 = (\ln t_x + \ln t_y) / 2. \quad \ldots\ldots\ldots\ldots\ldots\ldots (20)$$

The determination of the processing window for austempered ductile iron is of great interest not only academically but also very important in heat treating industry. An accurate processing window provides both the accuracy of controlled mechanical properties and the efficiency of heat-treating. A series of studies of the mechanical properties of austempered ductile iron were conducted to investigate the applicability of processing windows defined from curves of fatigue strength, impact toughness and retained austenites.

3.9 **RETAINED AUSTENITE ESTIMATION:**

Many of the properties of austempered ductile iron depend on the austenite, which is retained following the bainite reaction. A model to calculate the amount of retained austenite as a function of all austempering variables was adopted, using a neural network technique, using experimental data to model the retained austenite content. The model allows the quantity of retained austenite to be estimated as a function of the chemical composition and heat treatment parameters.

A neural network is a general method of regression analysis in which a flexible non-linear function is fitted to experimental data, the details of which have been reviewed extensively (Mackay and Cerjack 1997; Eberhart and Dobbins, 1990).

The heat treatment parameters used are T_γ = 850, 900 and 950^{0}C, t_γ= 60 minutes, T_A =250, 300 and 350^{0}C and t_A = 15, 30, 60,90 and 120 minutes. In order to predict the quantity of retained austenite a set of variables are chosen, which implicitly contain all the information, needed for the estimation.

3.10. MICROSTRUCTURAL EVOLUTION.

In discussing the microstructure, there is need to distinguish between the volume fraction of residual austenite ($V\gamma$), which is the untransformed austenite at the austempering temperature, and the volume fraction of retained austenite ($V\gamma_r$) which remains untransformed at ambient temperature.

The evolution of volume fraction with time in nucleation and growth reactions follows signoidal behaviour. This is because the bainite reaction associated with the first stage of austempering, and indeed, the subsequent decomposition of the austenite in stage two, should both follow an Avrami type of Equation with

$$\zeta = 1 - \exp\{-k_A t^n\}, \quad ..(23)$$

where ζ is the fraction of transformation. The detailed values of the Avrami parameter k_a and the time exponent n will depend on many different factors, as reviewed by Christian, 1975. If ζ is the fraction of bainitic ferrite then $V_\gamma = 1 - \zeta$ during stage I, so it is expected that

$$\ln\{-\ln\{V_\gamma\}\} \sim \ln\{t_A\}. \quad .....(24)$$

It is natural to use $\ln\{-\ln\{V\gamma\}\}$ as the output parameter in the model analysis, rather than $V_{\gamma r}$ directly. The former is physically justified on the basis of the Avrami equation, but is additionally important because $V_{\gamma r}$ and its associated error calculations become bounded between zero and one for all positive values of t, as they should be. On a similar rationale, the time parameter in the input set should be $\ln\{t_A\}$ rather than t_A.

The C content of the low C austenite, C_γ^o, formed during austenitizing depends on the iron composition and the austenitizing temperature. This dependence has been expressed by the equation:

C_γ^o = -0.435 + 0.335 x 10^{-3} TI + 1.61 x 10 T + 0.006(Mn wt %) – 0.11(Si wt %) – 0.07(Ni wt %) + 0.014(Cu wt %) – 0.030(Mo wt %). .....(25)

During austempering the carbon is redistributed between unreacted austenite, bainitic ferrite, high C austenite and carbide. A mass balance equation:

$C_\gamma^o = X_\gamma C_\gamma + X_\gamma^o C_\gamma^o + X_\alpha C_\alpha + X_C C_C$ .....(26):

Where X_γ, X_γ^o, X_α, X_C are the amounts of high C austenite, low C austenite, bainitic ferrite and carbide, respectively, and where C_γ, C_γ^o, C_α, and C_C are the carbon content of high C austenite, low C austenite, bainitic ferrite and carbide, respectively. As the value of C_α is small, the term $X_\alpha C_\alpha$ can be neglected, reducing equation 2 6to:

$C_\gamma^o = X_\gamma C_\gamma + X_\gamma^o C_\gamma^o + X_C C_C$ .....(27)

3.11. Model Analysis for Estimation of amount of Retained Austenite.

The general form of the model is as follows, with y representing the output variable (normalised) and x_j the set inputs.

$$y = \sum w_{ij}^{(2)} h_i + \theta^{(2)} \quad \text{.....(28); where } h_i = \tanh(w_{ij}^{(1)} x_j + \theta_i^{(1)},) \quad \text{.....(29)}$$

The subscript i represents the hidden units, the 0 terms are biases and ω, the weights. Thus, the statement of equation (28) together with the weights and coefficients defines the function giving the output as a function of the inputs. (Computer programme and graphic in Appendix I – III). All the variables were normalised within a range of ± 0.5 as follows:

$$y_N = \frac{(x - x_{min})}{(x - x_{max})} - 0.5 \text{ .....(30)}; \quad \text{(Yescas et al 2000).}$$

CHAPTER-FOUR.

4.0 METHODOLOGY

4.1. Preliminary Investigations

The research work was carried out in stages. The first stage involved preliminary investigations carried out on commercially available ductile irons. Preliminary investigations were carried out to verify the desirability of the project for industrial applications. Incessant machine breakdown due to metallurgical failures and the need to proffer solution has necessitated this research. A failed gear, obtained from Odua Textile Mills, Ado Ekiti, was subjected to visual, macroscopic and chemical analysis. Chemical analysis revealed that the material is a ductile cast iron going by the composition and the microstructure: 4.09 wt% C, 1.86 wt % Si, 0.552 wt% Mn, 0.025 wt%Ce. The chemical composition of ductile iron samples of a pump casing and water valve from Ondo State Water Corporation was also determined.

From all the investigations it was clear that there was a need to develop suitable alloys which would be readily available locally for the manufacture of replacement components for machinery.

4.2. PRODUCTION PROCESS

Various alloys of ductile iron with different silicon levels were produced. The production processes are as follows: (1). Selection of cast iron scraps (automobile cylinder heads, foundry returns, good quality low Mn steel scrap, high purity graphite as carburiser and ferrosilicon).

(2). Production of casting pattern and sand moulds (Moulds were prepared using silica sand with 5% bentonite as binder and 5% moisture).

(3) Charging of materials into the furnace for melting;

(4). Addition of inoculants (FeSi, CaSi)

(5). Addition of spheroidising agents (Mg, Ce...); (Sawdust addition of approximately 5wt% of sawdust to a nodulizing mixture of Mg and FeSi-75 in the compressed format was made).

(6). Pouring, casting with late inoculation;

(7). Removing the casting from the mold, shake out and fettling.

Three different silicon level ductile alloys were produced and designated as low silicon (LS), medium silicon (MS) and High silicon (HS) alloys. The amount of ferrosilicon added determined the quantity of silicon in the alloy.

Each alloy was cast into rods of 20mm diameter and 500mm length. From the rods, test samples were machined and prepared for various mechanical tests: fatigue, impact and hardness. The alloys generally contain 3.19 to 3.28% C and 2.0 - 3.0% Si. The composition of the various alloys determined spectrometrically at the Nigerian Foundries Lagos, are shown in Table 5.

4.3. HEAT TREATMENT

In order to determine the sensitivity of silicon content to heat treatment variables and mechanical properties, each sample was subjected to austempering heat treatment. Austempering heat treatment was carried out in two stages viz

1.Heating the casting to the austenitising temperature of 850, 900 or 950^{0}C for one hour.

2. Rapid quenching and holding in a salt bath maintained at temperatures of 280, 300 or 350^{0}C for different time intervals, (15,30,60,90,or 120). The heat-treated samples were later subjected to mechanical tests using standard procedures.

The three-austenitising and austempering temperatures with varying austempering time were conducted to generate the optimum strength and toughness and to determine whether fatigue resistance of ADI with different silicon levels is directly related to the impact toughness. According to Lin and Wei (1997), different matrix structures in ADI and the associated mechanical properties can be obtained by choosing proper combinations of heat treatment variables, including austenitising temperature and time and austempering temperature and time. The austempering time is selected to optimize the mechanical properties for a particular austempering and austenitising temperature.

The austempering cycle involves soaking the metal above the critical temperature (austenitisation) followed by a quench that is fast enough to prevent the transformation of austenite (γ) to pearlite and an isothermal hold in the bainitic transformation temperature range to transform the austenite to ferrite and stable high-carbon retained austenite, (Harding, 1996). In the first stage, the initial austenite (γ) is expected to decompose into ferrite (α) and high carbon or transformed austenite (γ_{HC}). The austempering temperature and time are selected so as to prevent a second reaction stage from taking place. During the second stage reaction, high-carbon austenite decomposes into ferrite and carbide in which case the structure of the alloys will contain a carbide, which makes the material brittle, (Gagne and Trudel, 1997). To obtain optimum values of the desired mechanical properties, this reaction must be avoided. According to Putatunda, 2000, the best combination of mechanical properties is obtained in ADI after the

completion of the first reaction but before the onset of the second reaction. That is the operation must remain within the time interval, referred to as the **Austempering-Processing Window,** Figure 11. Figure12(a) is the schematic diagram of the austempering process.

4.4 SPECIMEN PREPARATION

Specimens for the microstructure study of the low, medium and high silicon ductile irons were cut from the test specimens away from the fractured surfaces. The cutting operation was carried out slowly and under liberal cooling to minimise heating and machining stresses. The specimens were ground to 1200 grade using water lubricated silica carbide paper and then etched in 90% hydrogen peroxide plus 10% concentrated sulphuric acid for 10-15 minutes. This technique removed the work-affected surface and at the same time minimised the occurrence of a textured structure. Surface grinding removed any decarburised skin, which may have formed during heat treatment. To avoid the transformation of any metastable austenite to martensite the depth of cut and grinding speed were kept as low as practicable. Metallographic samples cut from each selected position were prepared for microstructural observation, using optical microscopes. Grinding and polishing of specimens were carried out using the electromet III etcher and cell. Automet II belt surfacer, Ecomet II polisher / grinder, Handimet strip grinder, specimen drier and metaserve universal polisher, available at Federal University of Technology Akure and Obafemi Awolowo University, Ile-Ife. The etched samples were used to take micrographs using optical microscope. These micrographs were later used for microstructural analysis.

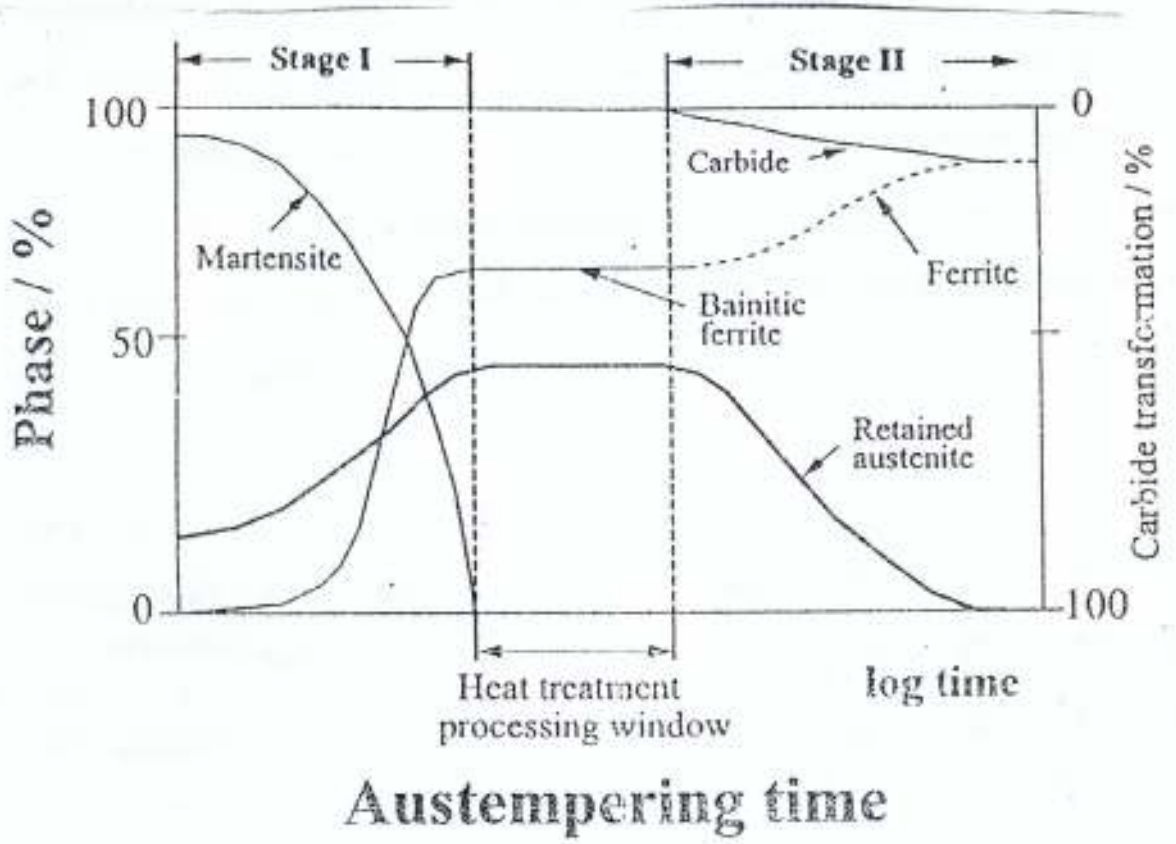

Figure 11. Schematic representation of the development of microscruture during austempering, together with an illustration of the 'Processing Window'.

4.5 MECHANICAL TESTING

Test specimens were machined from the castings into standard fatigue and impact toughness samples. The fatigue tests for all specimens were carried out using Avery Denison 7303 bi-axial fatigue testing machine at the Obafemi Awolowo University, Ile-Ife. The fatigue test was performed on all the specimens at varying bending stresses. The number of cycles to failure for each specimen and the bending stresses for the specimen was plotted against the number of cycles. The highest bending stress at which a run-out (failure) is obtained was taken as the fatigue limit. Notched Charpy impact test pieces were 10mm square cross section, 55mm long with a 2mm deep v-notch prepared in accordance with the normal standard. Appropriate specimens were prepared for hardness testing.

Table 5. Key To Specimen Identification.

AUSTENITISING/ AUSTEMPERING TEMPERATURES	850/ 280	850/ 300	850/ 350	900/ 280	900/ 300	900/ 350	950/ 280	950/ 300	950/ 350
IDENTIFICATION	11	12	13	21	22	23	31	32	33

LS20 - Low Silicon Alloy with average 2.0% silicon.

MS26 – Medium Silicon Alloy with (average 2.6% silicon).

HS30 – High Silicon Alloy with (average 3.0% silicon).

Austempering Time (Minutes):	15	30	60	90	120
N	1	2	3	4	5

Table 6. Chemical Composition of charged materials.

Material	C	Si	Mn	Mg	Ce	Ti	Al	Fe
FeMn	0.12	-	82.5	-	-	-	-	Bal
5%Mg. FeSi.		42.09	-	5. 33	0.10	-	0.55	Bal
FeSi 75	-	72.29	-	-	-	-	2.64	Bal
Mg			Analytical grade.					

Table 7. Chemical Composition of As-Cast Ductile Iron Alloys.

Alloy	C	Si	Mn	S	P	Mg	Cu	Ni	Mo	Fe
LS20	3.28	2.00	0.29	0.01	0.045	0.032	0.42	0.46	0.16	Bal
MS26	3.20	2.65	0.33	0.01	0.01	0.04	0.4	0.5	-	Bal
HS30	3.19	3.00	0.34	0.01	0.01	0.05	0.48	0.48	-	Bal.

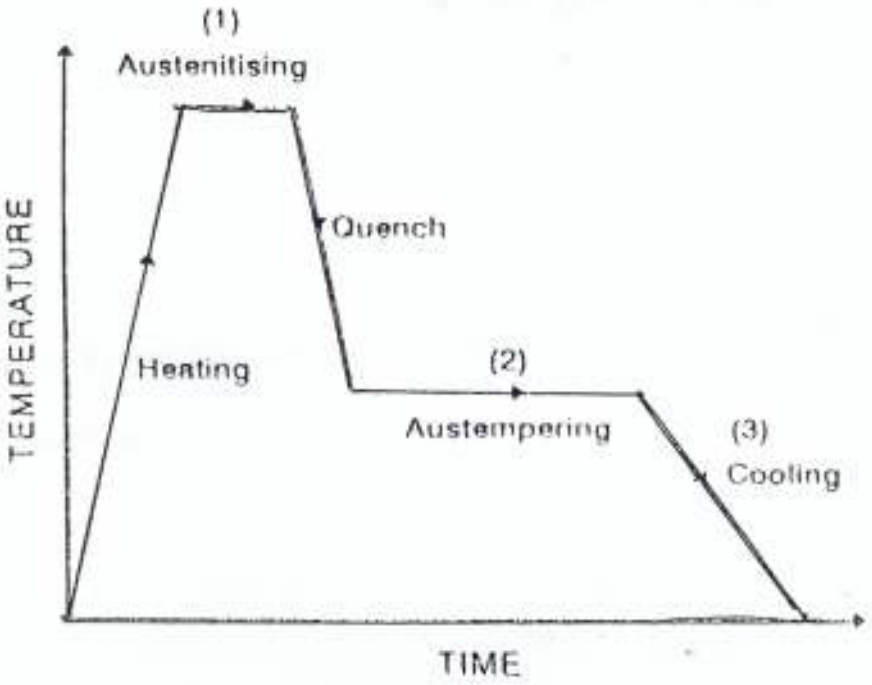

Figure 12a. Schematic diagram of austempering heat treatment cycle.

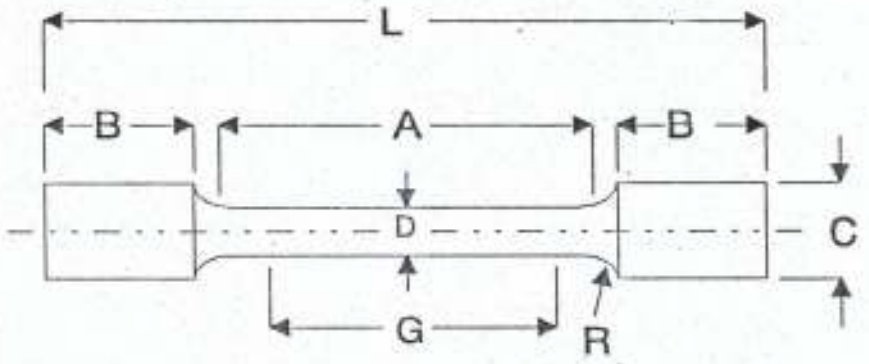

Figure 12 (b). Fatigue Specimen Standard Design. (L = 450, A = 260, B = 80, G = 150, C = 80, D = 50. Dimensions,in mm).

5.0 RESULTS AND DISCUSSIONS

The temperature and time of the isothermal transformation of austempered ductile irons have a marked influence on the relative amounts of bainite and retained austenite as shown in the tables and graphs. Table 7 contains data on the composition of the alloys produced. The sulphur and phosphorous levels were kept low because they are surface-active elements that tend to reduce graphite-iron interfacial energy thereby promoting interfacial characteristics of flake graphite. The role of inoculants and spheroidizers therefore is to promote spheroidization by their reaction with surface-active elements thus preventing their segregation at the graphite-iron interface. Plate 1 shows the as-cast structure of the three alloys. Nodules can be seen fairly distinctly in the high and medium silicon alloys. Table 8 shows the variations of iron carbon contents and equivalent carbon contents and austenite carbon content (wt%) with austenitising temperature and silicon content. It is observed that austenite carbon content increases with increasing austenitising temperature but decreases with increasing silicon content. This confirms earlier suggestion on the interdependence of austenite carbon content and silicon content. Table 9 shows the silicon level sensitivity and fatigue limit as a function of austempering time. It is clear from the data that silicon content affects the fatigue limit of austempered alloys.

The optical micrograph (plates1-14) show some examples of the most representative microstructures exhibited by the austempered samples. The effects of changes in austempering parameters (temperature and time) on the impact toughness, fatigue strength, volume fraction of retained austenite and hardness are presented in Figures 13 to 39.

The interdependence of fatigue strength on the silicon level obtained for the three austempered alloys are shown in Table 9. It can be seen that alloys with high fatigue strengths are produced when heat-treated at high austenitising temperature and austempering temperature (950^{0}C and 350^{0}C). Table 10 contains results of models developed to predict the fatigue limit from the impact strength data.

Table 11 shows the optimum values of fatigue limits, impact toughness and the amount of the retained austenite as a function of austempering time. The effect of austempering on hardness of the alloys is shown in Table 12. Table 13 and 14 establish optimum set of compositional variables for the production of ADI of high impact and fatigue strength suitable for the manufacture of automotive and other machine components.

5.1. Effects of Silicon on the Microstructure.

The important microstructural features obtained are the morphology of the ferrite, the retained austenite content, the carbon content of the retained austenite and the presence or absence of carbide in the austenite or ferrite. The different microstructures generated depending on silicon level, temperature and time of transformation, demonstrate how the silicon level and heat treatment affect the mechanical properties: impact, fatigue and hardness of the low, medium and high silicon alloys. As can be seen from Table 8, the amount of austenite carbon content in equilibrium with graphite decreases with increasing austenitising temperature and increasing silicon level. These values are only approximate, as it does not take into consideration the manganese content. However since the manganese content is moderate, it is expected to give a fairly approximate value. It follows therefore that in irons containing high silicon, sufficient

matrix carbon content can only be obtained when austenitising at 950^{0}C, a fact that may explain the superior fatigue strength and impact toughness obtained under these conditions.

Plate2 shows the microstructure of high and medium silicon alloys austenitised at 950^{0}C for 60 minutes and austempered at 350^{0}C for 90 minutes. The microstructure contains no pro-eutectoid ferrite but a mixture of coarse and fine ferrite platelets and uniformly distributed retained austenite. The coarse ferrite platelets occur as a result of high austempering and austenitising temperatures, while the formation of a finer ferrite structure is promoted by the high local concentration of silicon, particularly in dendrites and near the graphite nodule surfaces. The presence of silicon suppresses the carbide formation. When ferrite forms within the austenite the carbon rejected from these regions goes into solution in the surrounding austenite. As more and more ferrite forms the carbon content of the austenite increases. Since this high carbon austenite is stable at room temperature, the resulting microstructures consist of ferrite and retained austenite. This is the desired microstructure. Plate3 shows the microstructure of high silicon and medium silicon alloy austenitised at 950^{0}C for 60 minutes and austempered at 350^{0}C for 60 minutes. Bainitic morphology is seen as feather-like bainite and bainitic lath. In low silicon alloys austenitised at 850^{0}C for 60 minutes, after an austempering time of 15 min and 30 min at 350^0 C, the microstructure, (as shown in plate 4), contains closely parked acicular ferrite plates and high carbon austenite distributed uniformly between the plates. In comparison in plate 5, the same alloy austenitised at 950^{0}C for 60 minutes and austempered at 350^{0}C for 15 and 60 minutes show a continuous network of unreacted metastable austenite (a) and feather like bainite (b). Microstructure of high and medium silicon alloys austenitised at 900^{0}C for 60 minutes and austempered at 350^{0}C for 90 minutes are shown in plate 6. Most of the original pearlitic areas

had transformed, but the ferritic areas surrounding the graphite nodules had only started to transform. The structure reveals lower bainite, upper bainite (ausferrite), retained austenite and graphite. Samples austempered at 300^{0}C showed free ferrite characteristics of the lower ausferrite microstructure as revealed in plate7 for high and medium silicon alloys austenitised at 850^{0}C for 60 minutes and austempered at 300^{0}C for 60 minutes, while those austenitised at 950^{0}C and austempered at 300^{0}C is shown in plate 8. The microstructure reveals grain boundary lower bainite. At a lower value of austenitising temperature of 850^{0}C and high austempering temperature, high and medium silicon alloys have structures containing various proportions of proeutectoid ferrite, bainitic ferrite and retained austenite, (plate 9). Plate 10 shows the structure of low silicon alloy austenitised at 900 and austempered at 350^{0}C. Proeutectoid ferrite occurred as a result of low austenitising temperature. At low austenitising and low austempering temperatures, the microstructure of the alloys revealed bainitic ferrite and untransformed austenite as evidenced in the microstructure of samples of high and medium silicon alloys austenitise at 900^{0}C and austempered at 280^{0}C for 60 and 30 minutes as shown in plate 11. Plate 12 reveals the microstructure of low silicon alloys under the same austempering condition. In plate 13, the microstructures reveal the so-called 'pearlitic' bainite, (Bhadeshia, 1992), which is pearlite with alloy carbide formed as a result of low austempering temperature.

Plates 14 show the formation of columnar bainite in high and low silicon alloys austenitised at 950^{0}C and austempered at 280^{0}C. Columnar bainite is a non-lamellar aggregate of cementite and ferrite. The overall shape reveals an irregular and slightly elongated colony.

These structural features are controlled by the austempering kinetics. Figures 33 and 34 show that the maximum retained austenite volume is estimated at 30 – 41%.

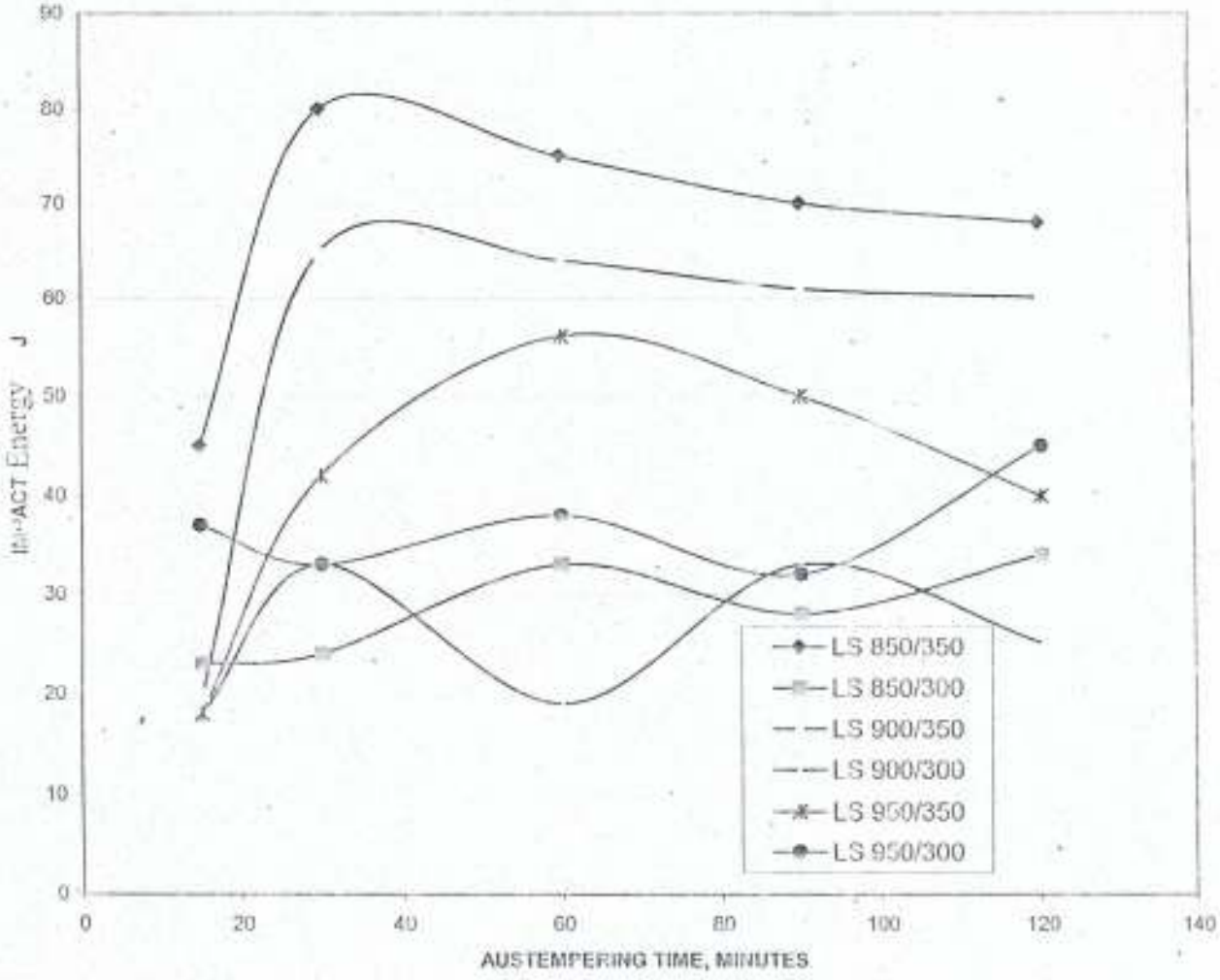

FIGURE 13 EFFECTS OF CHANGES IN AUSTENITISING AND AUSTEMPERING TOMPERATURE AND TIME ON IMPACT TOUGHNESS
OF LOW SILICON ALLOY LS20 13, 12,23,22,33and 32.

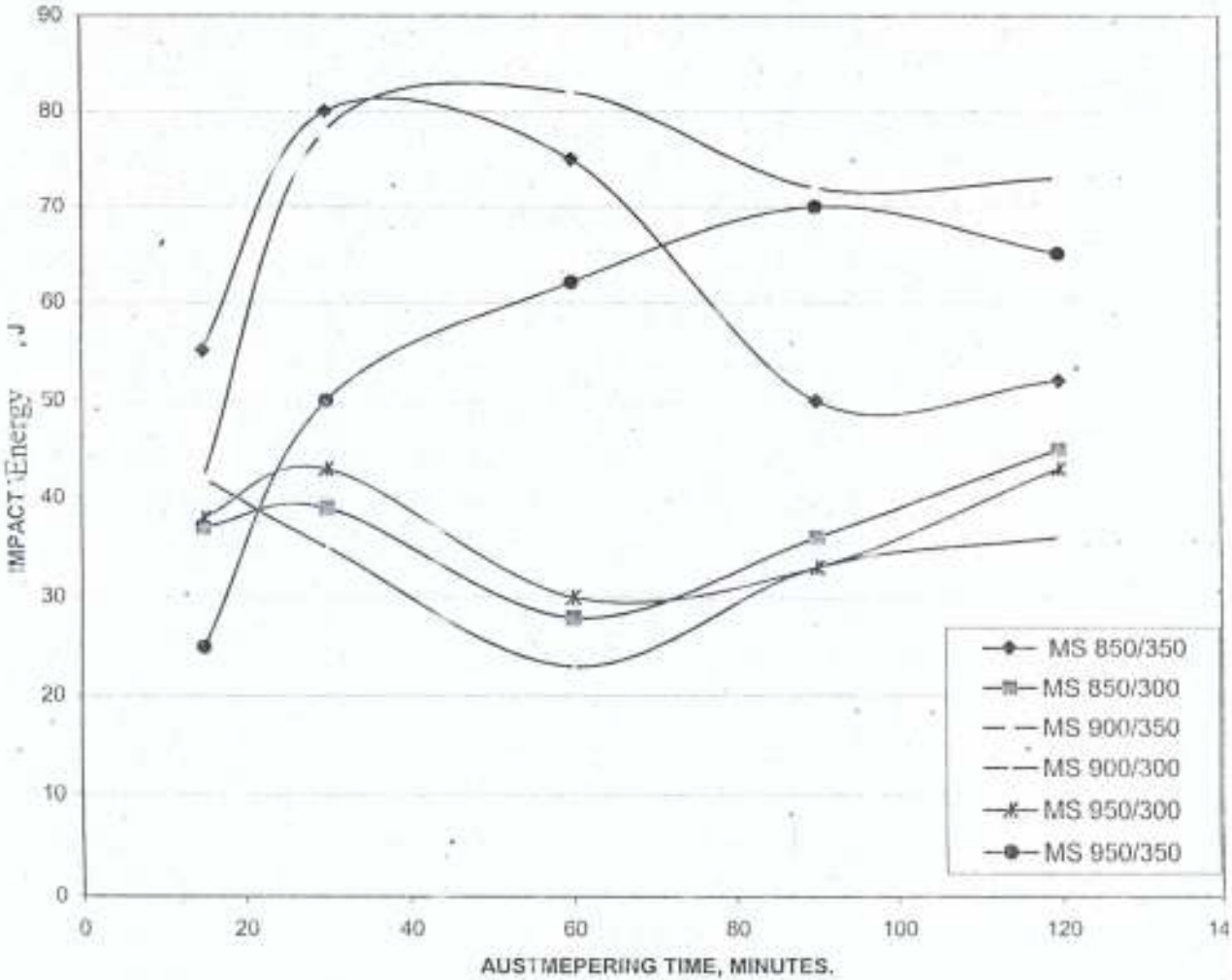

FIGURE 14 EFFECT OF CHANGES IN AUSTENITISING AND AUSTEMPERING TEMPERATURES AND TIME ON THE IMPACT STRENGTH OF MEDIUM SILICON ALLOYS MS 26 13,12,23,22,32and 33

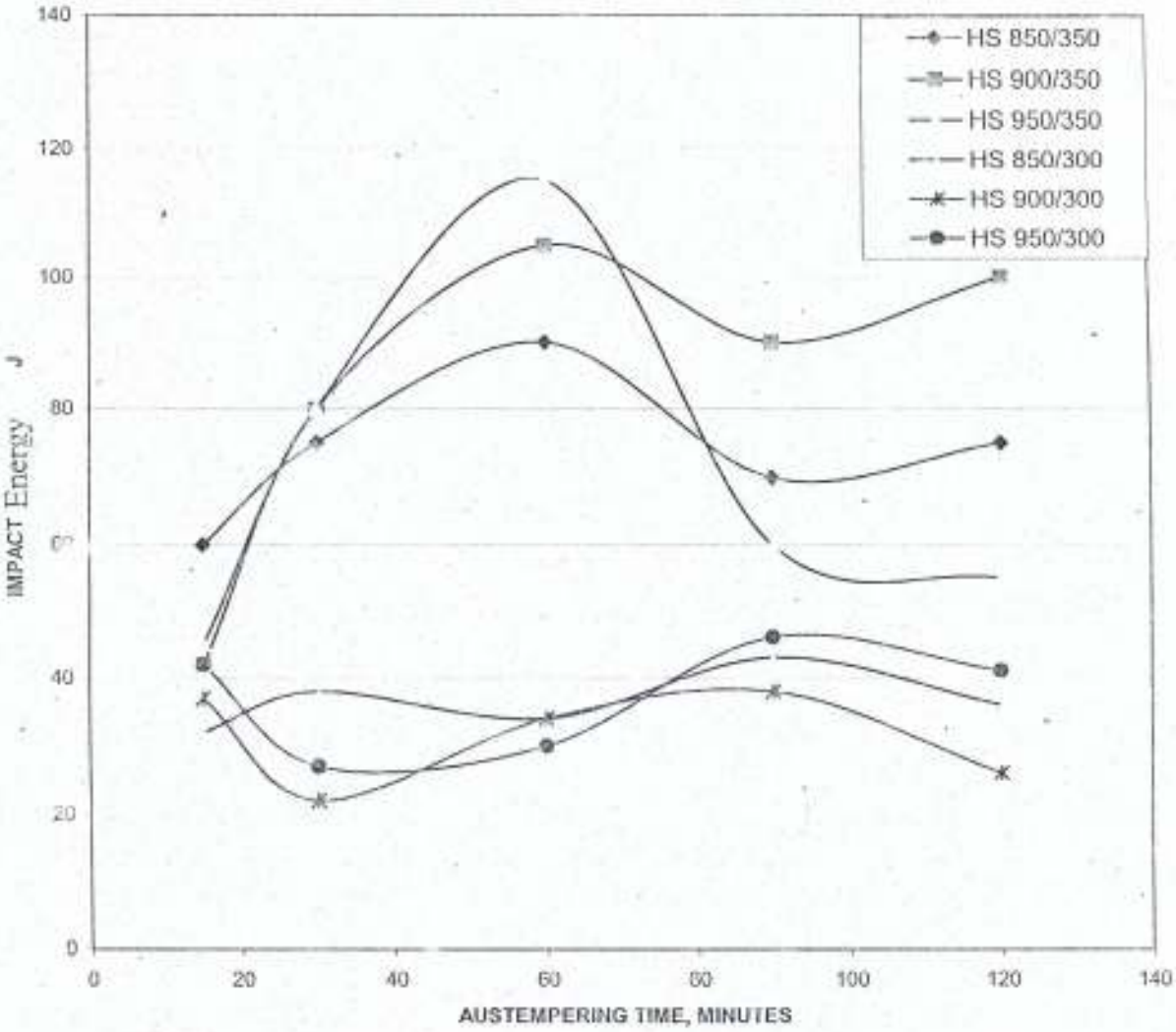

FIGURE 15 EFFECTS OF CHANGES IN AUSTENITISING AND AUSTEMPERING TEMPERATURE AND TIME ON THE MPACT TOUGHNESS OF THE HIGH SILICON ALLOY HS30 13, 23, 33, 12, 22, AND 32.

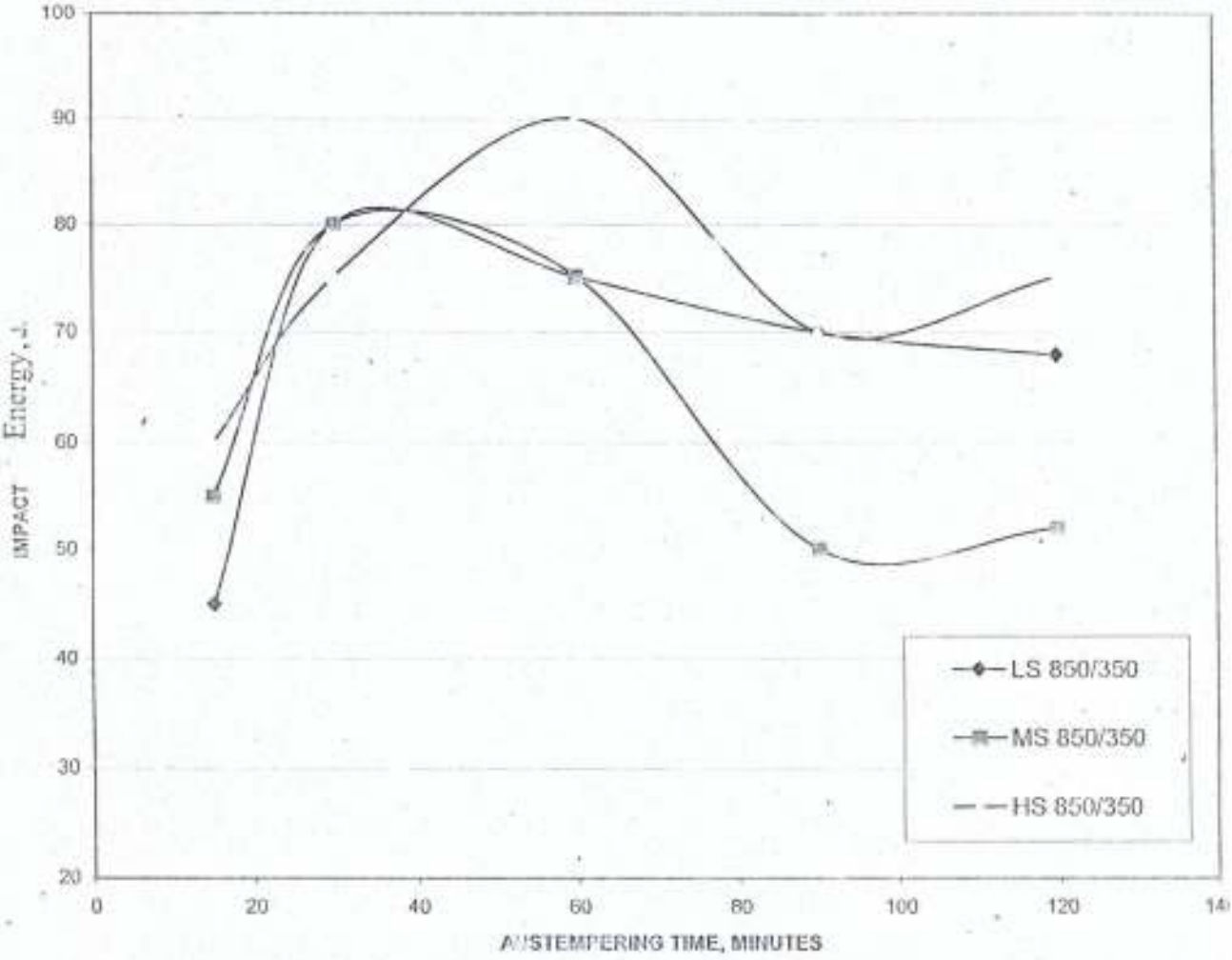

FIGURE 16 EFFECT OF AUSTEMPERING PARAMETERS AND SILICON LEVEL SENSITVITY ON IMPACT TOUGHNESS(850/350)

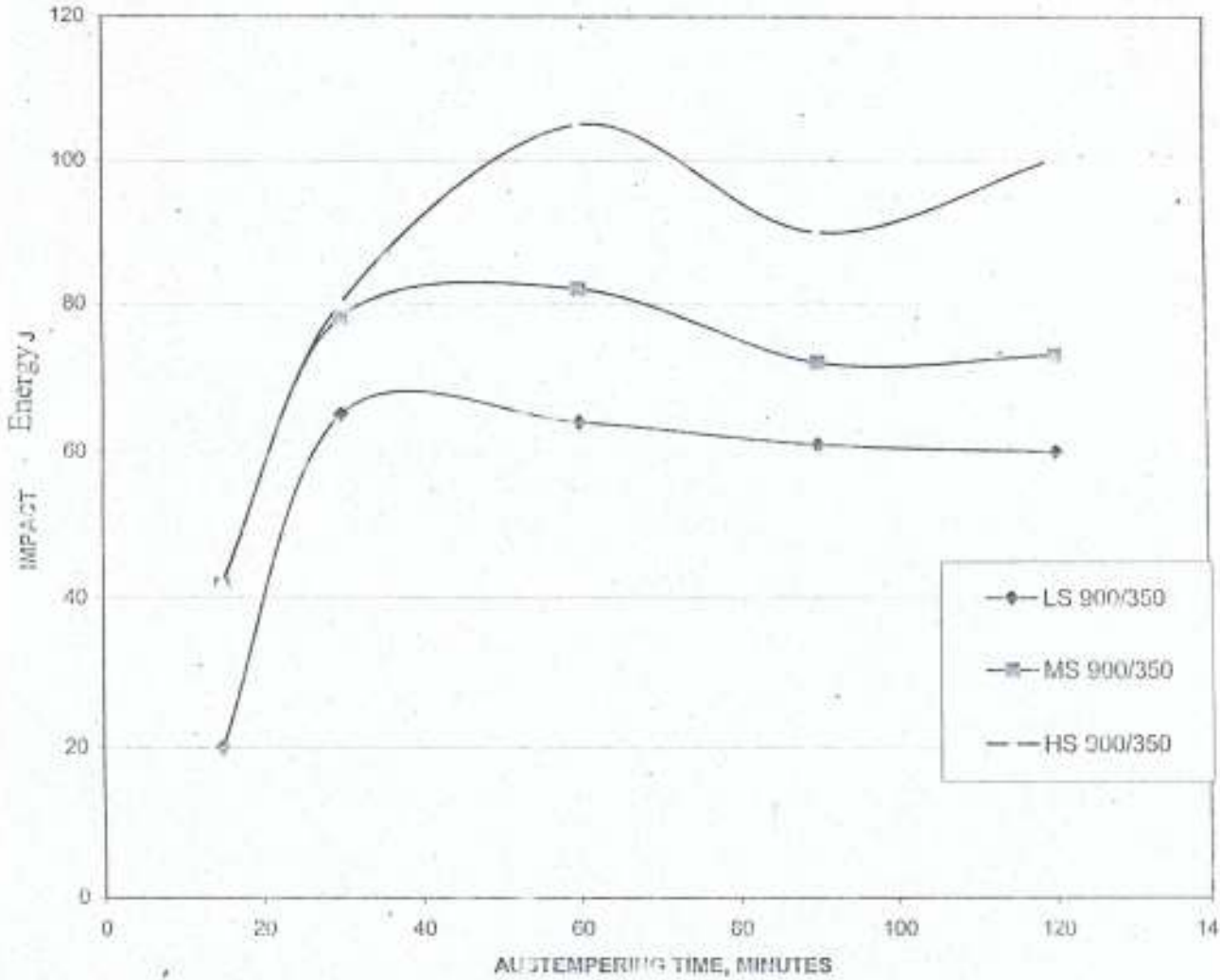

FIGURE 17 EFFECTS OF AUSTEMPERING PARAMETERS AND SILICON LEVEL SENSITIVITY ON IMPACT TOUGHNESS (900/350)

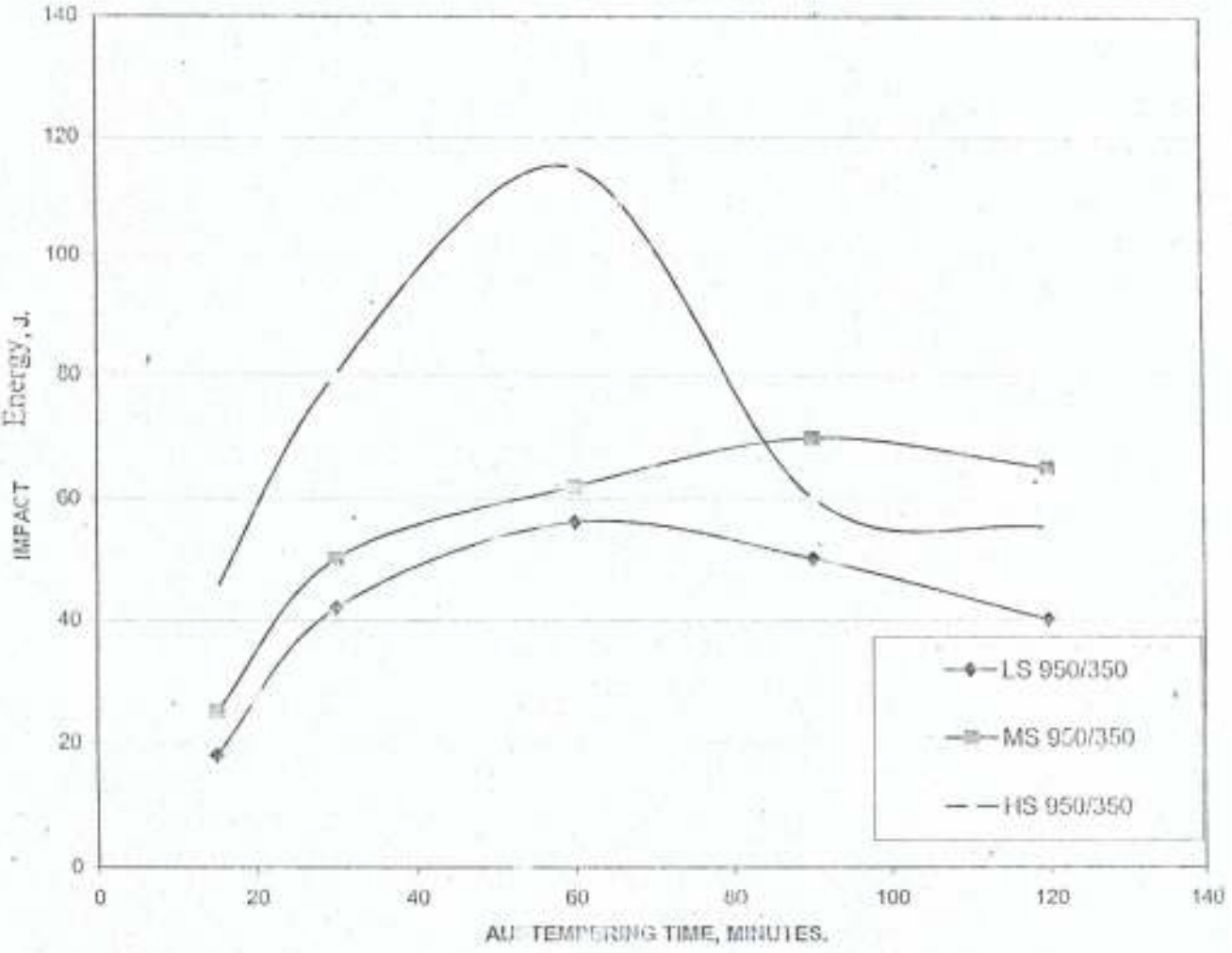

FIGURE 18 EFFECT OF AUSTEMPERING PARAMETERS AND SILICON LEVEL SENSITIVITY ON IMPACT TOUGHNESS (950/350).

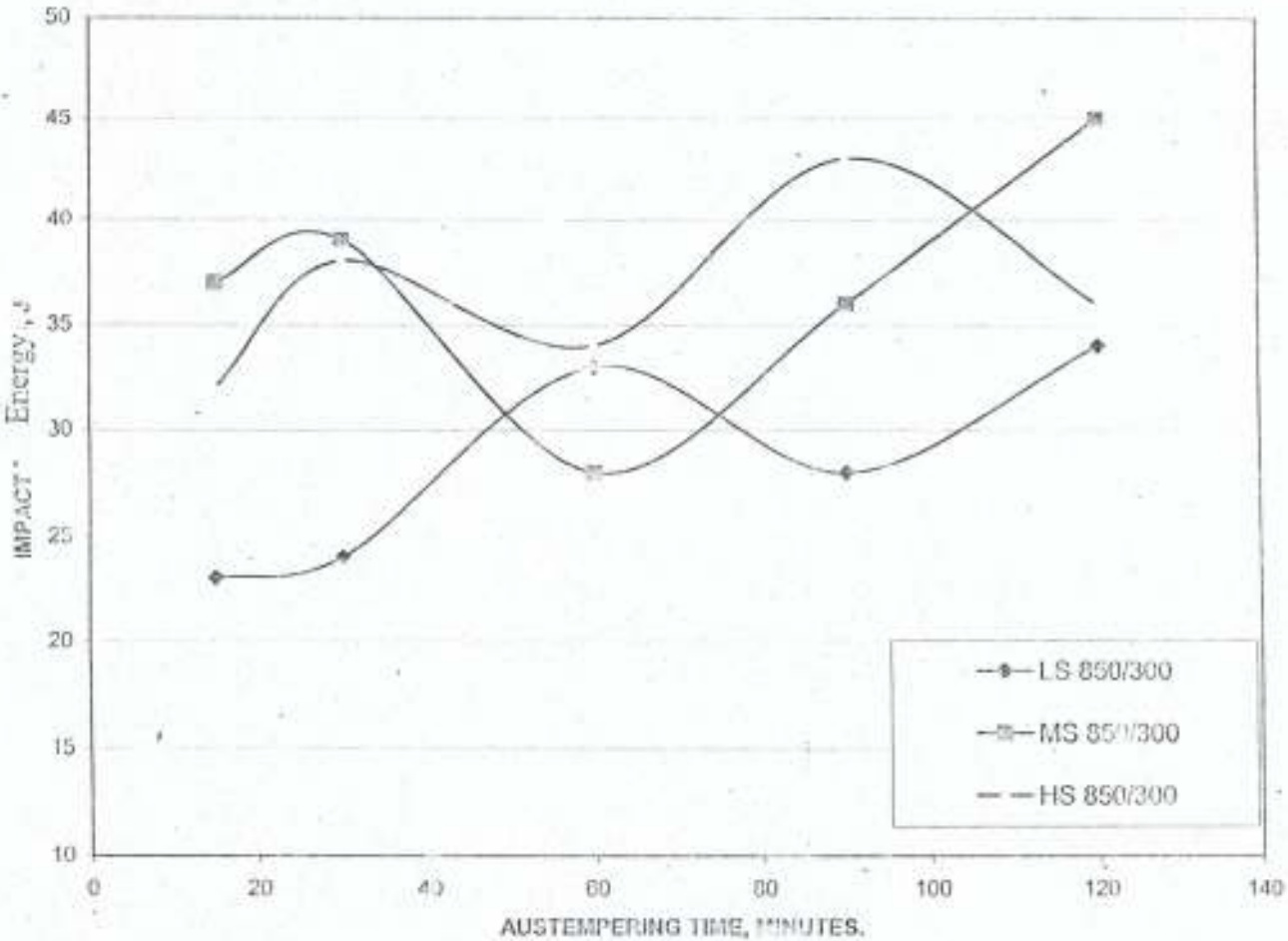

FIGURE 19 EFFECT OF AUSTEMPERING PARAMETERS AND SILICON LEVEL SENSITIVITY ON IMPACT TOUGHNESS (850/300)

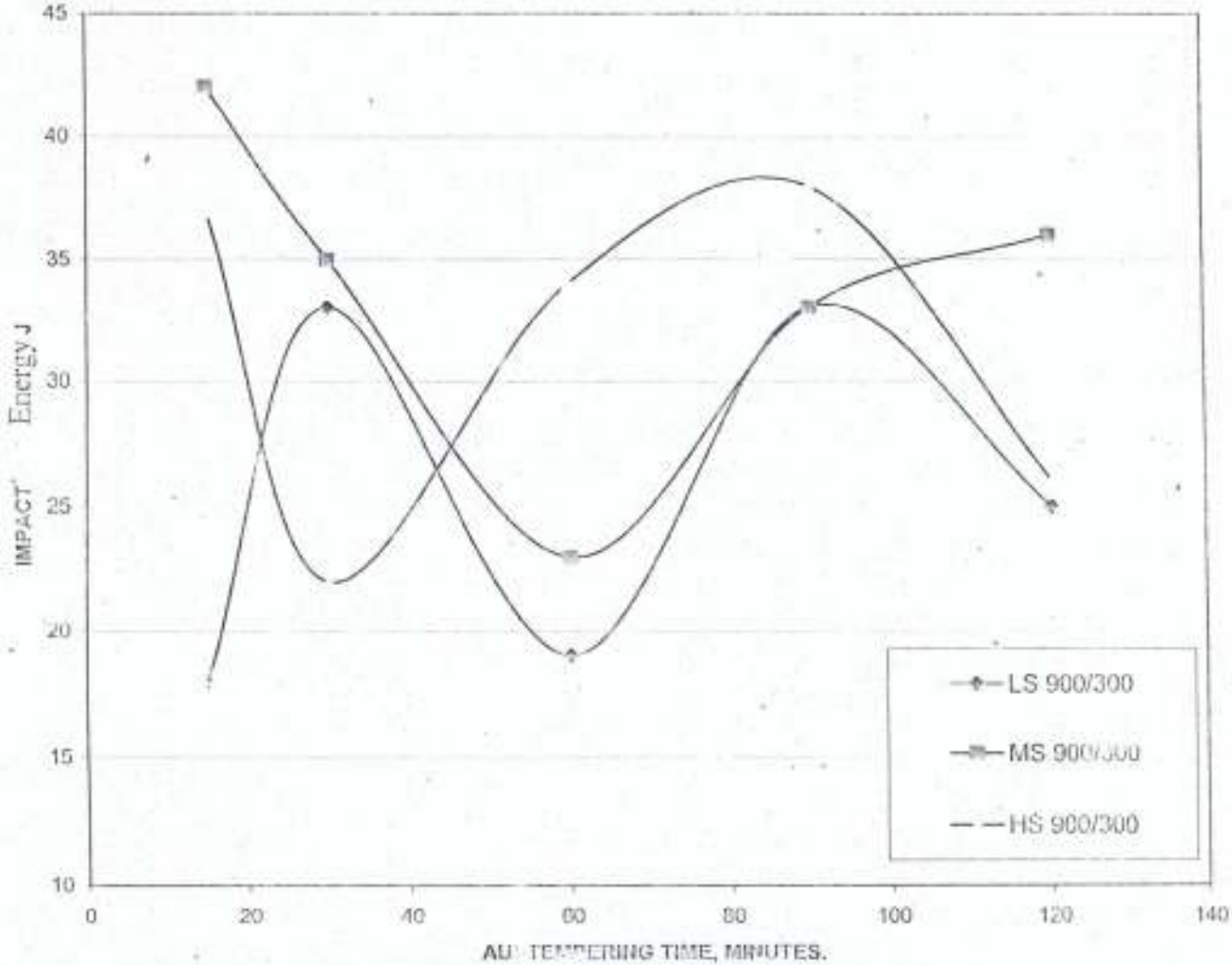

FIGURE 20 EFFECT OF AUSTEMPERING PARAMETERS AND SILICON LEVEL SENSITIVITY ON THE IMPACT TOUGHNESS (900/300)

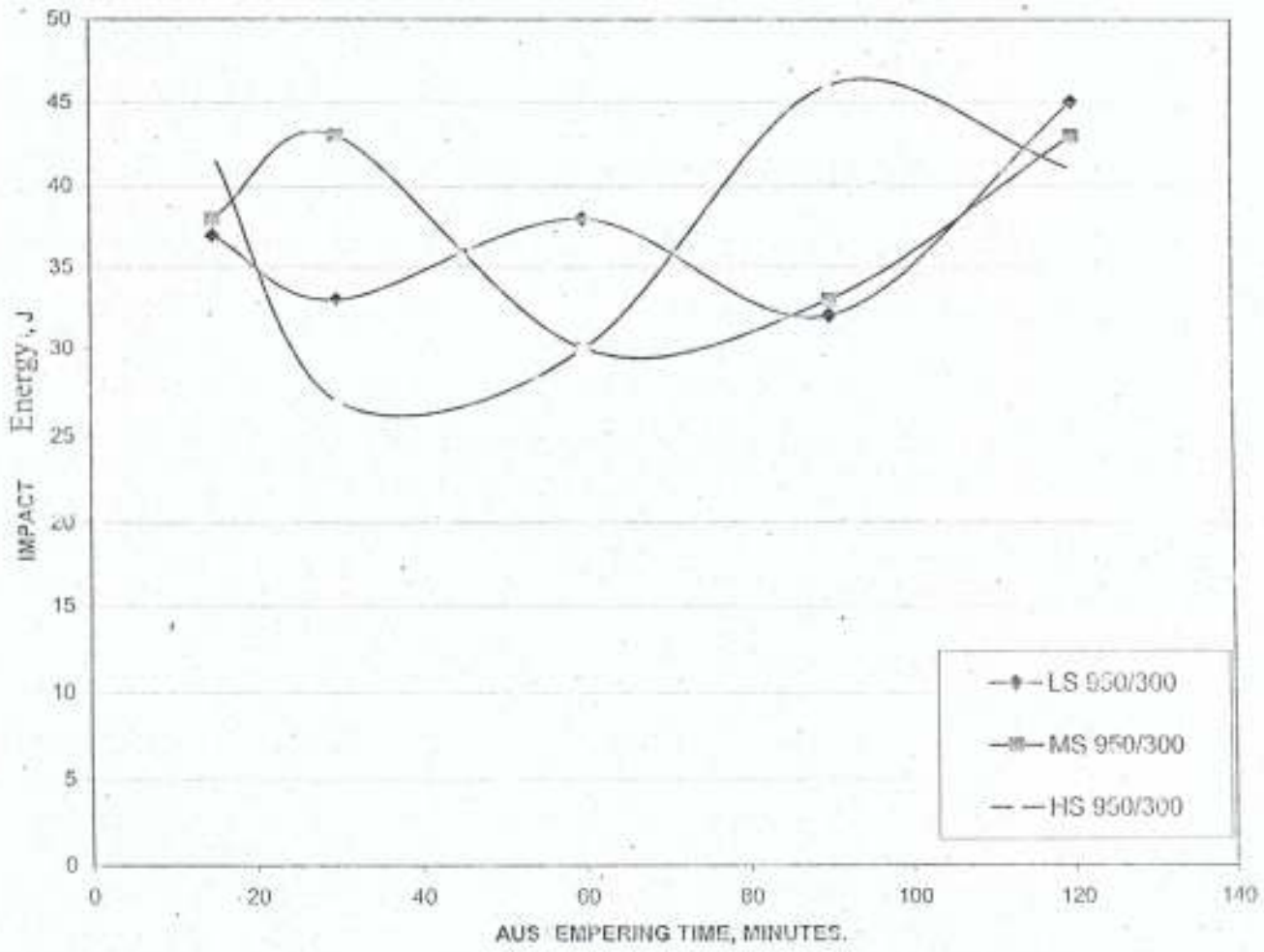

FIGURE 21 EFFECT OF AUSTEMPERING PARAMETERS AND SILICON LEVEL SENSITIVITY ON IMPACT TOUGHNESS(950/300)

The results of the estimated amount of retained austenite are shown in Figures 33 to 35.

The variation of volume fraction of austenite was found to depend on the silicon level, austenitising temperature and austempering temperatures and time. The high growth rate of bainitic ferrite needles and low diffusion rate of carbon results in a low retained austenite content at the low austenitising and austempering temperatures. For low, medium and high silicon alloys austenitised at 850^{0}C and austempered for 300^{0}C, the amounts of retained austenite are 10.03%, 19.96% and 26.797% respectively (Table 11). At higher austenitising temperature of 950^{0}C and austempering temperature of 350^{0}C the higher diffusion rate of carbon leads to carbon enrichment of the austenite region between the bainitic ferrite needles. Because of the higher matrix carbon content, sufficient carbon build up takes place ahead of the growing bainitic ferrite needle. This leads to appreciable retention of austenite hence the amount of retained austenite increased 34.92% for low silicon, 41.66% for medium silicon and 40.95% for high silicon. Thus the amount increases gradually with increasing silicon content and austempering temperature. For short treatment times, at each temperature, the bainite reaction is incomplete, and a pool of residual austenite subsequently transforms to martensite on cooling. For intermediate treatment times, after transformation at 300^{0}C, the retained austenite occurs mainly as inter-lath films, and some isolated pools of reduced dimensions appeared in the structure. Treatment at 350^{0}C lead to an increase in the amount of retained austenite volume fraction. This austenite, remaining after partial transformation of the original austenite, separates the ferrite plates from each other within a given sheaf of bainite and is also present as large pools called "blocky austenite". The differences in the amount of volume fraction of austenite on microstructures generated have an important influence on the properties.

TABLE 8. Relationship between austenitising temperature, silicon content, and austenite carbon content (wt%): iron carbon contents and equivalent carbon contents.

			Austenite carbon content, wt%		
Si content Wt%	C wt%	CE wt%	850^{0}C	900^{0}C	950^{0}C
2.0	3.28	3.95	0.733	0.853	0.97
2.60	3.2	4.066	0.631	0.778	0.868
3.0	3.19	4.19	0.563	0.68	0.8

5.2. Effect of austenitising temperature, austempering temperature and time and silicon level on the impact and fatigue strength of austempered ductile iron.

Figures 16 to 21 show the effect of silicon content on the impact toughness. The graphs show that silicon alloys are sensitive to changes in austempering conditions. It is apparent that each set of treatment conditions gives different combinations of impact, fatigue and hardness values.

For alloys heat-treated at 850/350, short austempering time at low austenitising and high austempering temperatures tends to favour low silicon and medium silicon alloys. They reach their peak within 35 minutes of austempering whereas, high silicon alloys take about 60 minutes to reach the optimum value with a higher value of impact toughness (90 Joules) than low and medium silicon alloys, Figure16. An increase in the amount of silicon in castings reduces the amount of pearlite but increase that of ferrite. In iron with high silicon content the matrix becomes completely ferritic (Silico-ferritic). Hence for alloys having high silicon content, more soaking time or austenitizing temperature is required to achieve the desired carbon dissolution and hardenability. From Figure 13 it is evident that low austenitising temperatures (850-900^{0}C) and high austempering temperature with short austempering time (15-30 minutes) favour

increase in impact of low silicon alloys. The highest impact toughness value for low silicon alloy (80 Joules) was obtained for alloy austenitised at 850^{0}C and austempered at 350^{0}C for 30 minutes. For all the alloys, impact toughness is observed to be low at low austempering temperatures and short austempering time, but increases with increase in austempering temperatures and time, (Figures 13,14 and 15). At low austenitising temperature (850^{0}C), high austempering temperature (350^{0}C) and short austempering time (30 minutes), both medium and low silicon alloys exhibit virtually the same impact characteristics (Figure16). At austenitising temperature (900^{0}C) and high austempering temperature (350^{0}C) and short austempering time (30 minutes), both high and medium silicon alloys have approximate the same value, 80 Joules. Prolonged austempering however increase the impact toughness value of high silicon alloys to 105 Joules but the medium and low silicon alloys do not show any appreciable increase (Figure 17 and 18).

Austempering at low temperature (300^{0}C) takes longer time for high silicon alloys to reach the optimum impact value. The impact values are generally low for all the alloys at low austempering temperatures, (Figures 19 to 21). Low silicon appears more stabilized at prolonged austempering time than medium silicon. High silicon alloy takes a longer time to reach optimum value but has a higher impact value. At austenitising temperature of 900^{0}C, the distinctions in changes in impact value are very apparent.

The effects of changes in austempering parameters on the fatigue stress for low silicon, medium silicon and high silicon alloys are shown in the S-N curves in Figures 22 to 29.

The number of cycles to failure for each specimen was plotted against the bending stresses for the specimen. The lowest bending stress at which a run-out (failure) is obtained was taken as the

fatigue limit. The variations of fatigue strength of austempered alloys with silicon level are shown in Figures 30 to 32. Comparing the effects of austenitising temperatures and austempering temperatures, it is apparent that each treatment condition gives different fatigue strengths. In high silicon alloy the highest fatigue strength (400 Nmm^{-2}) was obtained from an alloy austenitised at 950^0C and austempered at 350^0C (Figure 30). Similarly, medium silicon alloys austenitised at 950^0C and austempered a 350^0C also produce the highest fatigue strength, (Figure 31 and 32). In general it is observed that the fatigue strength increases with increasing austempering time, just as the retained austenite also increases with austempering time, (Figures 33 to 35). It can be seen that at each of the austenitising temperatures, as the austempering time increases from 15 to 90 minutes, the fatigue strength increases. At constant austempering time the effect is greater the higher the austenitising temperature.

For the high silicon alloy, the austenitising temperature (950^0C) and austempering temperature (350^0) that produce the optimum value of impact toughness (115 Joules) and fatigue strength (400 Nmm^{-2}) is the same that produce the highest amount of retained austenite (40.95%). For the medium silicon, the highest value of retained austenite (41.66%) was obtained at austenitising temperature of 950^0C and austempering temperature of 350^0C, however the optimum value of the impact toughness (82 Joules) was obtained at isothermal temperatures of 900^0C and 350^0C. For low silicon, high austenitising and austempering temperature ($950/350^0$C) favours the amount of retained austenite generated (34.92%), but low austenitising with high austempering temperature (850/350) tend to favour impact toughness of low silicon alloys hence the value at this isothermal condition is 80 Joules. Initial increase in hardness after austempering,

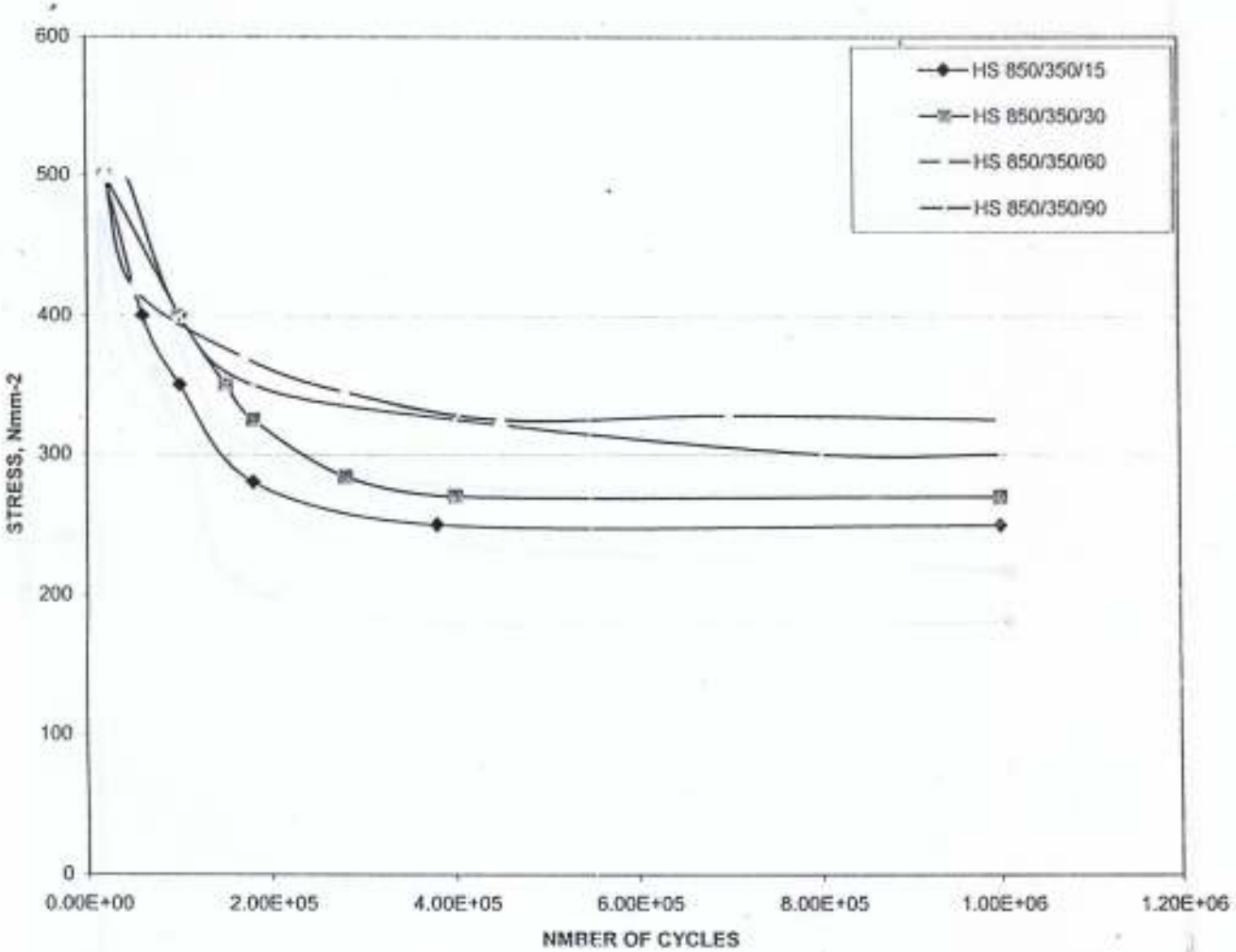

FIGURE 22 S -N CURVE SHOWING THE EFFECTS OF AUSTEMPERING PARAMETERS ON THE FATIGUE STRESS FOR HIGH SILICON ALLOYS HS30 131,132,133,AND 134.

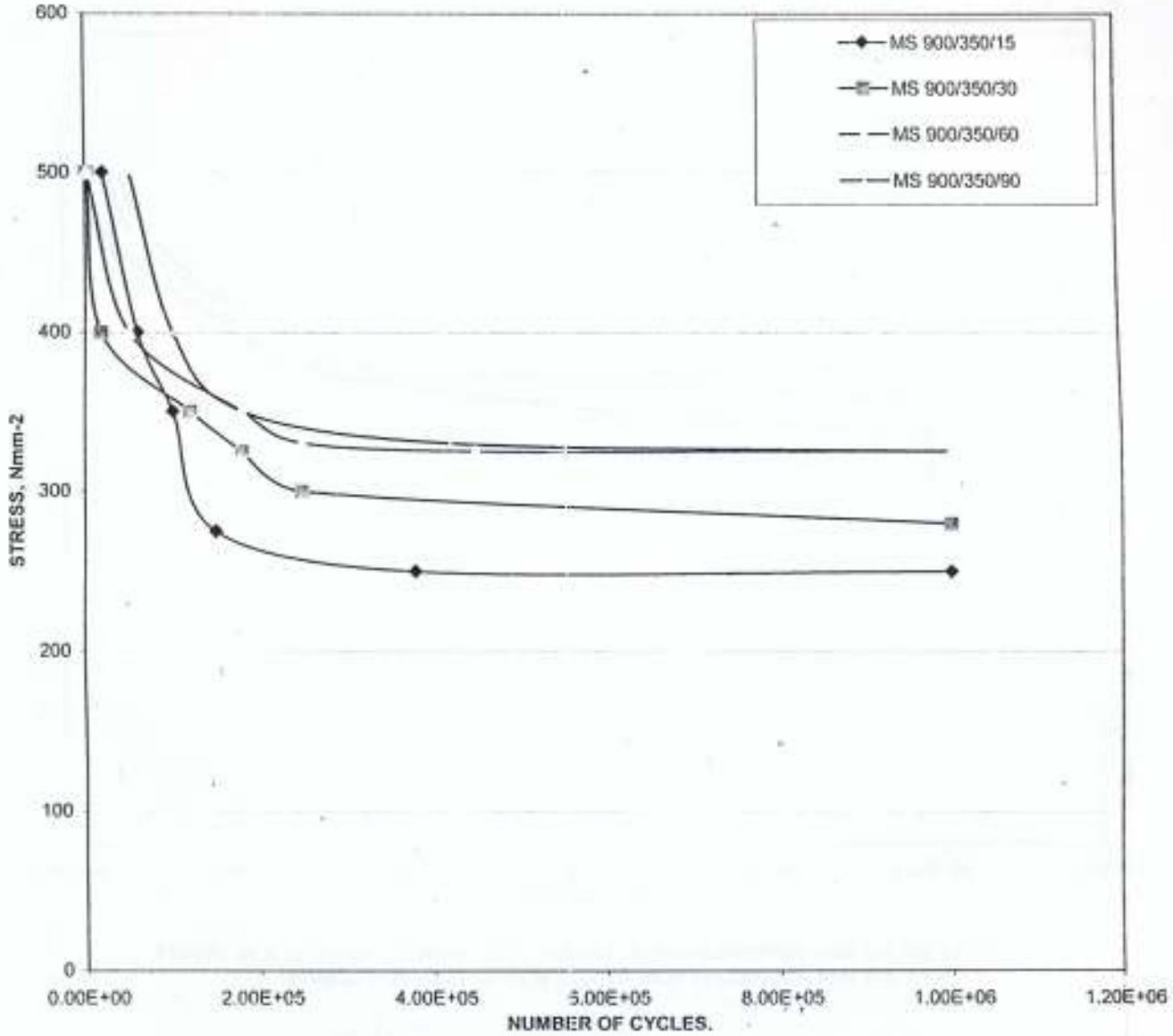

FIGURE 23 S-N CURVE SHOWING THE EFFECTS OF AUSTEMPERING TIME ON FATIGUE STRESS FOR MEDIUM SILICON ALLOYS MS26 231,232,233 AND 234 ,

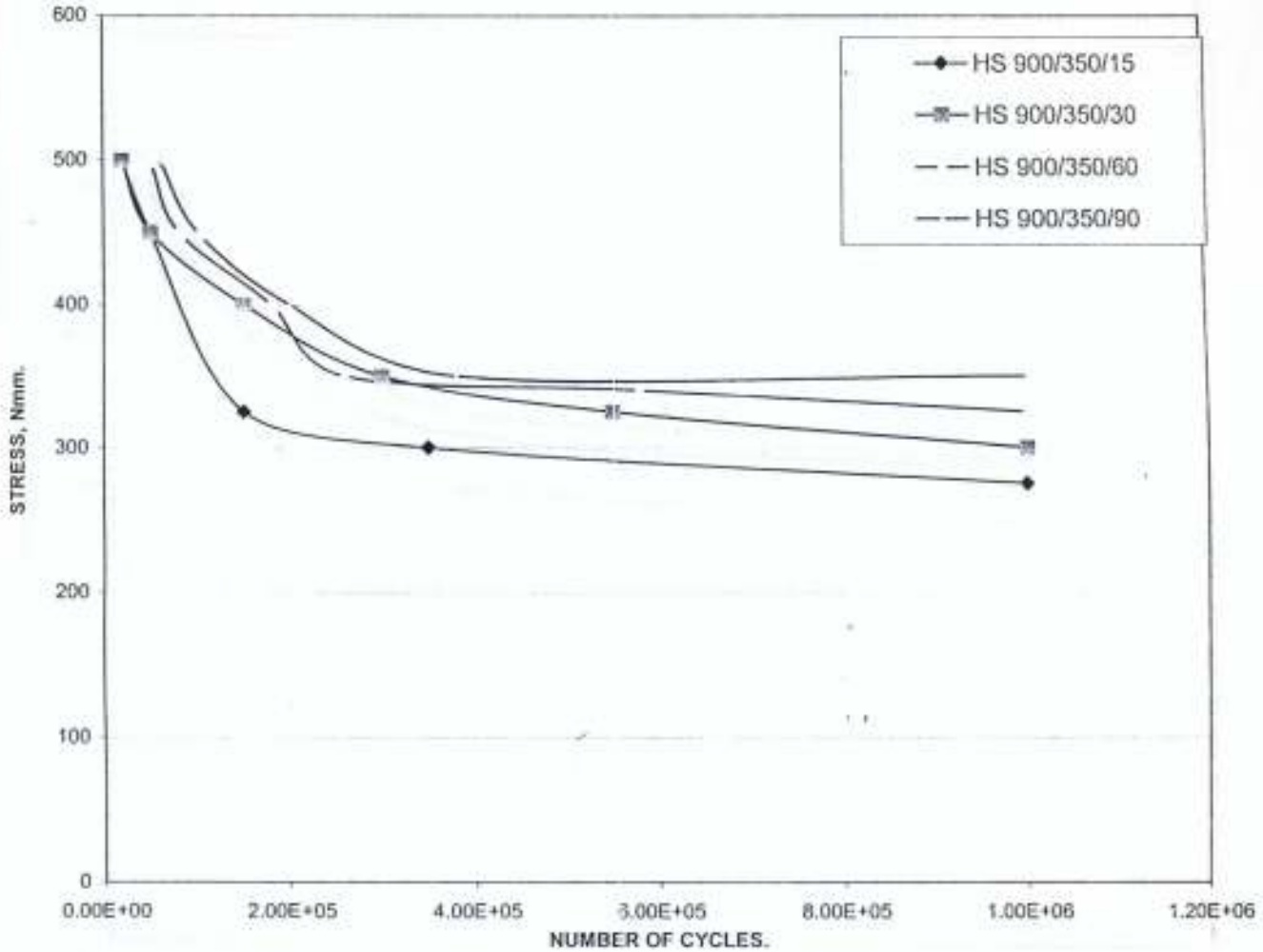

FIGURE 24 S -N CURVE SHOWING THE EFFECTS OF AUSTEMPERING TIME ON THE FATIGUE STRESS FOR HIGH SILICON ALLOYS HS30 231,232, 233, AND 234.

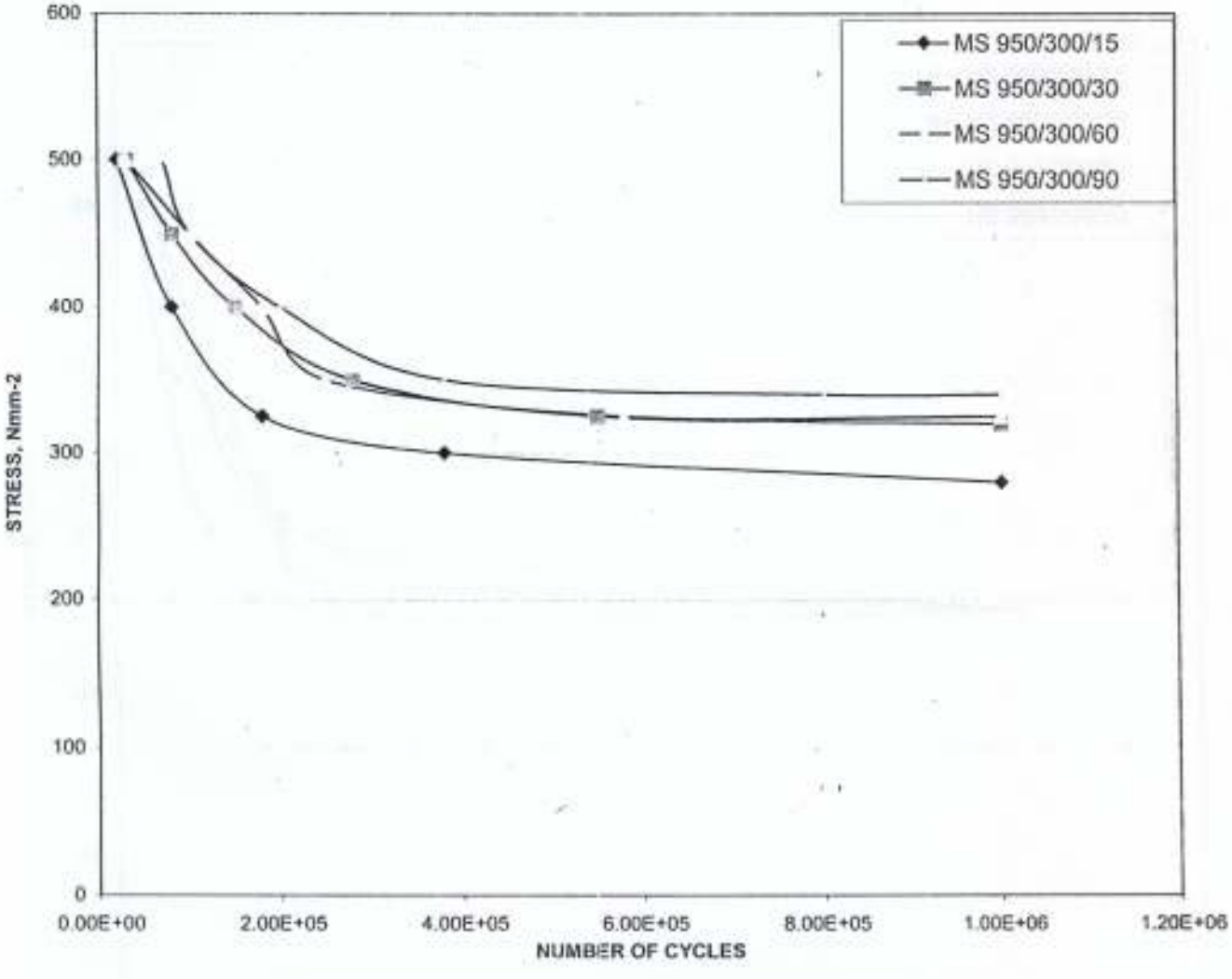

FIGURE 25 S-N CURVE SHOWING THE EFFECTS OF AUSTEMPERING TIME ON THE FATIGUE STRESS FOR MEDIUM SILICON ALLOYS MS26 321,322,323

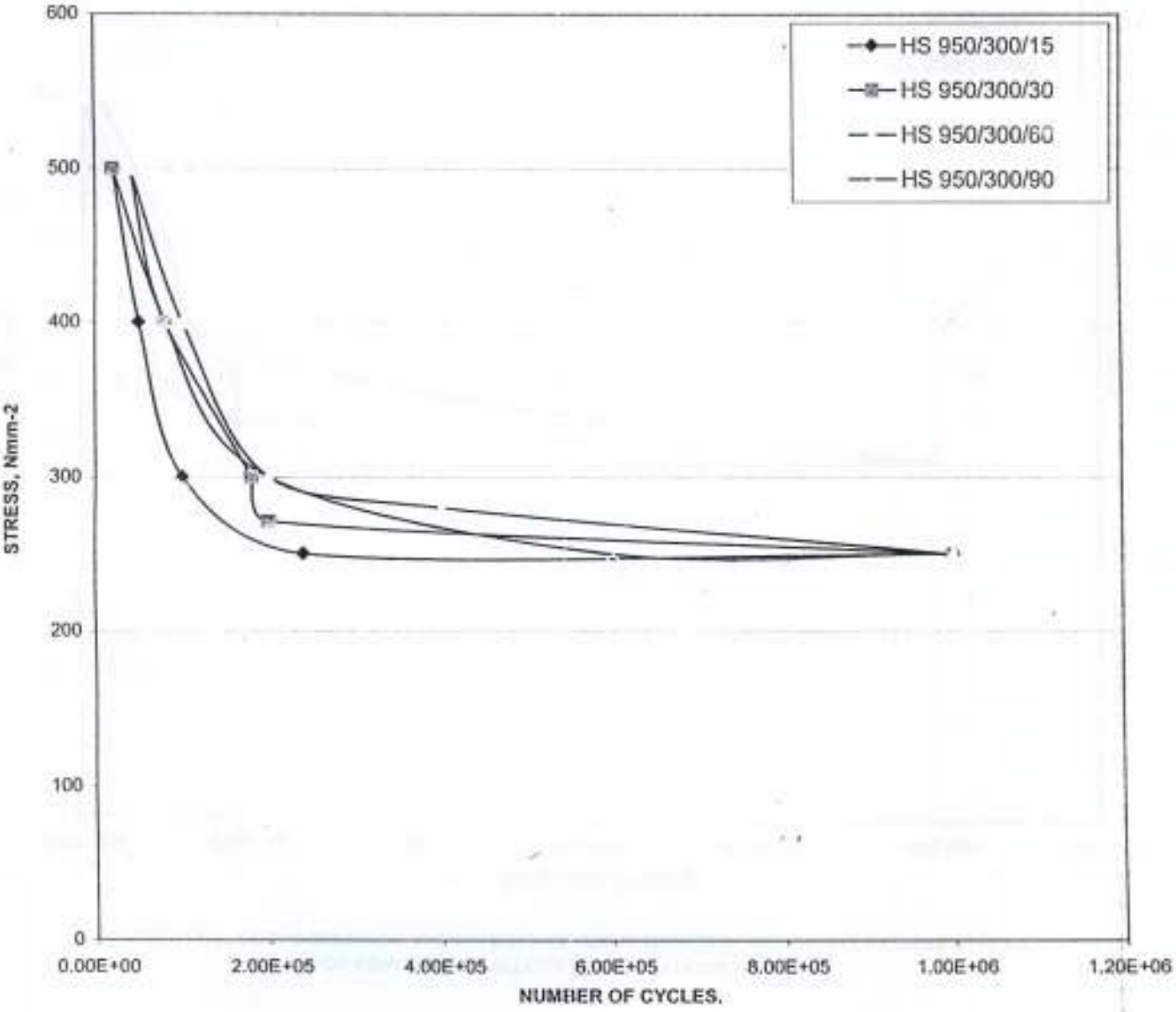

FIGURE 26 S-N CURVE SHOWING THE EFFECTS OF AUSTEMPERING TIME ON THE FATIGUE STRESS HIGH SILICON ALLOYS HS30 321,322,323 AND 324.

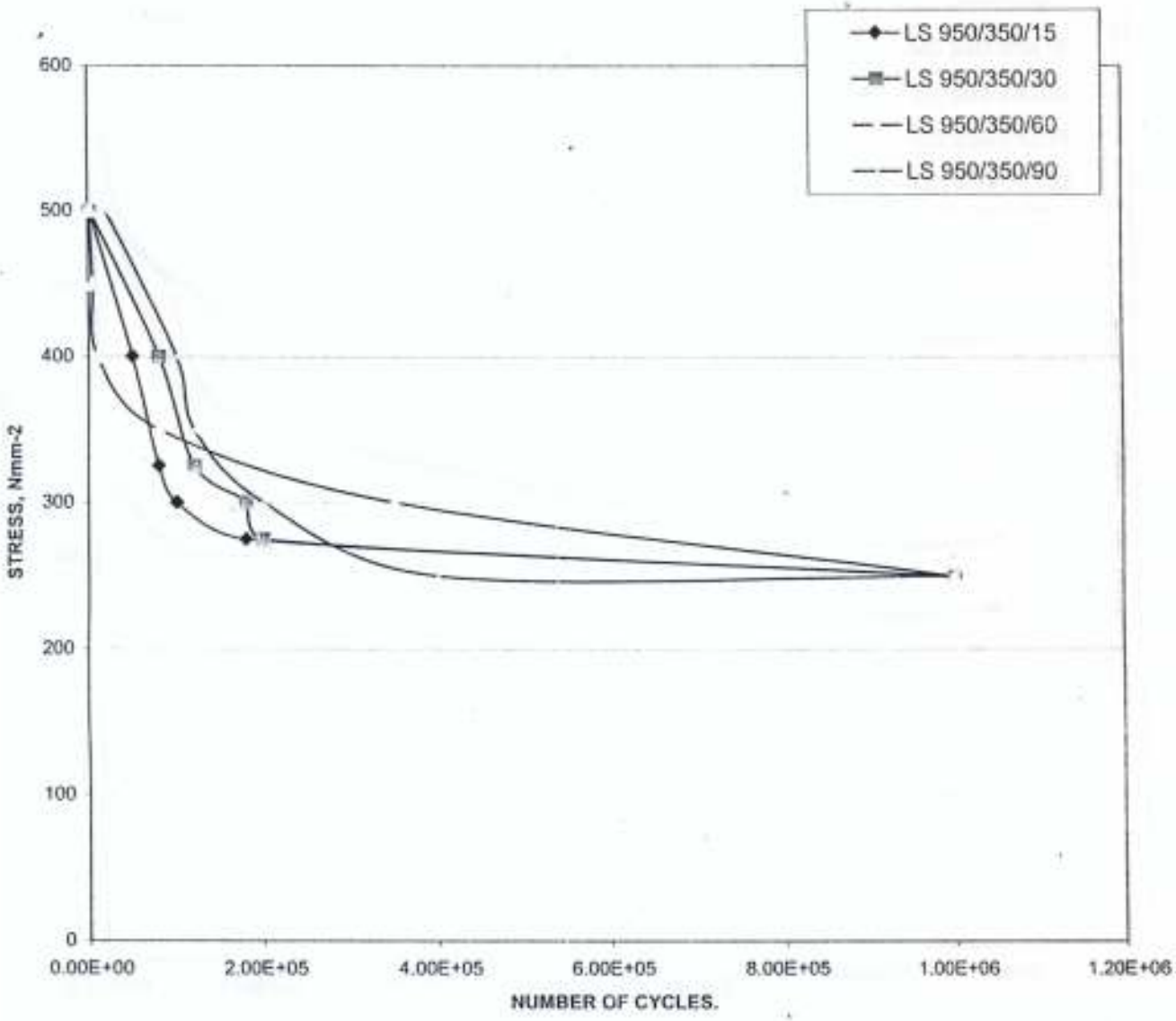

FIGURE 27 S-N CURVE SHOWING THE EFFECTS OF AUSTEMPERING TIME ON THE FATIGUE STRESS FOR LOW SILICON ALLOYS LS20 331,332,333 AND 334.

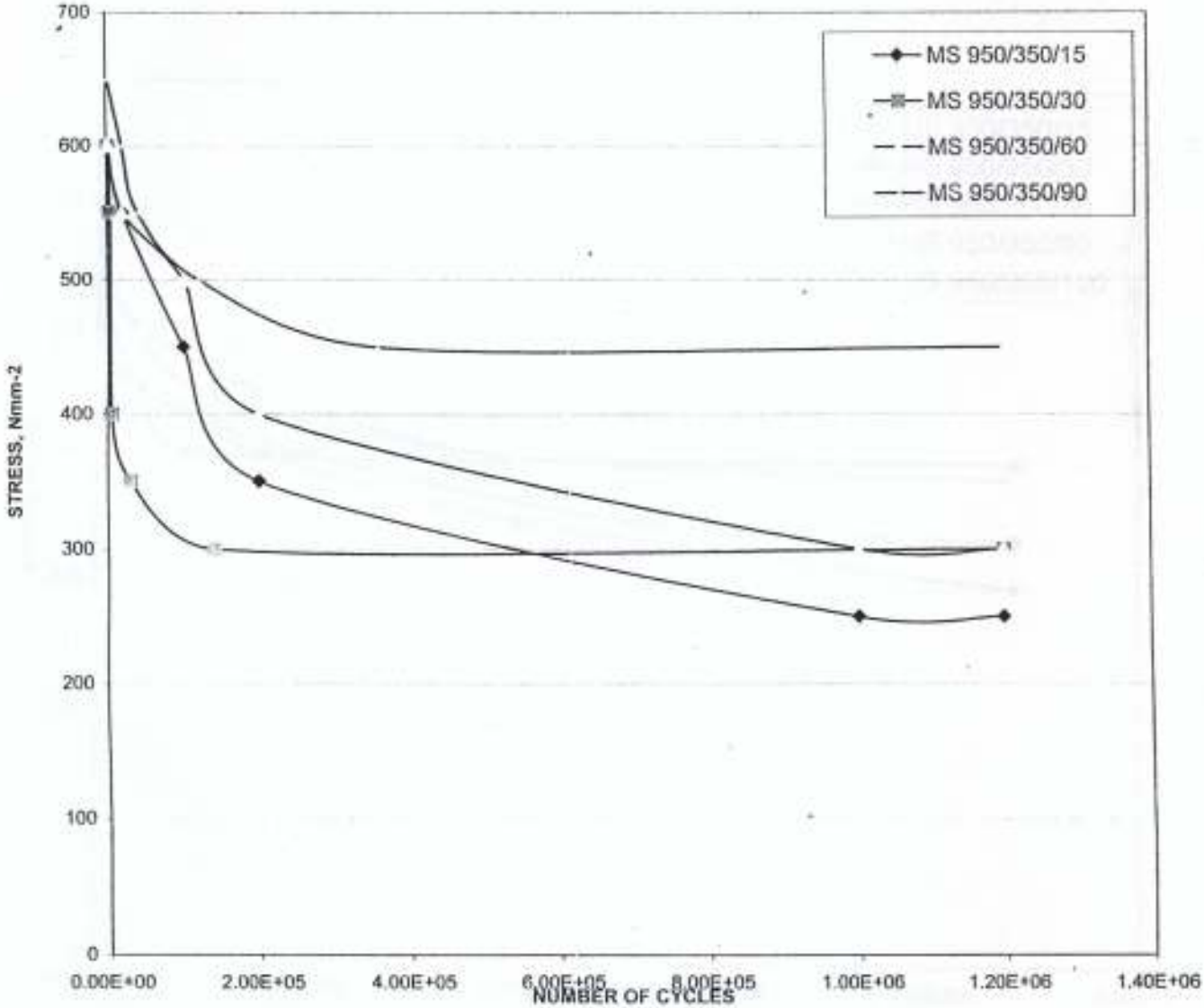

FIGURE 28 S-N CURVE SHOWING EFFECT OF AUSTEMPERING TIME ON FATIGUE STRESS FOR MEDIUM SILICON ALLOYS MS26 331,332,333 AND 334.

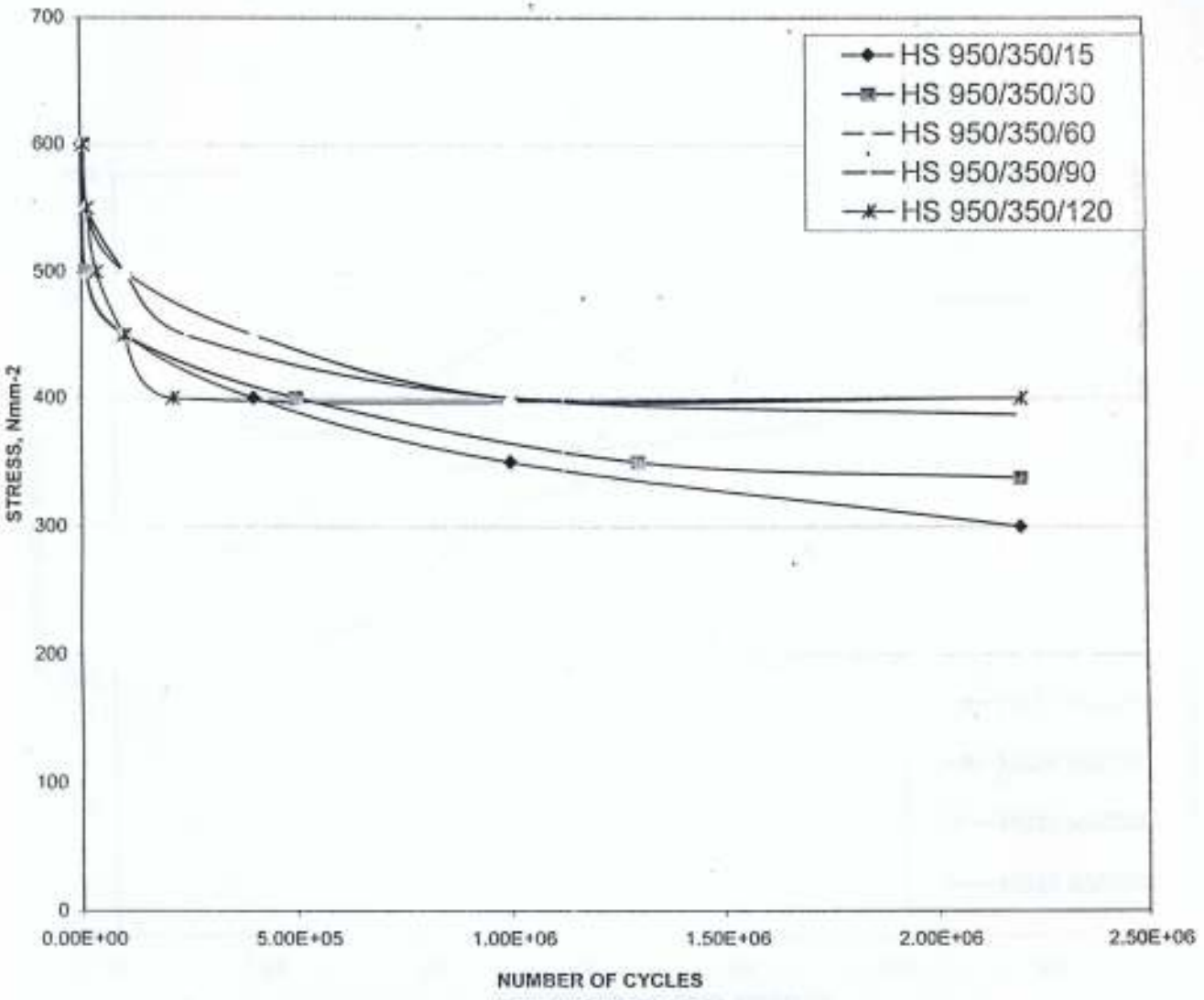

FIGURE 29 S-N CURVE SHOWING THE EFFECTS OF AUSTEMPERING TIME ON THE FATIGUE STRESSFOR HIGH SILICON ALLOYS LS30 331,332,333 AND334

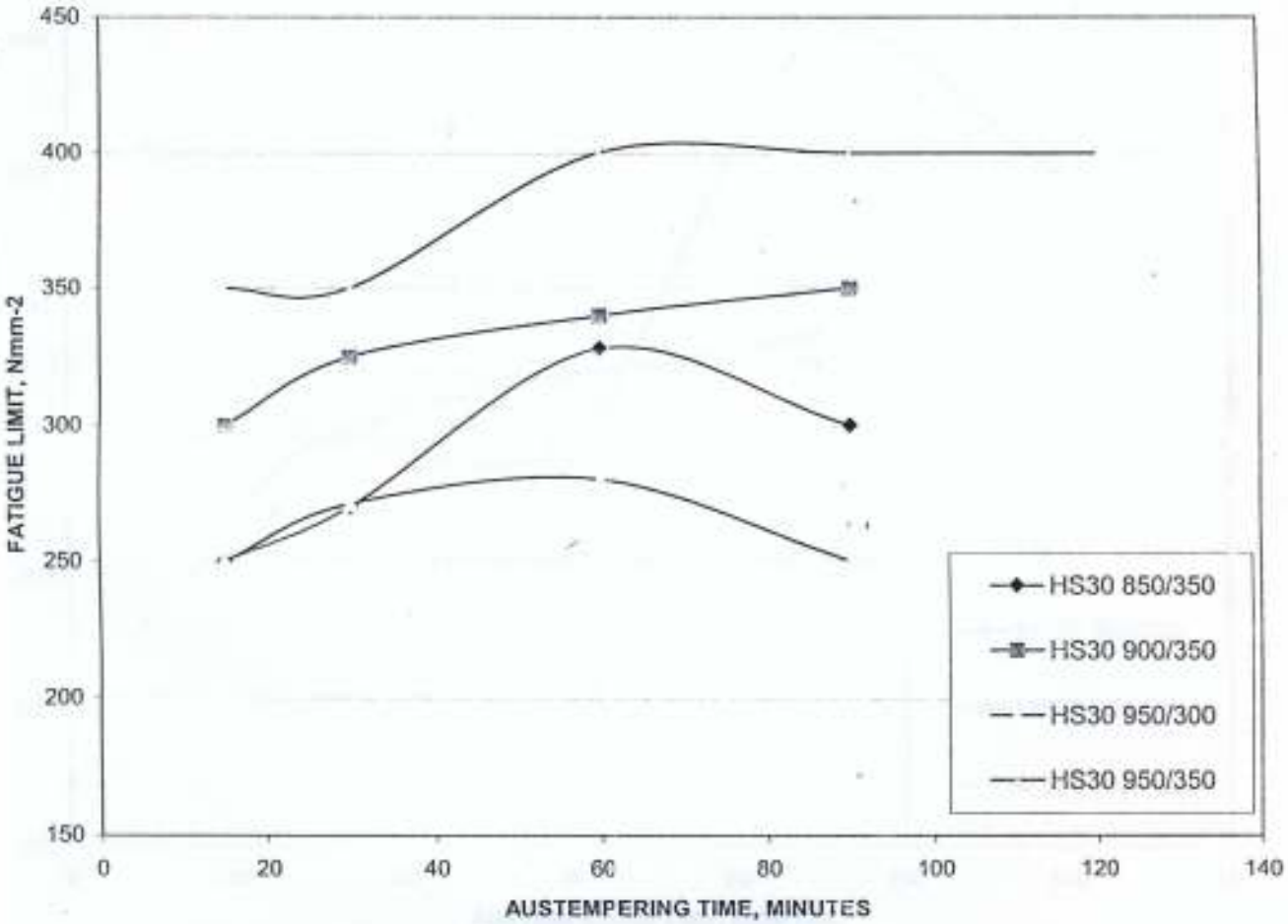

FIGURE 30 EFFECT OF CHANGES IN AUSTENITISING AND AUSTEMPERING TEMPERATURE AND AUSTEMPERING TIME ON THE FATIGUE LIMIT OF HIGH SILICON ALLOYS HS39 13,23,32 AND 33.

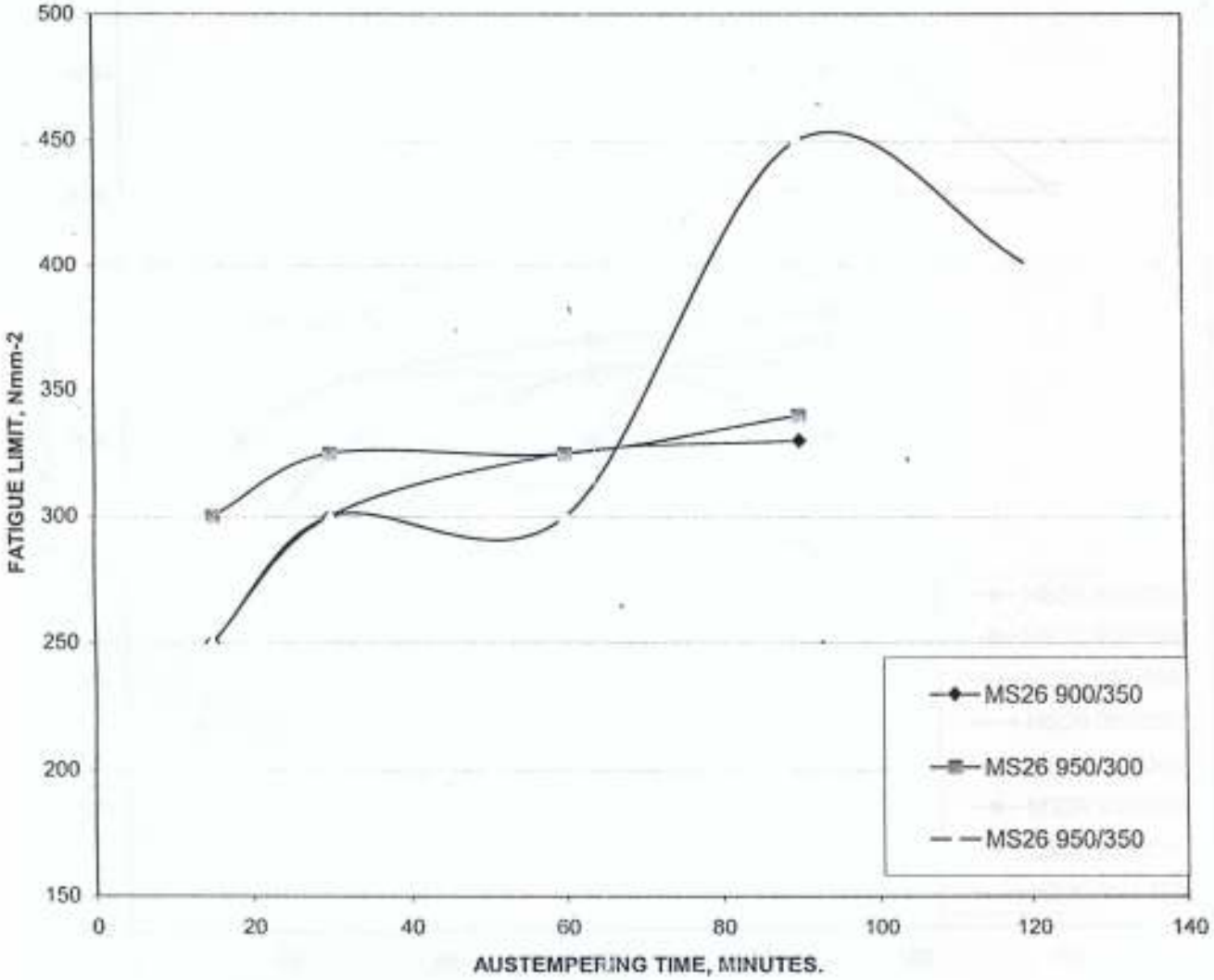

FIGURE 31 EFFECT OF CHANGES IN AUSTENITISING AND AUSTEMPERING TEMPERTURE AND AUSTMPERING TIME ON THE FATIGUE LIMIT OF MEDIUM SILICON ALLOYMS26 23, 32 AND 33.

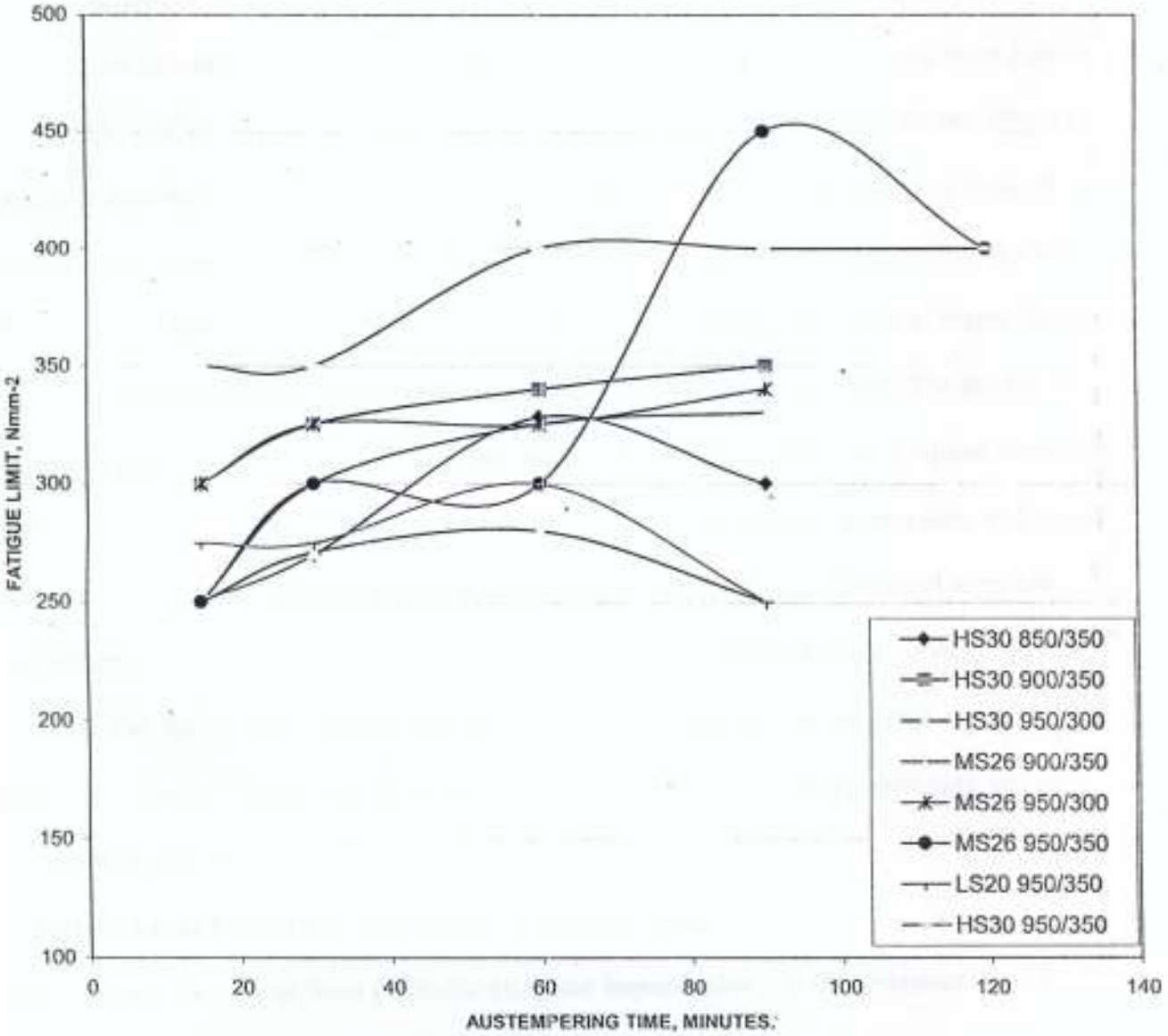

FIGURE 32 EFFECTS OF SILICON LEVEL SENSITIVITY AND CHANGES IN AUSTEMPERING PARAMETERS ON THE FATIGUE LIMIT AUSTEMPERED ALLOYS.

corresponds to the transformation of the as cast matrix structure to austenite. The hardness decreases at longer austempering times as the austenite grain size increases. The responses of various alloys to hardness after austempering are shown in Figures 36 to 38. From these figures it is evident that the alloys respond to hardness differently. The behaviour of the alloys to changes in austempering parameters is very complicated. Within the austempering period of 30 to 60 minutes, hardness decreases with increasing austempering time and temperature as shown in Figure 36 for low silicon alloys, in Figure 37 for medium silicon alloys and in Figure 38 for high silicon alloys. While the hardness decreases, the fatigue strength increases. The gradual rise in hardness can be attributed to carbide precipitation, which causes reduction in fatigue strength. The low fatigue strength and impact toughness at low austempering temperature and short austempering times can be attributed to the embrittling effect due to the presence of martensite at prior austenite grain boundaries. The changes can also be related to the amount of retained austenite. The higher the austenitising temperature, the hardness is expected to be lower. However the hardness increment of the specimen can be attributed to work hardening and phase transformation into martensite.

5.3. Fatigue Limit Prediction from Impact Toughness Data

Table 10 shows the fatigue limit predicted using the impact value and the estimated diameter of the nodules. Figure 38 is a graphical representation of the predictions.

It could be concluded that:

1. Fatigue limit of the various alloys is between 300 and 400Nmm^{-2}.
2. Fatigue limit increases with increasing austempering temperature.
3. The impact toughness and fatigue strength are closely related and the model can be used to

predict the fatigue limit from any given impact values irrespective of the silion level and austempering parameter employed.

4. The model indicates that ADI fatigue limit increases with increasing toughness and decreasing nodule size. This implies that toughness and nodule size are the two major factors controlling the fatigue limit of ADI.

TABLE 9 Silicon Level Sensitivity and Fatigue Limit as A Function of Austempering Time.

Austenitising / Austempering Temperature °C	Low Silicon Austempering Time (Minutes) /Fatigue limit					Medium Silicon Austempering Time (Minutes) /Fatigue limit					High Silicon Austempering Time (Minutes) /Fatigue limit				
	15	30	60	90	120	15	30	60	90	120	15	30	60	90	120
850/350	-	-	---	-	-	-	-	-	-	-	250	270	328	300	-
900/350	-	-	-	-	-	250	300	340	350		300	325	340	350	-
950/300	-	--	--	--	--	300	325	325	340		250	271	280	250	--
950/350	275	275	300	250	--	250	300	300	450	400	350	350	400	400	400

TABLE 10. Interrelationship between Impact Strength, Nodule Diameter and Fatigue Limit.

ALLOY TYPE	IMPACT VALUE (I), J	FATIGUE VALUE, (Experimental)	MEAN STRESS $S_C = \frac{1}{2}(S_{max} + S_{min})$	PREDICTED VALUE, $S_C = k * I^{0.31} * d^{-0.4}$ (k =70; d = 0.45μm)
HS30 850/350	90	328	387.5	371.609
MS26 900/350	82	330	387.5	361.4
HS30 900/350	105	350	425	389.197
MS26 950/300	43	340	420	309.163
HS26 950/300	46	280	300	303.836
LS20 950/350	56	300	387.5	322.307

5.3.2 Computer Model For the Prediction of the Amount of Retained Austenite.

Detailed computer model analyses are contained in Appendix I-IV. Appendix I gives information on the Operation of the computer model. This is already stored in the computer for future use. Appendix II and III is the FORTRAN programme for the prediction of any ADI alloy and the graphics. The results of the predicted amount of retained austenite is stored in the computer and are contained in Appendix IV and are graphically represented in Figures 33 to 35. From the results it is observed that the variation of volume fraction of austenite depends on the austenitising temperature and austempering temperatures and time.

Low Austenitising Temperature and Low Austemperimg Temperature

Retained Austenite of Low Silicon Alloys decreases with increasing austempering time. In the Medium and High Silicon alloys, the retained austenite increases between 15 and 30 minutes, thereafter it decreases with further increase in austempering time.

Low Austenitising with Moderate and High Austempering

Retained Austenite of Low Silicon and Medium Silicon Alloys decreases with increasing austempering time, while the High Silicon Alloys witness an increase between 15 and 30 minutes, thereafter there is decrease with further increase in austempering time.

Moderate austenitising with low austempering

Retained Austenite of Low Silicon and Medium Silicon Alloys increases between 15 and 30 minutes thereafter there is decrease with further increase in austempering time, while the High Silicon Alloys witness an increase with increasing austempering time between 15 and 60 minutes and thereafter there is slight decrease.

derate Austenitsing And Moderate Austempering

tained Austenite of Low Silicon and Medium Silicon Alloys decreases with increasing austempering ne. There is an increase between 15 and 30 minutes followed by slight reduction up to 90 minutes d slight increase at 120 minutes in the amount of retained austenite for the High Silicon Alloys.

derate Austenitising Temperature and High Austempering Temperature.

tained Austenite of Low Silicon and Medium Silicon and High Silicon Alloys increases between 15 d 30 minutes, thereafter there is decrease with further increase in austempering time.

igh austenitising Temperature; Low, Moderate and High Austempering Temperatures.

tained Austenite of Low Silicon increases with increasing austempering time up to 60 minutes, hile its value for Medium Silicon and High Silicon Alloys increase with increasing austempering ne extended up to 90 minutes.

4.Inter-Relationship between Microstructural Features and Impact and Fatigue Strength.

he inter-relationship between microstructural features and impact and fatigue strength are shown in able 14. The results show that silicon has been used successfully to control carbide and it has a lative effect on fatigue strength and impact toughness. It has earlier been suggested that silicon has e effect of modifying the Fe-C phase diagram such that a higher solution treatment temperature is eeded to fully austenitise the iron. The carbon that is present in the austenite renders it thermally and echanically stable and accounts for the high impact energy and fatigue strength obtained. Under the ustempering conditions, carbon stabilizes the austenite such that carbide precipitation does not occur mmediately resulting in a microstructure containing high carbon austenite plus acicular ferrite, leading o optimum fatigue and impact properties. As a result of second stage reaction, when the high carbon ustenite starts to decompose into ferrite plus carbide, the austenite carbon content is lowered, leading o further transformation to bainitic ferrite and carbides. The precipitation of carbides probably leads to eduction in fatigue strength and impact toughness. The amount of the retained austenite is lowest for

low silicon alloys. Hence medium and high silicon alloys exhibit more fatigue resistance than low

icon at all austempering conditions.

shown in plate 2, the microstructure contains a mixture of coarse and fine ferrite platelets and

ble11. Optimum Values of Fatigue Limits, Impact Toughness and Retained Austenite.

ustenit ustemp ing °C	Alloy Type	Fatigue limit Nmm^{-2}	Austem Pering Time (min)	Hardness	Austem pering Time (min)	Impact toughness (Joules)	Austem pering Time (min)	Retained austenite %	Austem-pering Time (min)
50/300	LS	-	-	-	-	34	120	10.03	15
	MS	-	-	-	-	45	120	19.96	15
	HS	-	-	-	-	43	90	26.797	30
50/350	LS	-	-	309	60	80	30	21.071	15
	MS	-	-	409	120	80	30	31.92	15
	HS	328	60	-	-	90	60	34.85	30
00/300	LS	-	-	-	-	33	30	8.62	15
	MS	-	-	-	-	45	15	18.99	30
	HS	-	-	-	-	38	90	25.68	90
00/350	LS	-				65	30	23.16	30
	MS	330	90	309	90	82	60	32.695	30
	HS	350	90	398	30	105	60	35.197	60
50/300	LS	-	-			38	60	14.46	60
	MS	340	90	426	90	43	30	25.32	90
	HS	280	60	409	15	46	90	30.19	90
50/350	LS	300	60	241	90	56	60	34.92	60
	MS	450	90	321	30	70	90	41.66	90
	HS	400	90	409	15	115	60	40.95	90

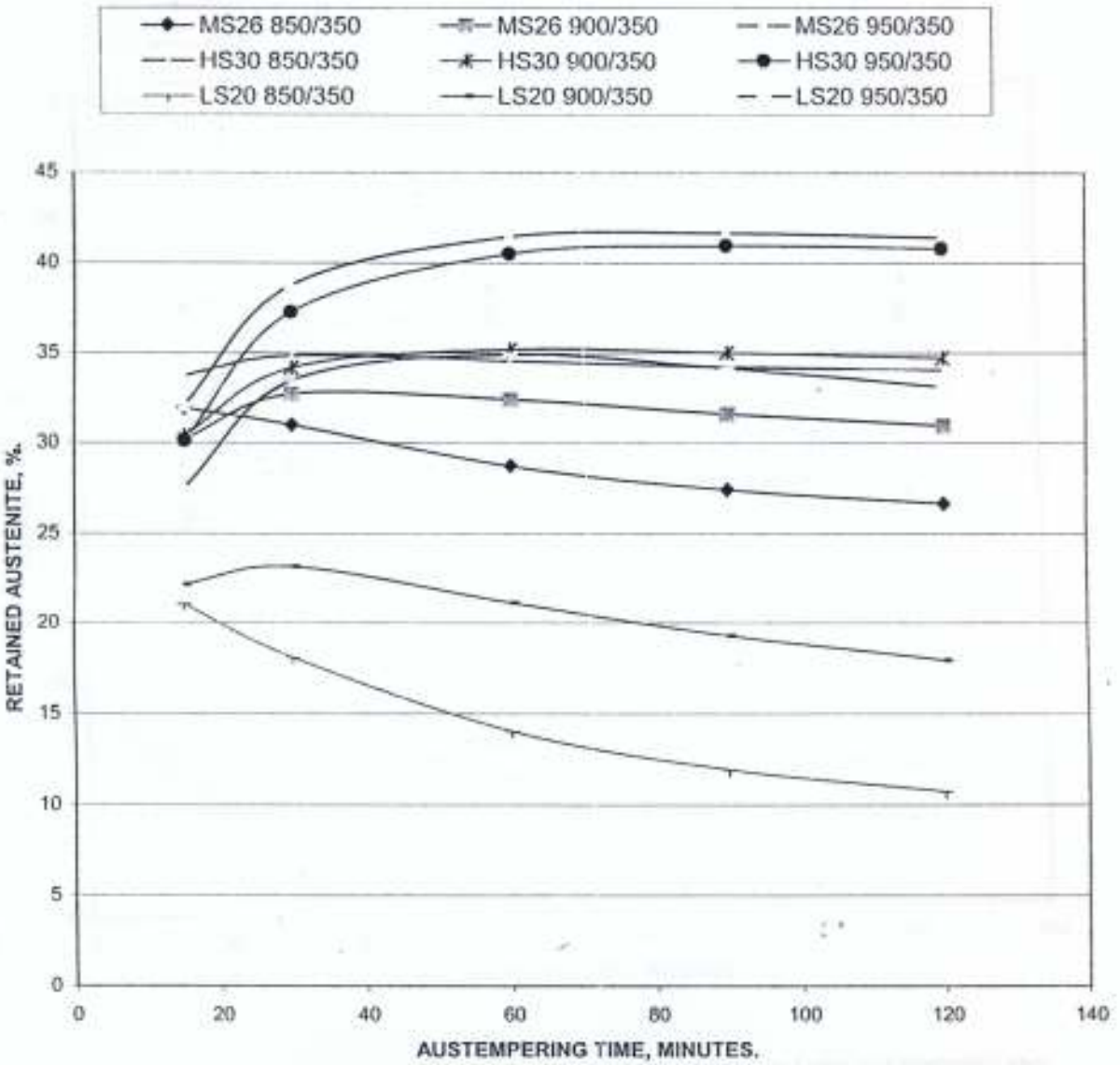

FIGURE 33 ESTIMATED RETAINED AUSTENITE FOR ALLOYS AUSTEMPERED AT 850/350, 900/350 AND 950/350

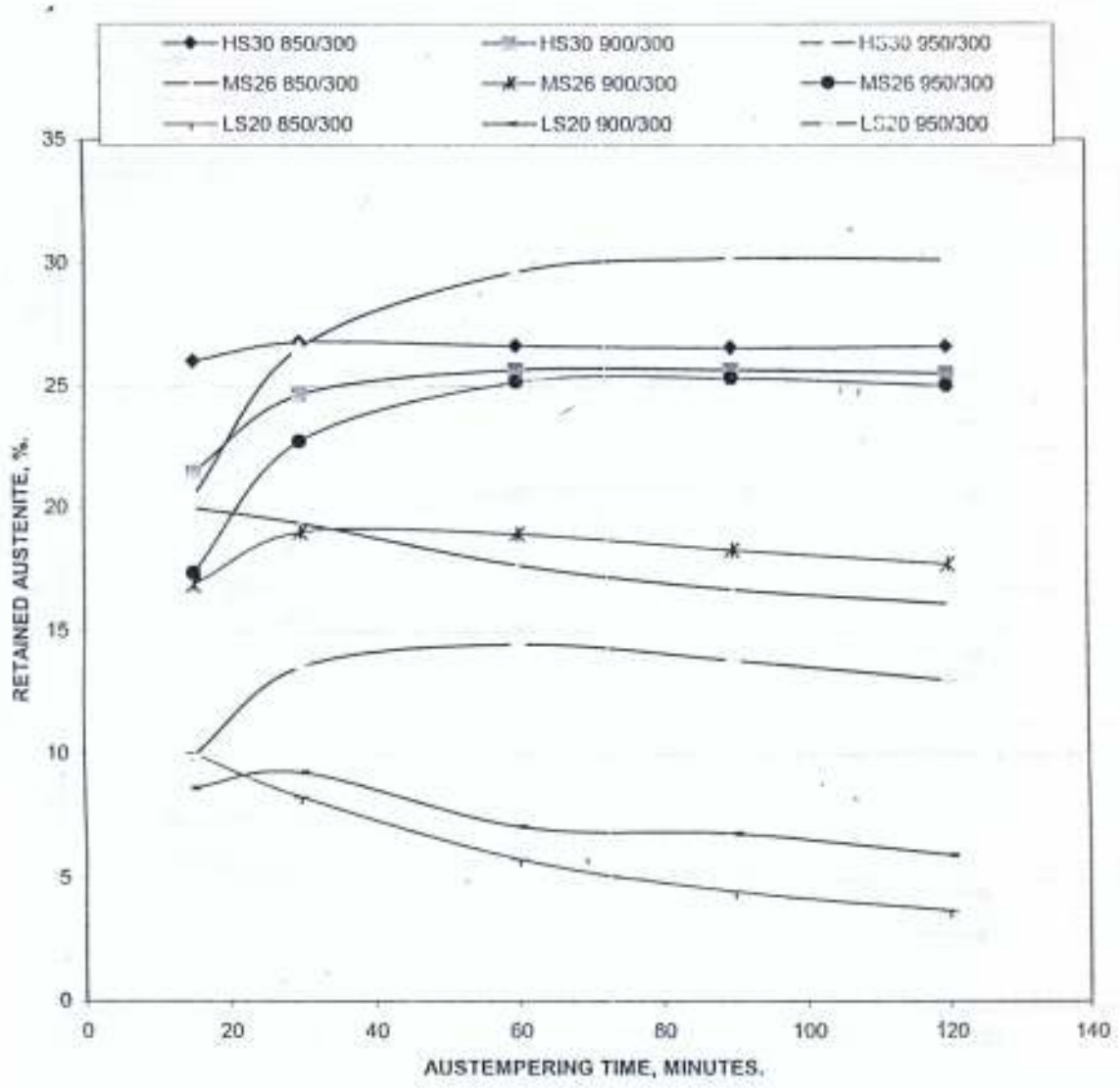

FIGURE 34 ESTIMATED AMOUNT OF RETAINED AUSTENITE FOR ALLOYS AUSTENITISED AND AUSTEMPERED AT 850/300, 900/300 AND 950/300.

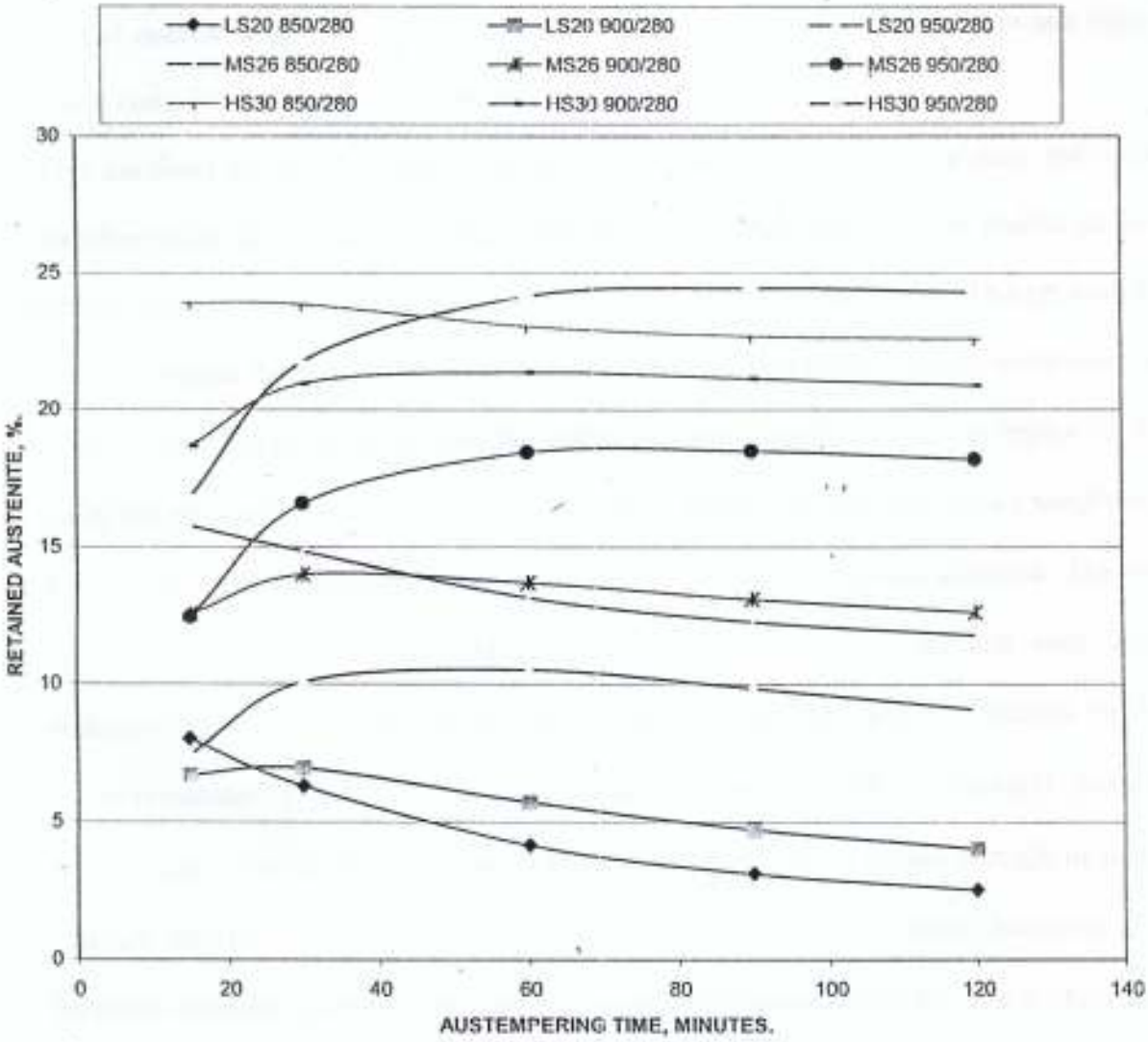

FIGURE 35 ESTIMATED AMOUNT OF RETAINED AUSTENITE FOR ALLOYS AUSTENITISED AND AUSTEMPERED AT 850/280, 900/280 AND 950/280.

uniformly distributed retained austenite. Since this high carbon austenite is stable at room temperature, the resulting microstructures consist of ferrite and retained austenite. This is the desired microstructure. From the retained austenite estimate, the low medium and high silicon alloys contain 34.92%, 41.66% and 40.95% respectively.

This confirms the earlier suggestions that silicon contracts the austenite zone and reduces the transformation rate of austenitizing. Furthermore, the eutectoid point is shifted to lower the carbon content and decrease the carbon solubility in austenite matrix. During austempering, silicon restrains the formation of carbide and makes carbon atoms saturate in retained austenite when bainitic ferrite grows, so that the stability of supercooled austenite is improved. This will delay the nucleation of fatigue crack. Increase in fatigue strength and impact toughness is also further enhanced by interstitial carbon, which is present in retained austenite. The interstitial carbon induces strain ageing. This increases with carbon content and with increase in austempering time. Thus we observe that fatigue strength and impact toughness increase with retained austenite, (Table 11). From the estimated amount of retained austenite (Figures 33 to 35) and the fatigue limits (Figures 30 to 32), it is confirmed that the fatigue strength increases as the retained austenite increases. This can be attributed to its strain-hardening behavour. There may be strain-induced martensite formation in some austenitic steels but this is not likely to occur in the austempered ductile iron because of its high carbon content. Proper austempering thus produces a unique bainitic structure (often called ausferrite) in ADI that consists of high carbon (plate 2 and 3). This unique microstructure provides excellent mechanical properties of ADI : high fatigue strength, high impact toughness and high retained austenite.

Acicular ferrite plates with high carbon austenite distributed uniformly in it (plate 4) obtained

from low silicon alloys austenitised at 850°C is responsible for the high impact obtained from this alloy.

Alloys with average fatigue strength and high impact strength is obtained from medium silicon austenitised at 900°C and-austempered at 350°C. The structure contains lower and upper bainite with graphite nodules dispersed in it (plate 6b).

Austenitising at low solution treatment temperature (850°C), high and medium silicon alloys produce structures containing free ferrite or procutectoid ferrite as a result of a three-phase region of austenite-ferrite-graphite phase, (plates 7and 9b). This structure is responsible for the poor fatigue, impact and low retained austenite of these alloys. Increasing the austenitising temperature to 950°C with moderate austempering temperature (300°C) leads to the formation of grain boundary lower bainite microstructure resulting in low fatigue and impact properties, (plate 8). Both pearlitic bainite and columnar bainite structures give poor mechanical properties.

5.5. Optimum Set of Compositional and Heat Treatment Variables.

Tables 13 show the time for the onsets of stage I reaction (processing window open) and the time indicating the termination of stage I reaction (processing window closed). The end of the first stage corresponds to the maximisation of the fraction of bainitic ferrite and the enrichment of the austenite, the second with the onset of carbide precipitation. The time interval between these two stages is the heat treatment window. From Table 13, the processing window or the time required to obtain the optimum amount of retained austenite in high silicon alloys austenitised and austempered at 850/350 is observed to open at a short austempering time (28 minutes) and closes after 60 minutes. For the fatigue strength and impact toughness, it takes a longer austempering time before the commencement of the first stage reaction (50 and 55 minutes respectively). In the

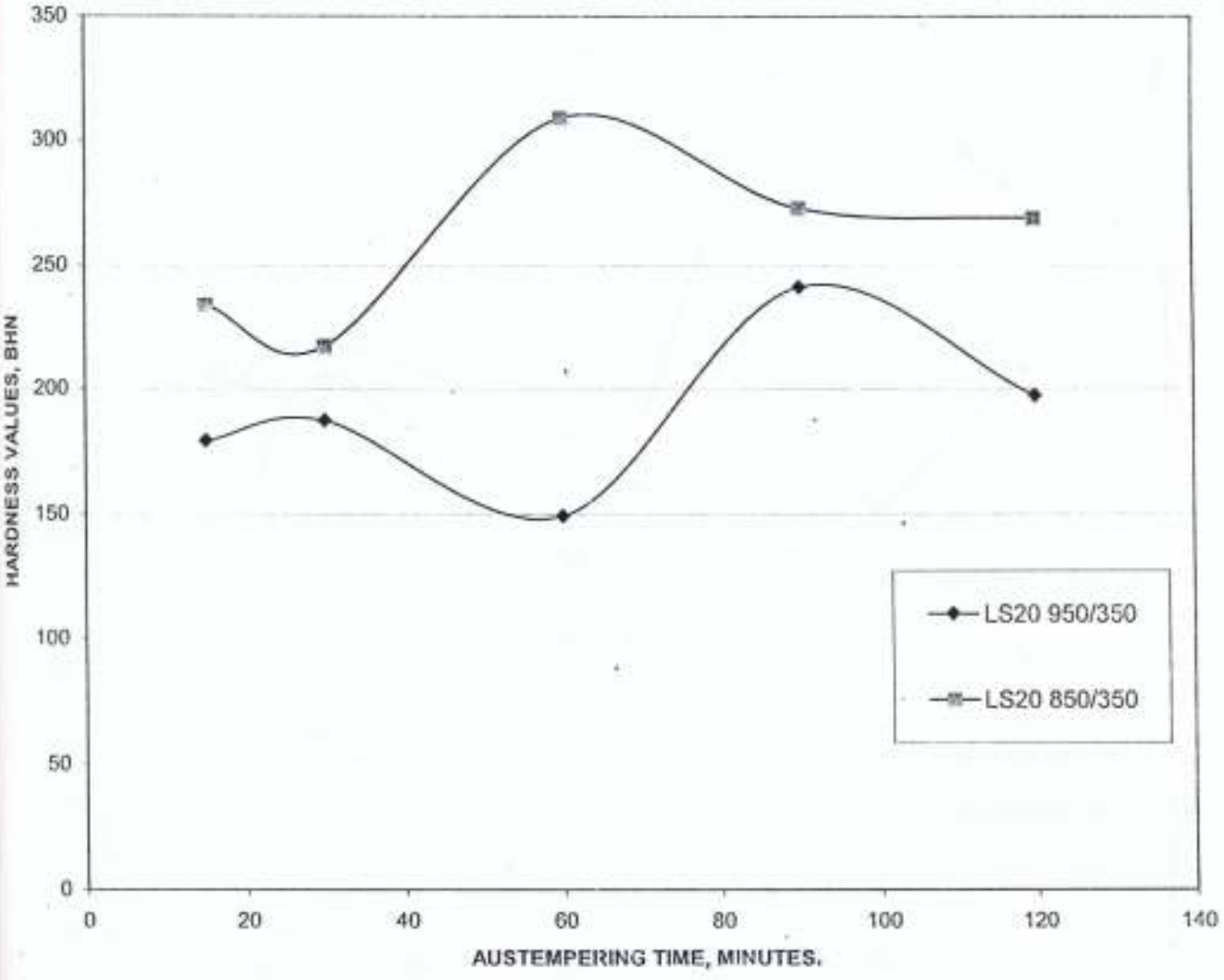

FIGURE 36 EFFECT OF CHANGES IN AUSTENITISING AND AUSTEMPERING TEMPERATURES WITH TIME ON THE HARDNESS OF LOW SILICON ALLOYS LS20 33 AND 13

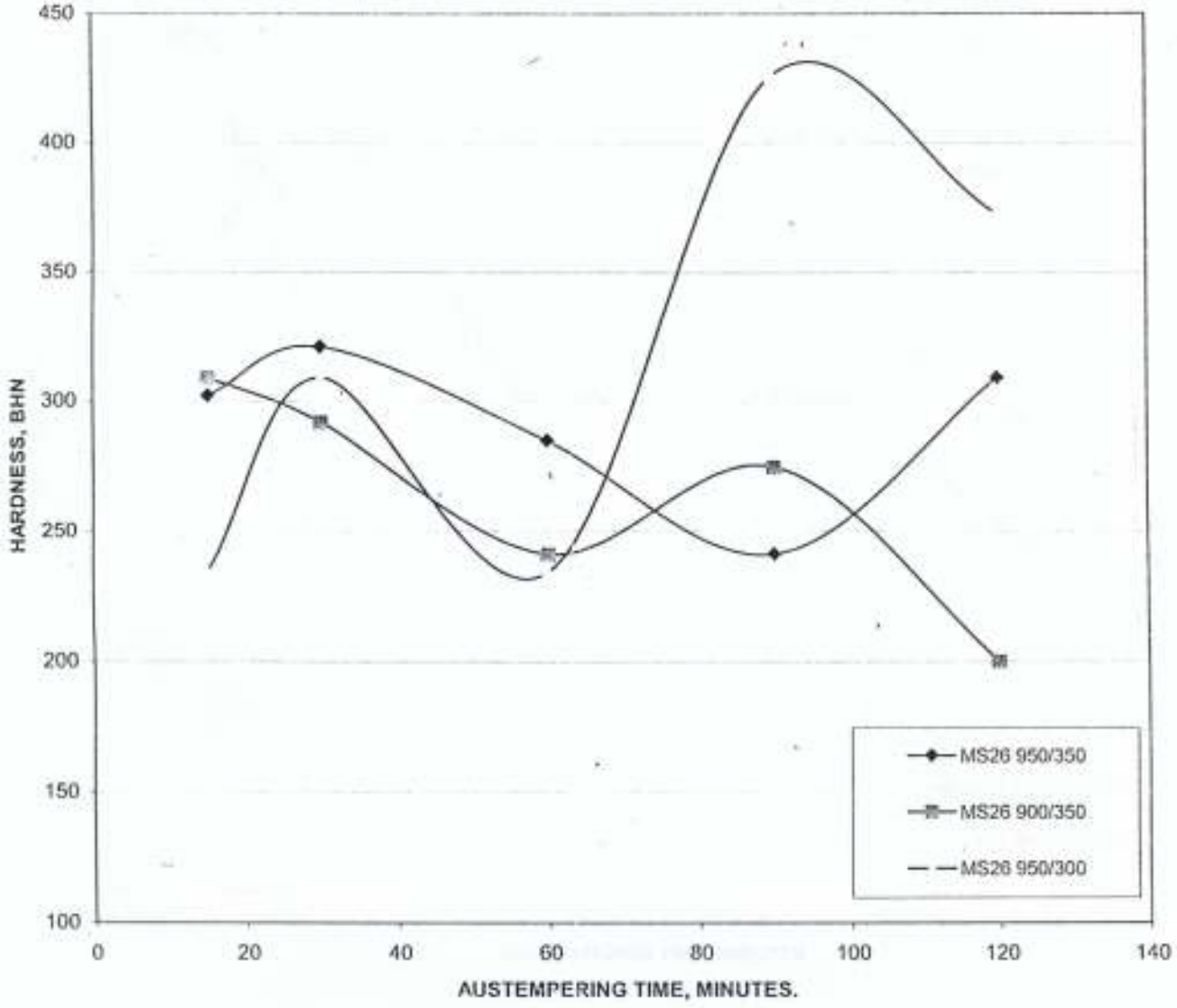

FIGURE 37 EFFECT OF CHANGES IN AUSTENITISING AND AUSTEMPERING TEMPERATURES WITH TIME ON THE HARDNESS OF MEDIUM SILICON ALLOYS MS26 33, 23 AND 32.

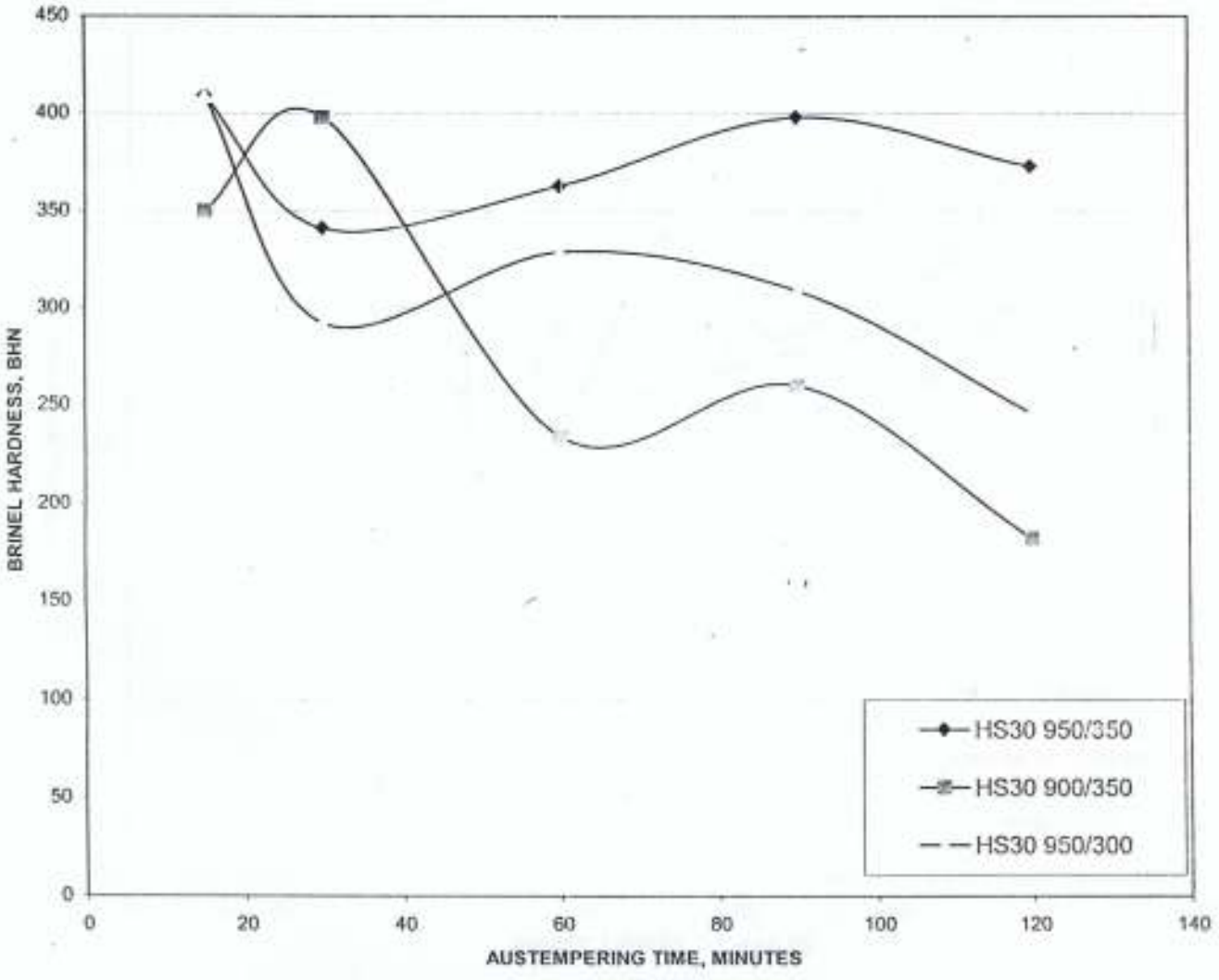

FIGURE 38 EFFECT OF CHANGES IN AUSTENITISING AND AUSTEMPERING TEMPERATURES AND TIMEON HARDNESS OF HIGH SILICON ALLOYS HS30 33,23, AND 32

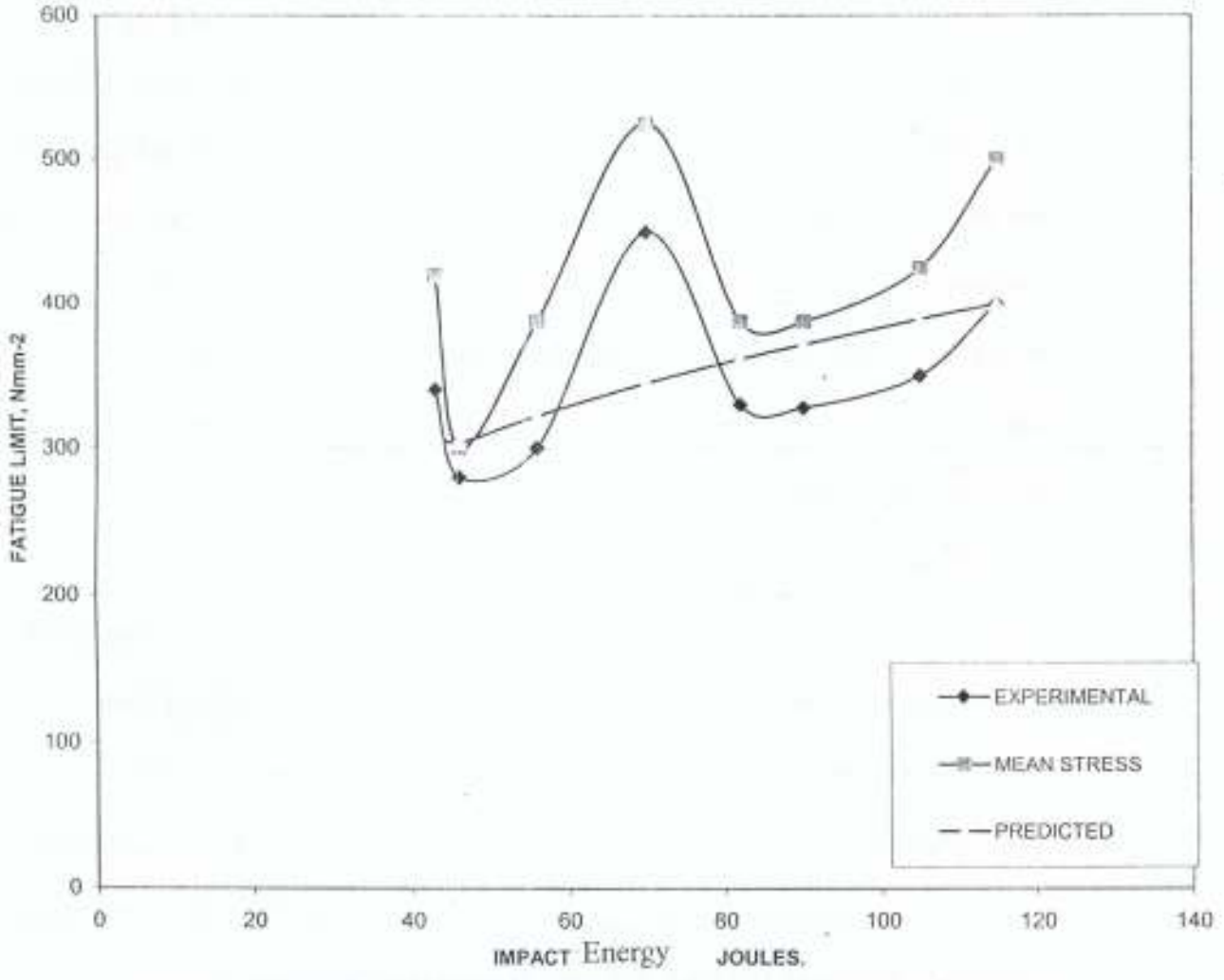

FIGURE 39 COMPARISON OF THE EXPERIMENTAL FATIGUE LIMIT AND THE PREDICTED VALUES.

austempering process, stage I and stage II are separated in time such that a plot of impact toughness and fatigue limit goes through a plateau (referred to as the processing window). It can be seen from these curves (from Figure 13), that three regions are actually visible: The initial part of stage I (opening period) which represents the nucleation and growth of ferrite in the relatively unsegregated volumes near the graphite nodules. This region obeyed the Johnson – Mehl equation as earlier stated. This is followed by the region of the processing window. The stage I reaction is a diffusion controlled plate growth of decreasing nucleation rate while the reaction of the processing window is a diffusion controlled plate growth of zero nucleation rate. The later part of stage I (the closure) represents the transformation as it extends into the segregated volumes and the beginning of stage II. Some parts of the structure had started in stage II of the reaction while other regions are still untransformed. This is responsible for the shrinking of the processing window. In the low silicon alloy, it is evident from Figure 13 that low austenitising temperature of 850 and 900^{0}C with high austempering temperature, 350^{0}C produce peaks while high austenitising (950^{0}C) produces a plateau. These peaks are caused by an overlap of the stage I and stage II reactions, which close the processing window. The segregation of elements like silicon and manganese promotes this type of behavior. Segregation of manganese to the cell boundaries increases the carbon solubility. As a result, the retained austenite reaches a peak after 60 minutes (Figure 33), followed by a steady decrease, which is the stage II. The relatively high silicon content in the vicinity of the graphite nodules improves the diffusion rate of carbon and consequently the first stage reaction starts early. In the high silicon iron, a sudden drop in impact toughness occurs after the optimum value is reached. This could be attributed to the segregation of the silicon and manganese, which has the effect of narrowing the

processing window. The time corresponding to low fatigue strength and impact toughness values can be attributed to precipitation of carbides.

It can be concluded that the effect of austempering can be optimised within the confines of processing window: too short an austempering time leads to an inadequate enrichment of the austenite and hence a lower retained austenite content. When the samples are held at the austempering temperature for too long beyond the processing window closure, a second reaction takes place, during which high-carbon austenite will decompose further into ferrite and carbide. In this case, the structure will contain epsilon carbide, which makes the material brittle. Therefore, this reaction must be avoided, hence the need to know the effective period at which the optimal property can be obtained. Also, if the austempering process is prematurely interrupted before the austenite is sufficiently stabilised through carbide enrichment, (that is before the processing window is opened), then some martensite will form on cooling to room temperature. The presence of martensite will increase hardness, (as could be seen in Table 12 and Figure 36, 37 and 38), but at the same time, reduce fatigue limit and impact toughness. For both situations, the loss of fatigue and impact toughness is not desirable. The optimum mechanical properties including strength and toughness can be achieved when setting the holding time of austempering within the range of the processing window.

TABLE 12. EFFECT OF AUSTEPERING PARAMETERS ON THE HARDNESS

ALLOY TYPE	HARDNESS (BHN)				
	AUSTEMPERING TIME				
	15	30	60	90	120
HS30 950/350	409	341	363	398	373
MS26 950/350	302	321	285	241	309
LS20 950/350	179	187	149	241	197
HS30 950/300	409	292	329	309	246
MS26 950/300	234	309	234	426	373
HS30 900/350	350	398	234	260	182
MS26 900/350	309	292	241	275	200
MS26 850/350	191	246	309	383	409
LS20 850/350	234	217	309	273	269

TABLE 13. Estimated Processing Window Duration (Minutes) For the Fatigue, Impact, Hardness and Retained Austenite Tests.

Austen / Austem. Temp. °C.	Process. Window (Minutes)	Retained Austenite			Fatigue Limit			Impact Toughness			Hardness		
		LS	MS	HS	LS	MS	HS	LS	MS	HS	LS	MS	HS
850/350	Open			28			50	30	30	55	60		
	Close			62			65	50	50	65	90		
900/350	Open		35	60		30	30	35	35	55		85	30
	Close		65	95		70	65	45	65	70		95	90
950/300	Open					30	50	55	25	70		30	55
	Close					60	70	80	30	100		90	80
950/350	Open	60	70	70	55	90	60	45	85	50	30	30	87
	Close	90	100	110	62	100	120	65	95	60	90	120	95

Table 14. Relationship between microstructural features and impact ans fatigue strength of ADI

ALLOY	AUSTEMPP ARAMETER	STRUCTURE OBTAINED	FATIGUE STRENGTH	IMPACT TOUGHNESS	RETAINED AUSTENITE
HS334	950/350/90	Coarse and fine ferrite with retained austenite	High	High	High
HS333	950/350/60	Feather like bainite with retained austenite	High	Average	High
HS234	900/350/90	Lower and upper bainite	High	Average	Average
HS123	850/300/60	Free ferrite	Low	Low	Low
HS322	950/300/30	Grain boundary bainite	Low	Low	Low
HS132	850/350/30	Pro-eutectoid ferrite	Low	High	High
HS213	900/280/60	Lower bainite	Low	Low	Low
HS223	900/300/60	Pearlitic bainite	Low	Low	Low
HS312	950/280/30	Columnar Bainite	Low	Low	Low
MS334	950/350/90	Coarse and fine ferrite	High	Average	High
MS333	950/350/60	Feather like bainite	High	Average	High
MS234	900/350/90	Lower and upper bainite	High	High	High
MS123	850/300/60	Free ferrite	Low	Low	Low
MS322	950/300/30	Grain boundary bainite	Average	Low	Average
MS132	850/350/30	Pro-eutectoid ferrite	Low	High	High
MS213	900/280/60	Lower bainite	Low	Low	Low
MS223	900/300/60	Pearlitic bainite	Low	Low	Low
MS312	950/280/30	Columnar Bainite	Low	Low	Low
LS131	850/350/15	Acicular ferrite	Low	High	Low
LS132	850/350/30	Acicilar ferrite	Low	High	Low
LS331	950/350/15	Metastable Austenite	Average	Average	Low
LS333	950/350/60	Featherlike bainie	Average	Average	Average
LS233	900/350/60	Proeutectoid ferrite	Low	Average	Low
LS232	900/350/30	Proeutectoid ferrite	Low	Average	Low

(a)

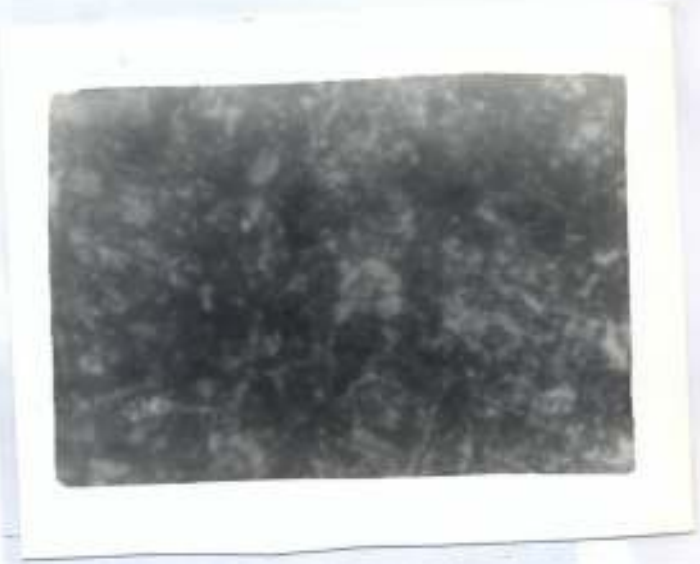

(b)

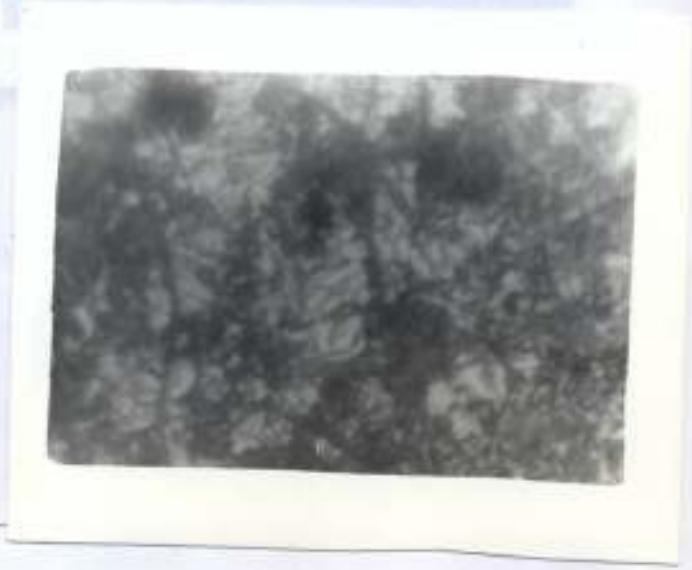

PLATE 1 As cast structures (a) High Silicon Alloys, (b) Medium Silicon Alloys. Some nodules are seen surrounded by ferrite (white). (X500)

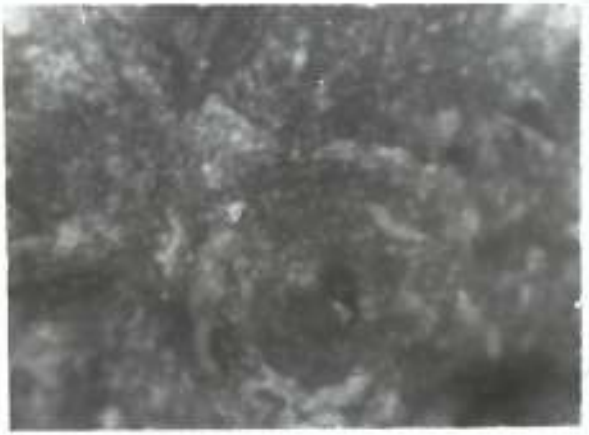

(c)

PLATE 1 (c). As cast structures Low Silicon Alloys.. (X500)

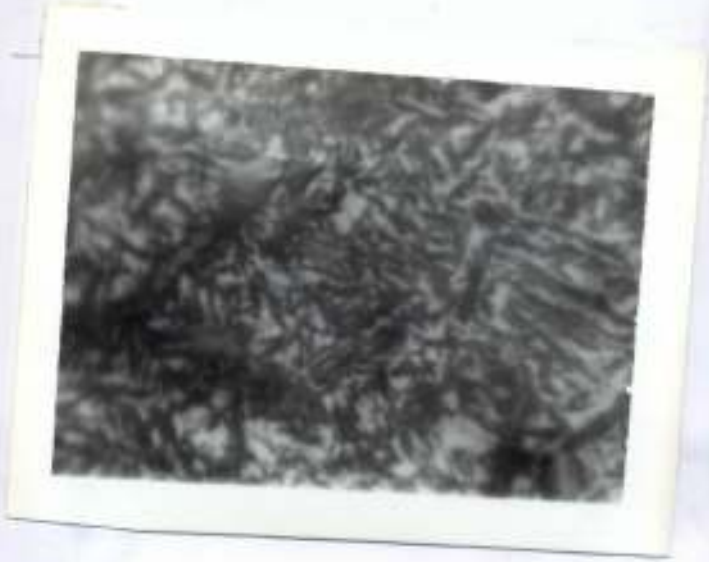

(a)

(b)

PLATE 2. Microstructure of high and medium silicon alloys austenitise at 950^{0}C for 60 minutes and austempered at 350^{0}C for 90 minutes (a) HS33 and (b) MS33. Microstructure contains a mixture of coarse and fine ferrite platelets and uniformly distributed retained austenite (light). (x500)

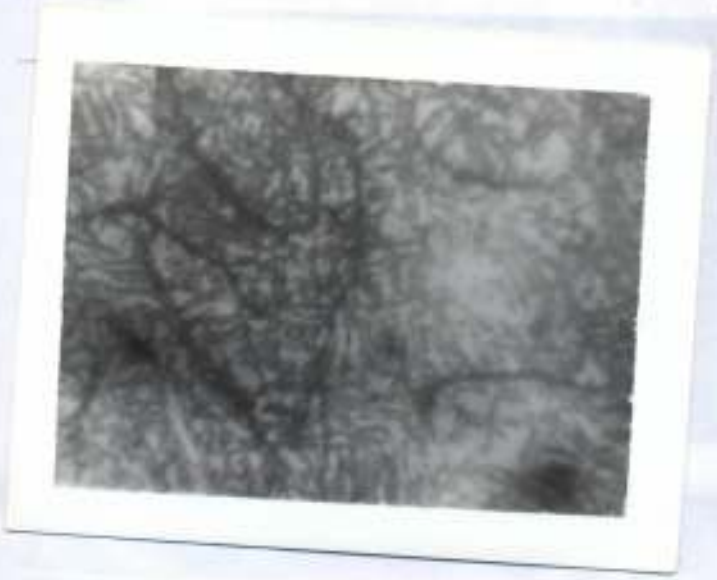

(a)

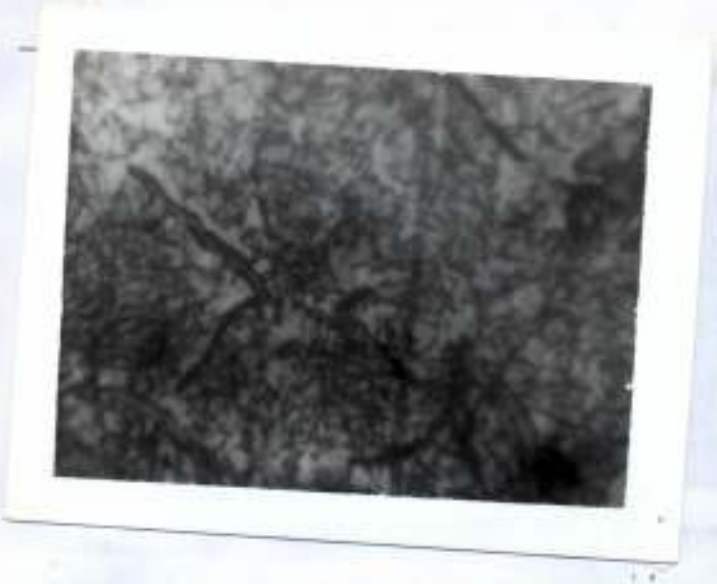

(b)

PLATE 3. Microstructure of alloys austenitised at 950^{0}C for 60 minutes and austempered at 350^{0}C for 60 minutes (a) HS33 and (b) MS33. Untransformed austenite remains at intercellular region. Bainitic morphology is seen as feather-like bainite and bainitic lath. (x500)

(a)

(b)

PLATE 4. Microstructure of low silicon alloys austenitise at 850^{0}C for 60 minutes and austempered at 350^{0}C (a) LS33 for 60 and (b) LS33 for 90 minutes. The microstructure contains closely parked acicular ferrite plates and high carbon austenite distributed uniformly between the plates. (x500)

(a)

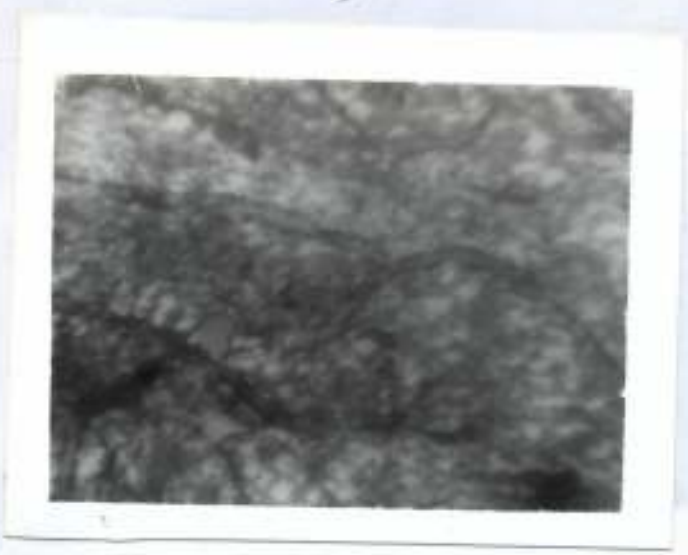

(b)

PLATE 5. Microstructure of low silicon alloys austenitise at 950^0C for 60 minutes and austempered at 350^0C (a) LS33 for 15 and (b) LS33 for 60 minutes. Microstructures show ferrite plates and a continuos network of metastable austenite and (b) featherlike bainite. (x500)

(a)

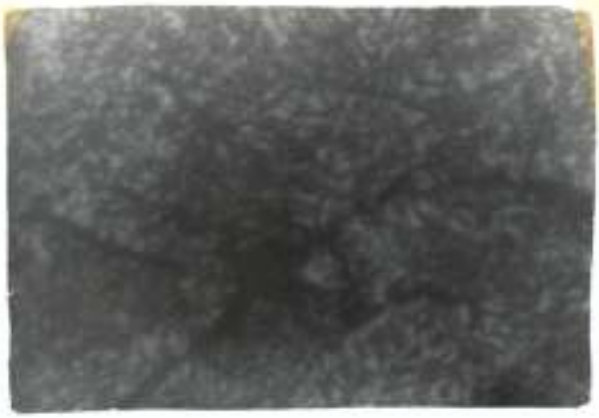

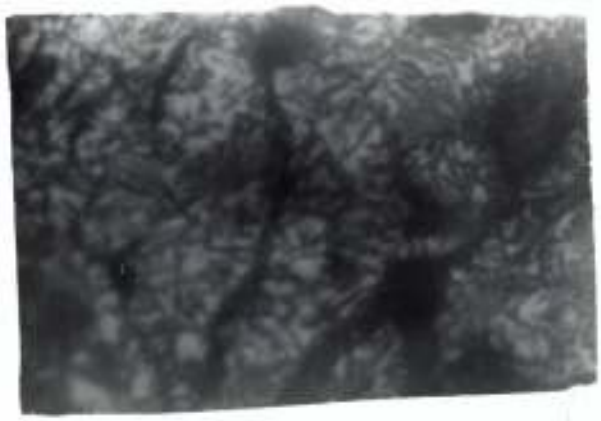

(b)

Plate 6. Microstructure of alloys austenitise at 900^{0}C for 60 minutes and austempered at 350^{0}C for 90 minutes (a) HS23 and (b) MS23. Structure reveals lower bainite + upper bainite (ausferrite) + retained austenite + graphite with dispersed nodules. (x500)

(a)

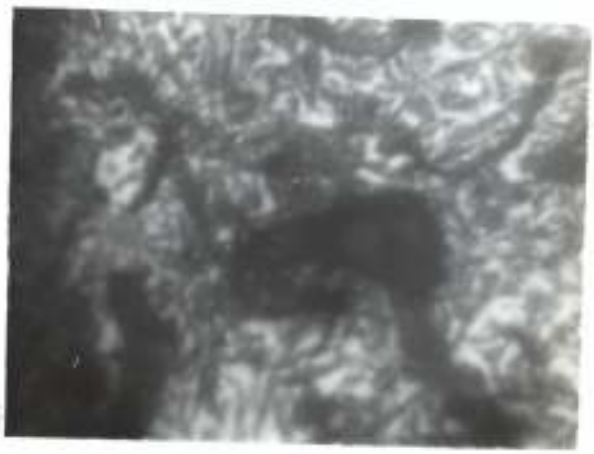

(b)

Plate7. Microstructure of alloys austenitise at 850^{0}C for 60 minutes and austempered at 300^{0}C (a) HS 12 and (b) MS12 for 60 minutes. Microstructure reveals free ferrite of the lower auferrite. (x500)

(a)

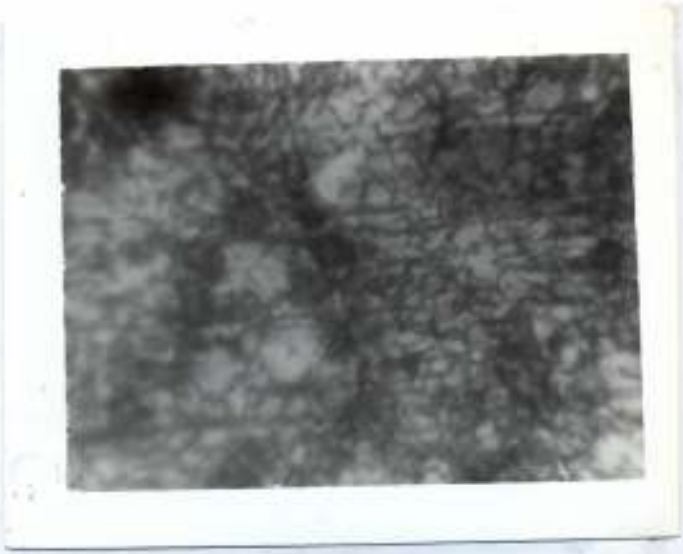

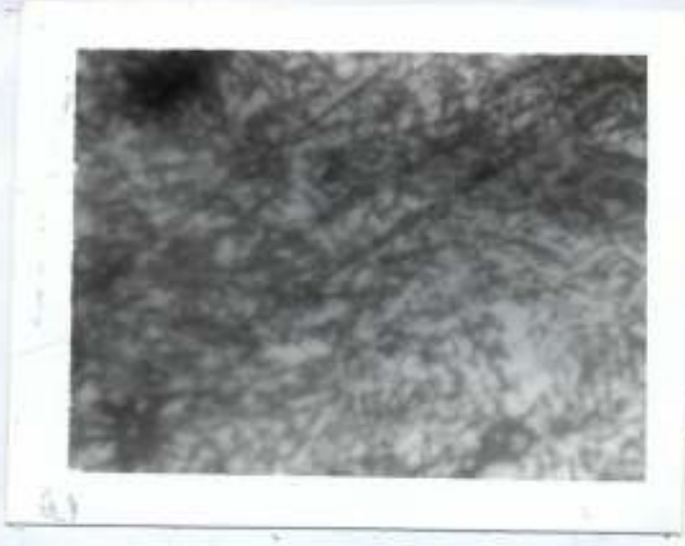

(b)

Plate 8. Changes in bainitic microstructure of alloy austenitise at 950^0C for 60 minutes and austempered at 300^0C for 30 minutes (a) HS32 and (b) MS32. Structure reveals grain boundary lower bainite with dispersed nodules at the centre. (x500)

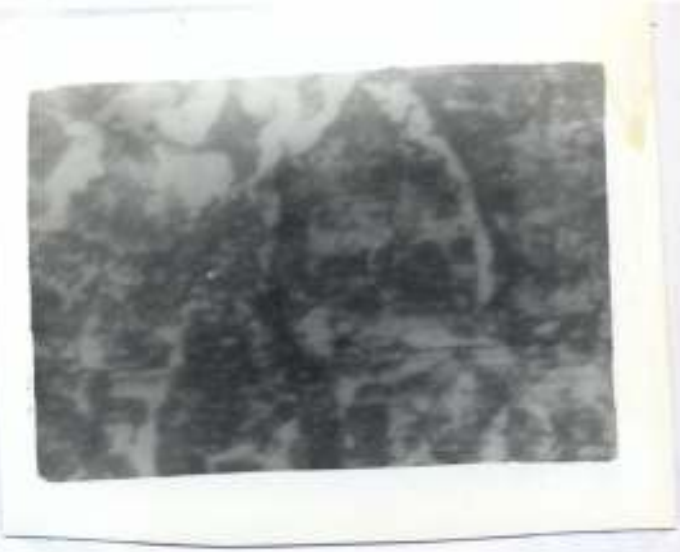

(a)

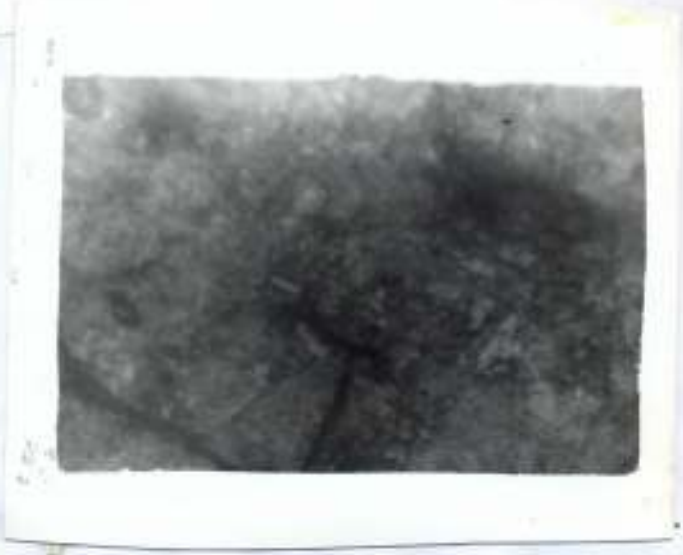

(b)

Plate 9 Microstructure of alloys austenitised at 850^{0}C for 60 minutes and austempered at 350^{0}C for 30 minutes (a) HS13 and (b) MS13. The microstructures consist of proeutectoid ferrite, bainite of coarse plates with islands of retained austenite. (x500)

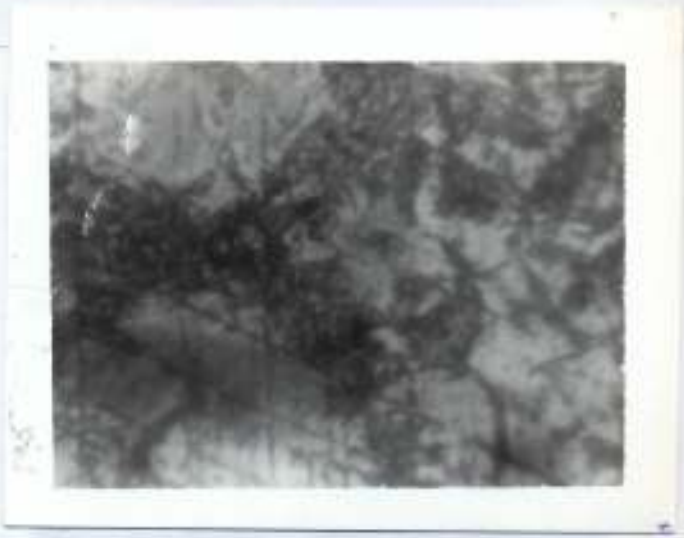

(a)

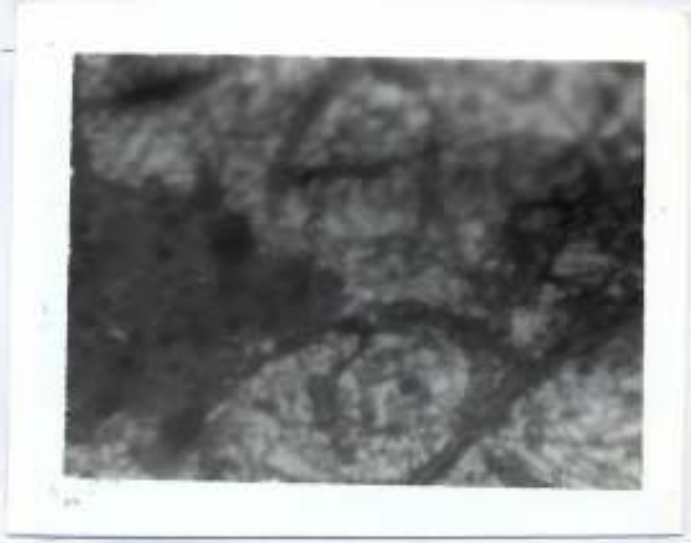

(b)

Plate 10. Microstructure of alloys austenitised at 900^0C for 60 minutes and austempered at 350^0C (a) LS23 for 60 and (b) LS23 for 30 minutes. Microstructures consist of proeutectoid ferrite (x500)

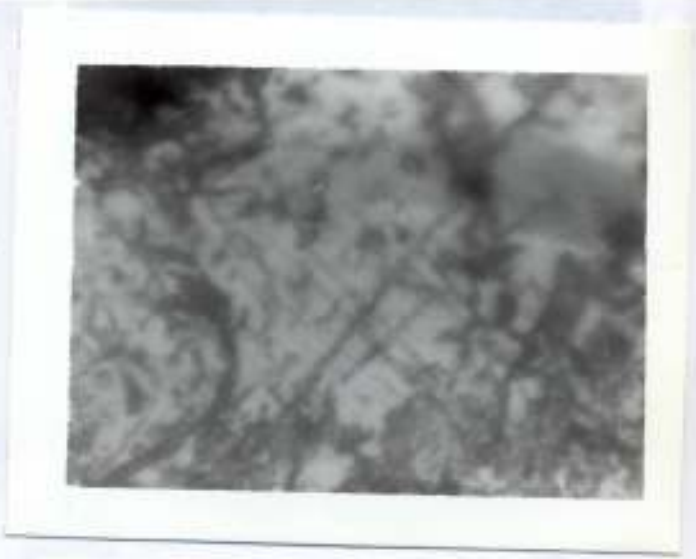

(a)

(b)

Plate 11. Microstructure of alloys austenitise at 900^{0}C for 60 minutes and austempered at 280^{0}C for 60 minutes (a) HS21 and (b) MS21. Bainitic Ferrite with untransformed austenite, (x500)

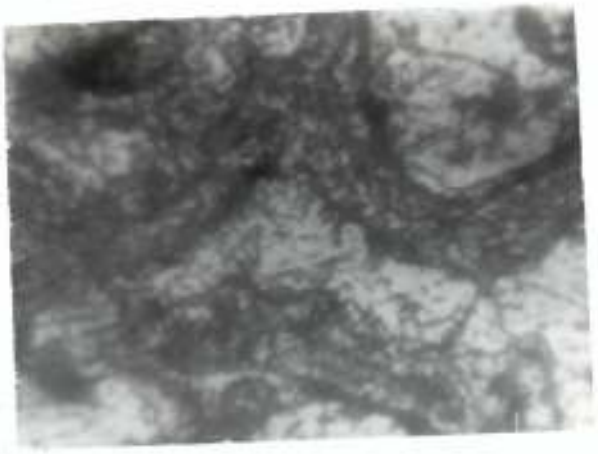

(a)

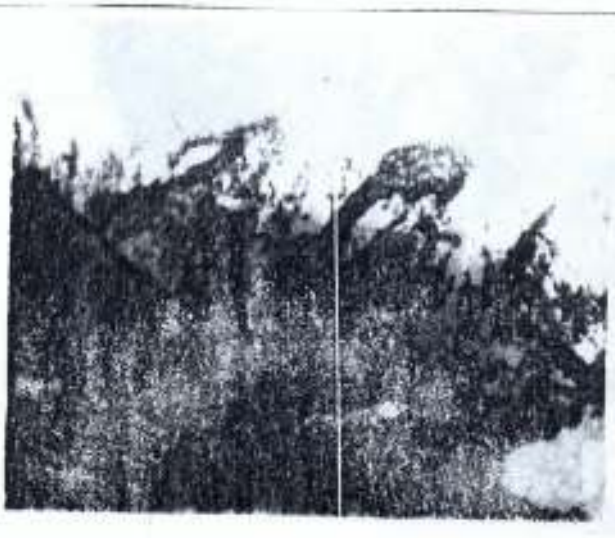

(b)

Plate 12. Microstructure of alloys austenitised at 900^{0}C for 60 minutes and austempered at 280^{0}C (a) LS21 for 90 and (b) LS13 for 30 minutes. (x500)

(a)

(b)

Plate 13. "Pearlitic" bainite microstructure in alloys austenitise at 900^{0}C for 60 minutes and austempered at 300^{0}C (a) HS22 for 60 and (b) MS22 for 60 minutes. (x500)

(a)

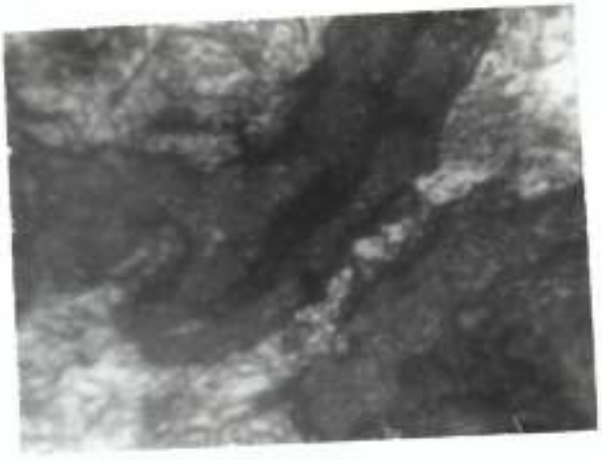

(b)

Plate 14. Columnar bainite in microstructure of alloys austenitise at 950^{0}C for 60 minutes and austempered at 280^{0}C (a) HS 31 and (b) MS 31 for 30 minutes. (x500).

CHAPTER 6

CONCLUSIONS AND SUGGESTIONS FOR FURTHER RESEARCH.

6.1 CONCLUSIONS

Developments in ADI will make replacement of costly engine components such as camshaft, crankshaft, connecting rods, axle shaft, steering knuckles and tractor parts possible with nodular iron castings. The prospects of ADI as alternative material to the rather expensive, forged, casehardened steel in other critical components operating under severe dynamic conditions will open new vistas for cast iron production. Furthermore, major engineering components requiring complicated manufacturing from high-grade steels by, for example, forging, rolling, welding, and surface hardening, all of which may preclude the use of normal machine tools, can be made in near-net shape casting in austempered nodular cast iron.

Nevertheless, like any other engineering materials, the production parameters have a significant influence on the performance of ADI castings. Of particular importance is the as-cast quality of the castings submitted to austempering, as the heat-treated castings remain sensitive to casting defects.

The results show that alloys of different silicon levels can be used to develop austempered ductile iron that is suitable for the production of automotive and machine parts by altering the austempering parameters.

As a summary, the results of this investigation have shown that:

1. High silicon ADI alloys with coarse and fine ferrite (ausferrite) structures generate the best impact value of 115 Joules.
2. Medium silicon alloys of ausferritic structure gave the best fatigue results of 450 Nmm^{-2}.

3. Impact properties of low silicon level ADI is favoured by low austenitising temperature and high austempering conditions. Acicular ferrite thus produced gave low silicon level ADI a low fatigue but high impact toughness of 80 Joules.
4. As a result of low austenitising temperatures, proeutectoid structures are formed in ADI with high and medium silicon levels. This structure adversely affects the fatigue and impact toughness of the material.
5. Moderate austenitising temperature and austempering temperature (900/300^{0}C), produces pearlitic bainite while high austenitising and low austempering generates columnar bainite in ADI with high and medium silicon alloys. Both structures exhibits poor fatigue and impact strength.
6. ADI with low silicon level austenitise at 950^{0}C and austempered at 350^{0}C show averagely high fatigue strength due to the featherlike ausferrite structure generated.
7. The optimum value of the retained austenite estimated for the various ADI alloys confirm the interrelationship between the amount of retained austenite, the fatigue strength and the impact toughness. The highest value of fatigue and impact obtained experimentally corresponds to highest amount of retained austenite estimated.
8. The predicted values of fatigue strength for ADI using developed model is relatively comparable to the experimental data obtained from various fatigue tests. This confirm the inter relationship between the fatigue strength and the impact toughness. Such a model is useful in obtaining fatigue data for materials of known impact toughness, thus saving costs and time spent in the cumbersome, time and energy consuming fatigue testing.
9. The austempering time duration as depicted in the predicted processing window obtained

from the fatigue, impacts and retained austenite test data is useful in optimising production process in foundries. Such optimisation will enable the industries to reduce product wastage, economise man-hour spent in production, increase productivity and improve product quality.

6.2 Suggestions for Further Researches.

Based on the findings from this research it is recommended that local spare-parts manufacturers should patronise indigenous foundry establishments for the source of their materials. Companies like Peugeot Automobiles Nigerian Ltd. can use this material apart from possible use for crankshaft and gearing system, it can be used as a replacement for the breakable door handles. Further research is envisaged on the mass production of silicon alloyed Austempered Ductile Iron for automobile and machine parts. Other local manufacturers of parts requiring shafts and gears can equally make use of these materials.

There is urgent need for ADI to be developed to the point where foundrymen, heat treaters and design engineers can have sufficient technical information to take full advantage of the engineering properties of the material

There is need for further work on the estimation of retained austenite. This could not be done now because of lack of facilities. There is need to correlate the amount generated by computer model with the actual mount obtained experimentally. The computer model was only adopted because it has been tested and is been used worldwide.

REFERENCES

1. Ahmadabadi, N. (1997). Bainitic Transformation in Austempered Ductile Iron With Reference To Untransformed Austenite Volume Phenomenon. Metallurgical and Materials Transactions A. 28A: 2159 –2170.

2. Ahmadabadi, M.N., Ghasemi, H.M., Osia, M. (1999). Effects of Successive Austempering on the Tribological Behaviour of Ductile Cast Iron. WEAR. 231: 293 –300.

3. American Society For Testing Materials A 8970-90, (1990) Standard Specifications For ADI Casting. Philadelphia ASTM.

4. Angus H.T. (1976) Cast Iron , Physical and Engineering Properties. Butterworths, 2nd Edition.

5. Aranzabai J, Gutierrecz I, Rodriguez-Ibade J M, Urcola J.J (1997), Influence of the Amount and Morphology of Retained Austenite on the Mechanical Properties of an Austempered Ductile Iron. Mechanical and Materials Transaction A, 28A: 1143-1156.

6. Archard J. F. (1960). Contact and Rubbing of Flat Surfaces. Journal of Applied Physics. 24: 981

7. Bahmani, M. and Elliott, R. (1994). Isothermal Transformation Diagrams For Alloyed Ductile Cast Iron. Materials Science And Technology. 10: 1050-1056

8. Bahmani, M. and Elliott, R. (1994). Effects of Pearlite Formation on Mechanical Properties of ADI. Materials Science and Technology. 10: 1068 – 1072.

9. Bayati, H. and Elliott R. (1995). Influence of T_γ on Mechanical Properties of High Manganese Alloyed Ductile Iron. Materials Science And Technology. 11: 909-912

10. Bayati, H. and Elliott, R. (1987). Role of Austenite In Promoting Ductility In An Austempered Ductile Iron. Materials science and technology. 13: 319 – 326

11. Bhadeshia H.K.D.H (1992).. The Institute of Materials. Cambridge University Press. Bainite in Steels, p 347-397.

12.Bhadeshia H.K.D.H and Svenson LE (1937): Mathematical Modeling of Weld Phenomena. The Institute of Materials. 109:80

13. Briggs, J., and Simmons, W., (1986). Influence Of Filtration On Machinability And Mechanical Properties Of Ductile Iron, presented at 2nd International Conference on ADI, Ann-Arbor, Michigan, USA, 17-19 March.

14. Dai, W. S., Chen, L.H., Lui, T.S. (2000). A Study on SiO_2 Particle Erosion of Slag, Graphite And Spheroidal Graphite Cast Irons. WEAR 239; 143 –152

15. Dieter, G 1988, , McGraw Hill, 4th Edition . Mechanical Metallurgy p 275-330

16. Dommarco, R., Galarrieta I,.Ortiz, H David P.,.Maghieri G (2001). The Use of Ductile Iron for Wheel Loader Bucket Tips. WEAR, 249: 101-108.

17. Dommarco, R.C., Bastias, P.C., Dall'O, H.A., Hahn, G.T., Rubbin, C.A. (1998). Rolling Contact Fatigue (RCF) Resistance of Austempered Ductile Iron (ADI). WEAR. 221: 69–74.

18. Fan. H., Keer, L.M, Chang, W., Cheng H.S. (1993). Competition between Fatigue Crack Propagation And Wear. Journal of Tribology, 115: 141-146.

19. Fan, Z.K. and Smallman, R. E (1994). Some Observations on the Fracture of Austempered Ductile Iron. Scripta Metallurgica Et Materiala. 31 2: 137 - 142.

20. Gates, J.D. (1994). Two Body And Three.Body Abrasion - A Critical Discussion. WEAR 214: 139–146.

21. Harding, (1986). Effect Of Metallurgical Process Variables On Austempered Ductile Irons. Metals and Materials. 2 2: 65 – 71.

23. Haseeb, M. A., Islam, A. Bepari, A. (2000). Tribological Behaviour of Quenched and Tempered and Austempered Ductile Iron At The Same Hardness Level, WEAR 244. 15: 9

24. Hemanth J. (2000) The Solidification And Corrosion Behaviour of Austempered Chilled Ductile Iron, Journal Of Materials Processing Technology. 101: 159 – 166.

25. Higgins, R.(1993). Engineering Metallurgy Part I; Applied Physical Metallurgy. Hodder and Stonghton, 6th Edition. p359-301.

26. Hsu, C. H. and Chuang, T.L. (2001). Influence of Stepped Austempering Process on the Fracture Toughness of Austempered Ductile Iron. Metallurgical and Materials Transaction A. 32A, 2509-2512

27. Imasogie B.I. (1994). Development and Characterisation of Isothermally Heat Treated Nodular Cast Irons. Ph.D. Thesis. Obafemi Awolowo University, Ile-Ife.

28. Imasogie B.I. Afonja A.A. and Ali J.A. (2000). Properties of Ductile Iron Nodularised With Multiple Calcium-Magnesium Based Master Alloy. Materials Science and Technology, 16: 194-201.

29. James, J.S. and Thomson, R.C. (1999) Microstructural Modeling of Austempered Ductile Iron. Presented at Phase Transformations Meeting '99, Kyoto, Japan.

30. Kobayashi , T. and Yamada, S. (1996). Effects of Holding Time in the (α and γ) Temperature range on Toughness of Specially Austempered Ductile Iron. Metallurgical and Materials Transactions A. 27A: 1961-1971.

31. Krauze, L.A., Kurganov,V.A., Lesovoi, V.V., (1988). Mechanism of Formation of Graphite in Iron-Carbon Alloys. Izvestia VUZ Chernaya Metalla. 12: 83-89.

32.Lin, C. K. and Fu, C.S. (1997), Low Cycle Fatigue of Austempered. Ductile Irons In Various Sized Y-Block Castings, Materials Transactions, JIM. 38 8: 692-700.

33. Lin, C-K and Wei, J.Y. (1997), High-Cycle Fatigue of Austempered Ductile Irons In Various-Sized Y-Block Castings. Materials Transactions, JIM 18 8: 682 – 691.

34. Magalhaes, L; Seabra, J. and Sa, C. (2000) Experimental Observation Of Contact Fatigue Crack Mechanisms For Austempered Ductile Iron (ADI) Discs, WEAR. 246: 134 –148.

35. 'Marks' Standard Handbook for Engineers' (1996). 10th Ed. McGraw-Hill

36. Neuman, F. (1965). Recent Research in Cast Iron. Gordon and Beach, 659.

37. Prasad, P. R. and Putatunda, S.K (1998) Comparative Study of Fracture Toughness Of Austempered Ductile Irons With Upper And Lower Ausferrite Microstructure. Materials Science And Technology. 14: 1257 – 1264

38. Prasad R, and Putatunda, S.K. (1990). Effect of Over-Stressing on Fatigue Behaviour of Austempered Ductile Iron. Engineering Materials Structure. 18 60: 693 – 697.

39. Putatunda, S.K. (2001). Development of Ductile Cast Iron with Simultaneous High Yield Strength And Fracture Toughness By A Novel two-step Austempering Process. Materials Science and Engineering. A315: 70-80.

40. Rajan T.V., Sharma C.P., Ashok, S. (1988). Heat Treatment Principles And Techniques. Prentice Hall, 3rd Edition 117 - 119.

41. Roberts M., (1992). Machine Elements In Mechanical Design. Macmillan, Singapore, 2nd ed. P 376 - 408.

42. Santos, H., Pinto A, Tornes V. (1991). Cu-Mn ADI: A Low Cost High Performance Material. Proceedings Of The 58th World Foundry Congress. Poland, September 23-25, p23.

43. Schisser,J.M, Chobanut, J.P. (1988). S.E.M. Study Of The Influence Of Intercellular Segregation On The ADI Structures, paper presented at XXII International Metallurgy Congress: Innovation For Quality, (Conf. Proc.), Bologna, Italy, 17-19th May.

44. Shaker, M.A. and Salamoni M.A. (1988). Improvement of Structure Homogeneities of S.G. Iron Casting by the Addition of Sawdust to the Nodulising Mixture. XXII International Congress: Innovation For Quality Miliano Italy.

45. Shieh, C.S., Lui, T.S., Chen, L.H. (1995). Tensile Characteristics of Austempered Ductile Cast Iron in the Temperature Regime of 300 K to 693 K. Materials Transactions, JIM, 36, 5: 620-625.

46. Smith J.H. (2001). An Introduction to Modern vehicle design. Butterworth-Heinmann.

47. Tanaka Y. and Kage H., (1995). Development of Austempered Spheroidal Graphite Cast Iron. Materials Transaction JIM 33,6:543-557.

48. Tripodo, R. Bertozzi, R. Gabrielli, V. (1988). Evaluation Of Mechanical Behaviour Of Austempered Ductile Iron For Possible Use In Gears. paper presented at XXII International Metallurgy Congress: Innovation For Quality, (Conf. Proc.), Bologna, Italy, 17-19th May.

49. Trudel, A. and Gagne, M. (1997). Effect of Composition and Heat Treatment Parameters on the Characteristics of Austempered Ductile Irons. Canadian Metallurgical Quarterly. 36, 5 : 289-298.

50. Vasatuk, J. Sinatora, A. Goldenstein, H. Albertin, E. Fuoso, R. (1988). paper presented at XXII International Metallurgy Congress: Innovation For Quality, (Conf. Proc.), Bologna, Italy, 17-19th May.

51. Wen D. C. and Lei T. S. (1997). The Mechanical Properties Of A Low Alloyed Austempered Ductile Iron In The Upper Ausferrite Region. ISIJ International, 39 5: 493-500.

52. Yescas M. A., Bhadeshia, H.K.D.H., Mackay, D.J. (2000). Estimation of The Amount of Retained Austenite in Austempered Ductile Irons Using Neural Networks. Material Science and Engineering A311; 162-173.

53. Yan, M. (1995) Effect of Cu, Mo, Si on the content of Retained Austenite of Austempered Ductile Iron. Scrita Metallurgica

APPENDIX I

PROGRAM NEURAL ADI RETAINED AUSTENITE

The purpose of this program if for the estimation of the amount in percent of retained austenite for any austempered ductile irons (ADI) as a function of chemical composition and heat treatment conditions (austenitising temperature, austenitising time, austempering temperature and austempering time). The language used is FORTRAN.

How To Generate The % Amount Of Retained Austenite.

STEP I. Input variables. The input variables for the model are listed below.

1	Carbon (wt%)	3.28; 3.20; 3.19
2	Silicon (wt%)	2.00; 2.65; 3.00
3	Manganese (wt%)	0.29 0.33 0.34
4	Molybdenum (wt%)	0.16 - -
5	Nickel (wt%)	0.46; 0.5 0.48
6	Copper (wt%)	0.42 0.4 0.48
7	Austenitising temperature (^{0}C)	850; 900; 950
8	Austenitising time (min)	60
9	Austempering temperature (^{0}C)	280; 300, 350
10	Austempering time (min)	15; 30; 60; 90; 120

STEP II. Output parameters. This program generate the amount of retained austenite value in %. (To run the program, double click on "RET_AUST.exe" icon).

STEP III. To obtain results double click on "RESULTS . exe" icon. The Results (Volume % of retained austenite) are stored in a file called 'Result.dat'. The format of the output results is:

Prediction (%) Upper-limit (%) Lower-limit (%).

End of task.

FORTRAN PROGRAMME TO PREDICT RETAINED AUSTENITE FORMATION IN ADI

Introduction

IPAUSE allows a pause if the value is set to 1;
X contains normalized values of the input variables;
W1 and W2 contain the weights;
THETA1 and THETA2 are the biases;
Y is the output (normalized);
AMIN and AMAX contain the minimum and maximum unnormalized values of the input variables and of the output

```
SUBROUTINE MAP_NEURAL_ACITEMP(AW,W1,W2,THETA1,THETA2,
&AMIN,AMAX,IMAX,Y,HT,IERR,IN,IHID,ERROR)  IMPLICIT NONE
DOUBLE PRECISION  W1(4,22),W2(4),THETA1(4),H(4),ERROR,
&AMIN(23),AMAX(23),AW(22),X(22),HT(20),Y(20),A,THETA2
INTEGER IMAX, IERR(20), I, J, IN, IHID, II
```

Remember to set matrix dimensions according to number of inputs and number of hidden units. Currently set at 100 and 10 respectively.

```
ERROR = 40D0
Read a set of unnormalized inputs
DO 222 I=1,IN
X(I)=AW(I)

222     CONTINUE
```

One of the variables, in this case the heating rate HT, is to be varied, so at first normalize IN-1 variables

```
      DO 1 I=1,IN-1
        X(I) = ((X(I) -AMIN(I))/(AMAX(I)-AMIN(I)))-0.5D+00

1       CONTINUE

      DO 20 II=1,IMAX
      HT(II) = 10.0D+00**(II)/1000.0D+00
      X(IN) = ((HT(II) -AMIN(IN))/(AMAX(IN)-AMIN(IN)))-0.5D+00
```

IERR = 0 (implies that all inputs are within the range of the training dataset for the neural network. Thus, the 95% confidence error bars amount to about +- 11%)

```
C IERR = 1 (implies that some inputs are out of the range of the training dataset for the neural
network. The 95% confidence error bars MAY then be greater than +-11%. )

      IERR(II)=0
      DO 11 J=1,IN
       IF(X(J) .LT. -0.5D+00 .OR. X(J) .GT. 0.5D+00) THEN
       IERR(II)=1
        END IF
11    CONTINUE
Read all weights, and theta parameters
Do calculation of the normalized output value for the given set of
 normalized input  First equation

      DO 6 I=1,IIIID
        A=0.0D+00
            DO 5 J=1,IN
             A=A+W1(I,J)*X(J)

5           CONTINUE

        H(I)=DTANH(A+THETA1(I))

6     CONTINUE

 Second equation
      A=0.0D+00
      DO 7 I=1,IIIID
        A=A+W2(I)*H(I)

7     CONTINUE

      Y(II) = A+THETA2
      Y(II)=(Y(II)+0.5D+00)*(AMAX(IN+1)-AMIN(IN+1))+AMIN(IN+1)

 Prevent temperature from acquiring a negative value
   IF (Y(II) .LT. 0.0D+00) Y(II)=0.0D+00

 20   CONTINUE

      RETURN

      END
```

APPENDIX III

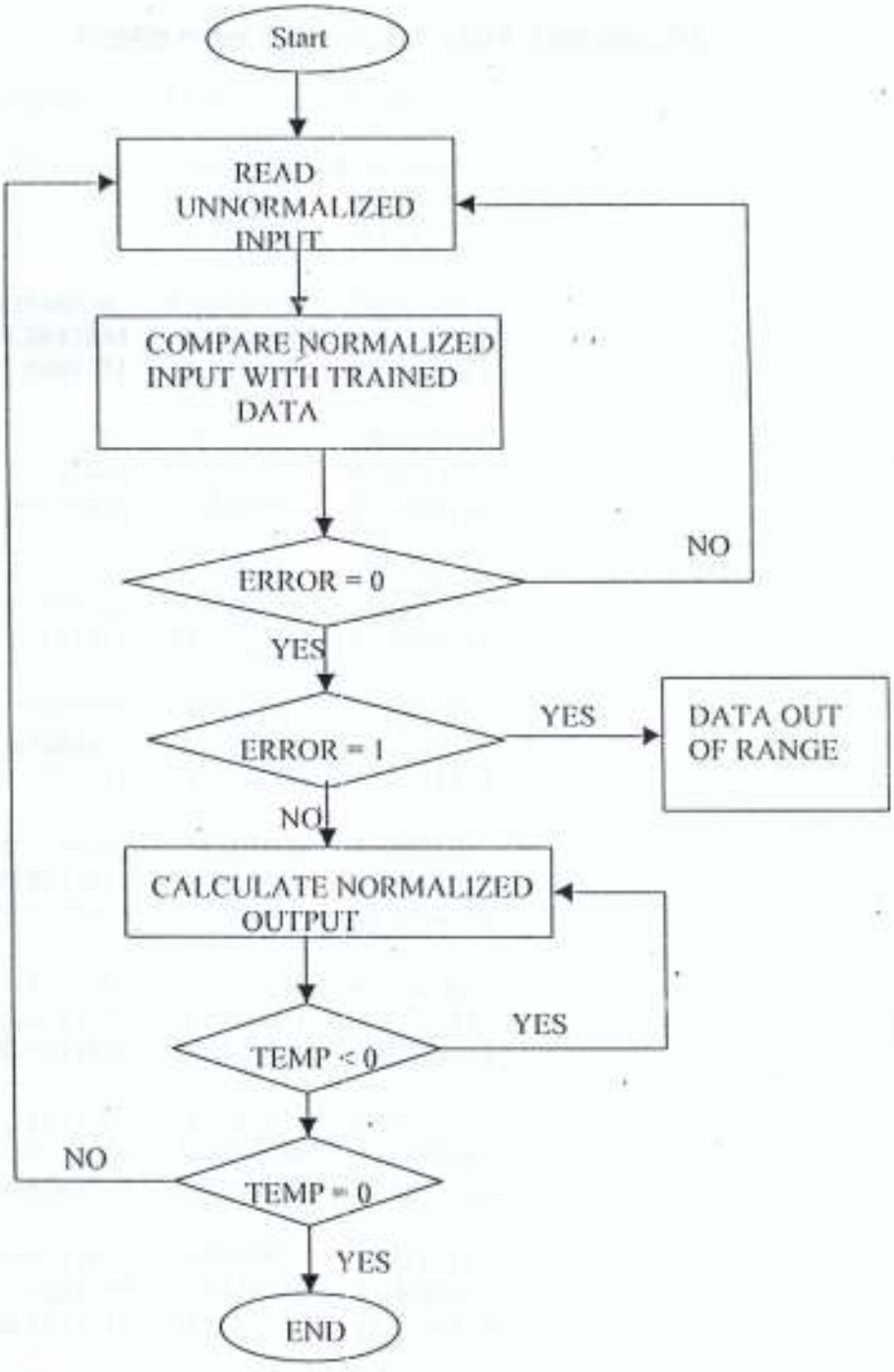

Figure Appendix I Flow Chart for Estimation of retained austenite in ADI

Results of the Amount of Retained Austenite (%).

	Prediction	Upper-limit	Lower-limit
850/280/15			
	6.9556695	6.7638388	4.1601667
	14.0034461	6.1906911	5.0732373
	20.9488171	10.4170616	8.7915643
850/280/30			
	6.2958326	6.6113732	3.9082908
	14.8445844	8.7809640	6.8138243
	23.8462321	15.3710991	12.7153243
850/280/60			
	4.1450810	4.9745696	2.6918576
	13.1497860	8.4700304	6.3438913
	23.0499403	15.2502571	12.4463167
850/280/90			
	3.1066238	4.2362421	2.1165710
	12.2571120	8.2905059	6.0803593
	22.6941111	15.1546758	12.2990534
850/280/120			
	2.5231585	3.8757506	1.7971122
	11.7695832	8.2129241	5.9444757
	22.5957651	15.0886738	12.2331279
850/300/15			
	10.0288394	7.6188100	5.2880663
	19.9644542	9.0815641	7.7169599
	26.0349043	14.0958544	12.2763043
850/300/30			
	8.2553250	6.5491058	4.4048087
	19.3453302	9.2535007	7.7632280
	26.7973515	14.4058539	12.6525496
850/300/60			
	5.7561472	5.4854037	3.3550520
	17.6598429	9.1484599	7.4686764
	26.6583470	14.6761658	12.8293335
850/300/90			
	4.4627165	5.0490647	2.8213111
	16.6838354	9.0171060	7.2440161
	26.5839212	14.7775906	12.8904039
850/300/120			
	3.7029128	4.8501150	2.4973722
	16.1117099	8.9576556	7.1211564
	26.6315450	14.8273748	12.9370634
850/350/15			
	21.0711384	10.6224176	8.9533335
	31.9194700	8.7065211	8.4090866
	33.7493390	13.3360172	12.8704972
850/350/30			

	18.0674891	10.4146207	8.3493712
	30.9754118	8.6358182	8.2843783
	34.8498279	12.8259439	12.5384052
850/350/60			
	14.0211125	10.0201563	7.3526983
	28.7074522	8.5959504	8.0999602
	34.5525284	12.6577051	12.3424211
850/350/90			
	11.9375857	9.7177671	6.7186508
	27.4094429	8.6523459	8.0583835
	34.2103504	12.6858734	12.3266383
850/350/120			
	10.7278709	9.4894072	6.2998218
	26.6671562	8.7533412	8.0898611
	34.0297521	12.7481845	12.3623088
900/280/15			
	6.7030816	6.8298428	4.1090308
	12.5510529	5.7944913	4.6637269
	18.6691406	10.2069148	8.3128376
900/280/30			
	6.9556695	6.7638388	4.1601667
	14.0034461	6.1906911	5.0732373
	20.9488171	10.4170616	8.7915643
900/280/60			
	5.7065221	6.0370371	3.5321466
	13.7004179	6.2974201	5.1124391
	21.3709519	10.4751373	8.8912646
900/280/90			
	4.7059112	5.5125156	3.0408328
	13.0934997	6.2790336	5.0337886
	21.1367095	10.5134747	8.8859077
900/280/120			
	4.0170144	5.1826564	2.7016200
	12.6130681	6.2712133	4.9729443
	20.8909100	10.5673507	8.8888501
900/300/15			
	10.0288394	7.6188100	5.2880663
	19.9644542	9.0815641	7.7169599
	26.0349043	14.0958544	12.2763043
900/300/30			
	8.2553250	6.5491058	4.4048087
	19.3453302	9.2535007	7.7632280
	26.7973515	14.4058539	12.6525496
900/300/60			
	5.7561472	5.4854037	3.3550520
	17.6598429	9.1484599	7.4686764
	26.6583470	14.6761658	12.8293335
900/300/90			
	4.4627165	5.0490647	2.8213111

	16.6838354	9.0171060	7.2440161
	26.5839212	14.7775906	12.8904039
900/300/120			
	3.7029128	4.8501150	2.4973722
	16.1117099	8.9576556	7.1211564
	26.6315450	14.8273748	12.9370634
900/350/15			
	22.1593331	9.2054794	8.0515374
	30.1841180	8.1494660	7.7915985
	30.3641453	11.5140580	10.8135582
900/350/30			
	23.1624686	9.8570085	8.6571656
	32.6950452	8.0570189	7.8443911
	34.1702141	10.8688191	10.6100760
900/350/60			
	1.1324280	10.3985478	8.8039561
	32.4103621	7.9069058	7.6878237
	35.1974006	10.3369565	10.1893712
900/350/90			
	19.2947103	10.6660280	8.7132254
	31.5889822	7.8627400	7.6041273
	35.0108528	10.1255469	9.9701173
900/350/120			
	17.9443951	10.8393946	8.5937348
	30.9292488	7.8868007	7.5918723
	34.7080214	10.0284721	9.8529831
950/280/15			
	7.4390050	8.5035761	4.9094504
	12.4431955	7.3616024	5.6015202
	16.8293743	9.5212734	7.5849218
950/280/30			
	10.0687533	9.5462069	6.1350813
	16.5754518	8.2477467	6.7299560
	21.7333517	10.1972924	8.7394433
950/280/60			
	10.5161305	9.8644457	6.3955749
	18.4172350	8.6467018	7.2273560
	24.1356785	10.5050494	9.2679544
950/280/90			
	9.8246914	9.8746473	6.1871687
	18.4635349	8.7907117	7.3325207
	24.4403311	10.7080680	9.4616467
950/280/120			
	9.0696914	9.8696572	5.9341125
	18.1711651	8.9052070	7.3742022
	24.2930683	10.9025933	9.5931637
950/300/15			
	9.9042831	8.3037969	5.5706812
	17.3496319	8.4657563	6.9730370

	20.4938144	10.6015985	8.8547489
950/300/30			
	13.5327908	9.0950998	6.7579911
	22.7169772	9.1946840	8.1008041
	26.5378615	11.2119666	10.1148771
950/300/60			
	14.4632460	9.6753904	7.2578584
	25.1609338	9.3854657	8.4889522
	29.6478822	11.2770427	10.5278095
950/300/90			
	13.8076493	10.1071141	7.3512671
	25.3247558	9.4596725	8.5646359
	30.1925673	11.3035440	10.6103924
950/300/120			
	12.9811261	10.4762176	7.3384233
	25.0279937	9.5543808	8.6132676
	30.1403349	11.3647081	10.6581463
950/350/15			
	27.5256005	11.1488057	10.1802381
	32.1019015	9.0670368	8.7561651
	30.1070219	12.4520361	11.5957800
950/350/30			
	33.4455777	11.8686086	11.4751773
	38.7380330	8.8492065	8.9508856
	37.2575290	11.5881417	11.6038728
950/350/60			
	34.9197025	12.8470952	12.5672381
	41.4461083	8.5238277	8.7601456
	40.5095983	10.5664260	10.8494419
950/350/90			
	34.1381009	13.5376503	13.1112961
	41.6560459	8.4553225	8.6986330
	40.9531465	10.1294322	10.4236181
950/350/120			
	33.0812976	14.0781646	13.4496492
	41.4115921	8.4989344	8.7321227
	40.8113679	9.9293874	10.2024558